The University Of Sheffield.

Pyrene Based Donor-Acceptor Conjugated Polymers for Photovoltaic Applications

Bakhet Ahmad M Alqurashy

A thesis submitted to
The University of Sheffield
as partial fulfilment for the degree of Doctor of Philosophy

Department of Chemistry

Declaration

I hereby declare that the dissertation entitled "**Pyrene Based Donor-Acceptor Conjugated Polymers for Photovoltaic Applications**" is submitted for the degree of doctorate of philosophy (PhD) at the University of Sheffield. It records the research carried out from January 2014 to February 2017. I further declare that all work reported were carried out under the supervision of Dr. Ahmed Iraqi who also helped with the editing of this dissertation.

Dr. A. Iraqi, Professor David. G. Lidzey, Yiwei Zhang and Luke Cartwright are co-authors on articles published from the work conducted in this dissertation.

All results presented in this dissertation were undertaken myself, unless where referenced.

Signed:……....
February 2017

Acknowledgements

First and foremost, I am truly grateful to my parents for their unending moral support and encouraging me all the times. I am also thankful to my brothers and sisters for their support. Honestly, I would not be able to finish my PhD without them.

I am deeply grateful to my supervisor Dr. Ahmed Iraqi for allowing me to take a place in his research project. Special thanks to him for his encouragement, support, guidance and advice throughout my PhD in both lab work and writing the thesis.

I particularly would like to express my gratitude to Sulaiman Al-isaee for his continuous help, support, suggestions regarding the work and co-operation. Without you Sulaiman my experimental work would not have been accomplished. I would also like to thank Ary Murad who should have a mention. Special thanks to Luke Cartwright and Nathan Rutland who has been enormously patient when I was asking for help and advice on many occasions. Specials acknowledgements to my friends Hamza Qasem, Majed Alawad, Omar Esmaeel and Bader Altayeb for their sustained help and valuable suggestions. If you all guys were not with me in the lab I would certainly still struggling. These acknowledgements would not be complete without mentioning my colleague: Ali Alkorbi, Wael Alsaedi, Osama Alharbi and Sami Alalawi. It was a great pleasure to work with you all.

I would like to thank Sue Bradshow and Sandra Meurs for fitting NMR spectra measurements, Rob Hanson for his great help in GPC and TGA analysis, Simon Thorpe for help with mass spectrometry, Sharon for help with XRD, Mel Hannah, Heather Grievson, Peter, Nick, and to everyone at the department who has helped me.

Last but not least I would also like to express my thankful to the Royal Embassy of Saudi Arabian, Culture Bureau in London for their sustained help and Taibah University for sponsoring my education and funding this project.

Publications from this Thesis

1- **B. A. Alqurashy**, L. Cartwright, A. Iraqi, Y. Zhang and D. G. Lidzey, Pyrene-Benzothiadiazole Based Copolymers for Application in Photovoltaic Devices, *Polymer. Adv. Tech.*, 2017, **28**, 193-200.

2- **B. A. Alqurashy**, A. Iraqi, Y. Zhang and D. G. Lidzey, Preparation and photovoltaic properties of pyrene-thieno[3,4-c]pyrrole-4,6-dione-based donor-acceptor polymers, *Eur. Polym. J.*, 2016, **85**, 225-235.

3- **B. A. Alqurashy**, A. Iraqi, Y. Zhang and D. G. Lidzey, Pyrene-Benzo[1,2,5]thiadiazole Based Conjugated polymers for Application in BHJ solar cells is submitted for publication.

Abstract

Photovoltaic devices have emerged as a promising and efficient technology to address rising global energy demands as the current energy source, which depends on fossil fuels is running out. This technology has the ability to directly convert sunlight to electricity. Inorganic photovoltaic devices exhibit relatively high power conversion efficiencies from 8 to 29%. However, the high cost of these devices has impeded their widespread usage. Intensive research has been done in order to find different approaches to explore less expensive materials to maintain a technology path for photovoltaic devices. Organic photovoltaic devices based on conjugated polymers have gained a large amount of attention from researchers and academicians owing to their potential characteristics when compared with inorganic solar cells. The potential characteristics of organic photovoltaic devices are as follows: they are economical, light weight, and their roll to-roll production is fast and inexpensive. Several types of π-conjugated polymers have been synthesized and applied as electron donor materials in organic photovoltaic devices, either as homopolymers or alternating donor-acceptor copolymers.

In this project, different type of donor-acceptor conjugated polymers, consisting of pyrene as the electron donor and benzothiadiazole or thieno[3,4-c]pyrrole-4,6-dione as the electron acceptor, have been prepared via palladium catalysed cross-coupling reactions such as Stille or direct arylation. The purity and identity of all monomers were confirmed by ^{1}H and ^{13}C NMR spectroscopy, GC-MS and elemental analysis. The structures of all synthesised polymers have been confirmed by ^{1}H NMR spectroscopy and elemental analysis. The thermal, optical and electrochemical properties of all polymers have been investigated using TGA, UV-vis, CV and XRD in order to evaluate their suitability for application in organic photovoltaic devices. The optical band gap of all polymers ranged between 1.76 and 2.06 eV. Bulk heterojunction devices were fabricated from all polymers using $PC_{70}BM$ as the electron acceptor. Preliminary studies indicated that the power conversion efficiencies of the polymers ranged from 0.33 and 2.06 %.

Table of Contents

List of abbreviations

A	Acceptor
Acetone-d6	Deuterated acetone
AM	Air Mass
bm	Broad multiple (NMR)
br	Broad (NMR)
Br_2	Bromine
CB	Conduction band
$CDCl_3$	Deuterated Chloroform
$CHCl_3$	Chloroform
CH_2Cl_2	Dichloromethane
$C_2D_2Cl_4$	Deuterated 1,1,2,2-Tetrachlorethan
CV	Cyclic voltammetry
D	Donor
d	Doublet (NMR)
dd	Doublet of doublets (NMR)
DCM	Dichloromethane
DMF	*N*,*N*-dimethylformamide
DMSO	Dimethyl sulfoxide
DP	Degree of polymerization
E_g (opt)	Optical band gap
E_g (elec)	Electrochemical band gap
EtOAc	Ethyl Acetate
eV	Electron volt
Fc	Ferrocene
FET	Field-Effect Transistor
GPC	Gel Permeation Chromatography
HCl	Hydrochloric acid
HNO_3	Nitric acid

HOMO	Highest Occupied Molecular Orbital
H_2SO_4	Sulfuric acid
Hz	Hertz
ICT	Intramolecular charge transfer
IR	Infra-Red spectroscopy
ITO	Indium Tin Oxide
IPCE	Incident Photon to Current Efficiency
J_{SC}	Short Circuit Voltage
J-V	Current-Voltage
LED	Light-Emitting Diode
LUMO	Lowest Unoccupied Molecular Orbital
λ_{max}	Maximum absorption wavelength
m	Multiplet (NMR)
M_n	Number average molecular weight
M_w	Weight average molecular weight
NMR	Nuclear Magnetic Resonance
NBS	*N*-Bromosuccinide
OFETs	Organic field-effect transistors
OLED	Organic light emitting diode
OSC	Organic Solar Cell
OPV	Organic Photovoltaic
PA	Polyacetylene
$PC_{70}BM$	Phenyl-C_{70} Butyric Acid Methyl Ester
PCE	Power conversion efficiency
PDI	Polydispersity Index
P3HT	Poly(3-hexylthiophene)
PivOH	Pivalic acid
PLEDs	Polymer light emitting diodes
PPV	Poly(*para*-phenylenevinylene)
PV	Photovoltaic
PSC	Polymer solar cell

$P(o\text{-}tol)_3$	Tri-*ortho*-tolylphosphine
$Pd(PPh_3)_2Cl_2$	Bis(triphenylphosphine)palladium(II)dichloride
$Pd_2(dba)_3$	Tris(dibenzylidene acetone) palladium (0)
$Pd(OAc)_2$	Palladium(II) acetate
PEDOT:PSS	Poly(3,4-ethylenedioxythiophene): Poly(styrenesulfonate)
s	Singlet (NMR)
t	Triplet (NMR)
TGA	Thermogravimetric analysis
THF	Tetrahydrofuran
TPD	Thieno[3,4-c]pyrrole-4,6-dione
UV-vis	Ultra Violet-visible spectroscopy
V_{OC}	Open-Circuit Voltage
V	Volt
XRD	X-ray diffraction

List of Tables

List of Figures

List of Schemes

Chapter I: Introduction

1. Photovoltaic cells

1.1. Introduction

Increasing world population in addition to the economic expansion led to growing global energy demands, however, the current energy source (fossil fuels) such as oil, coal and gas is running out. It is realised that fossil fuels affect the environment and caused other problems such as pollution and global warming. Therefore, a clean and renewable energy source is needed to be developed to address these issues.[1,2] Solar cells or the so-called photovoltaic (PV) devices have emerged as a promising and efficient technology to address rising global energy demands. This technology has the ability to absorb sunlight and directly convert it to electricity.[3]

Inorganic solar cells based on silicon (Si), cadmium-indium-selenide (CIS), copper indium germanium selenide (CIGS) or cadmium telluride (CdTe) exhibit high power conversion efficiencies from 8 to 29% (figure 1.1 (a)).[2,3] However, the high cost of these devices has impeded their widespread usage. Intensive research has been done in order to find different approaches to explore less expensive materials to maintain a technology path for solar cells.[2,3,4]

Organic solar cells (OSCs) based on conjugated polymers (or organic semiconductors) have gained a large amount of attention because of their potential characteristics when compared with inorganic solar cells. The potential characteristics of OSCs are as follows: they are economical, light weight, and their roll-to-roll production is fast and inexpensive (figure 1.1 (b)).[5,6]

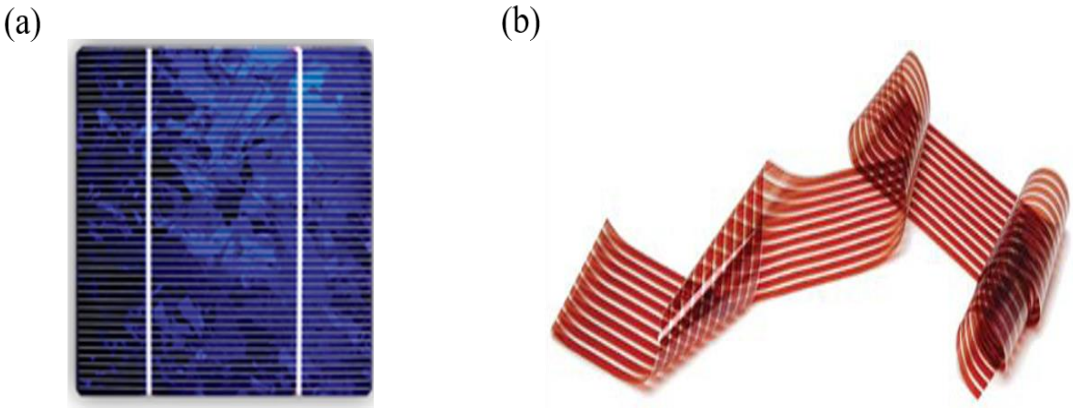

Figure 1.1. (a) Inorganic solar cells and (b) Organic solar cells.

Photovoltaic cells fabricated with single layers of pure conjugated polymers as the active layers exhibit a very poor power conversion efficiency (PCE) ranging from 10^{-3} to 10^{-2}%, too low in terms of being used in solar cell applications. However, the development of photo-induced electron transfer between conducting polymers which act as electron donors and fullerene derivatives which act as electron acceptors enabled a new promising method towards higher power conversion efficiency.[7]

1.2. Development of organic photovoltaic devices

The first generation of organic photovoltaic cells was a single-component active layer. It is the simplest organic semiconductor device. The structure of the single layer device consists of an active layer, two conducting electrodes and a substrate. The active layer is sandwiched between the two electrodes. The two metal electrodes have different work functions.[8,9] In such devices, glass is used as a substrate and is usually coated with indium tin oxide (ITO) (figure 1.2). ITO electrodes are mostly used since they are conductive and transparent but they are expensive.[10] Due to the electrostatic binding of photoexcited electrons to the hole left in the valence band, photovoltaic devices that only have one semiconductor cannot work efficiently. Excitons are neutral hence are not affected by an electric field and are hardly split into electron-hole charges that reach the electrodes.[11] As a result, such cells have less than 0.1% energy conversion efficiency.[12] Adding another semiconductor that has a lower-energy conduction band can help solve this problem.[11]

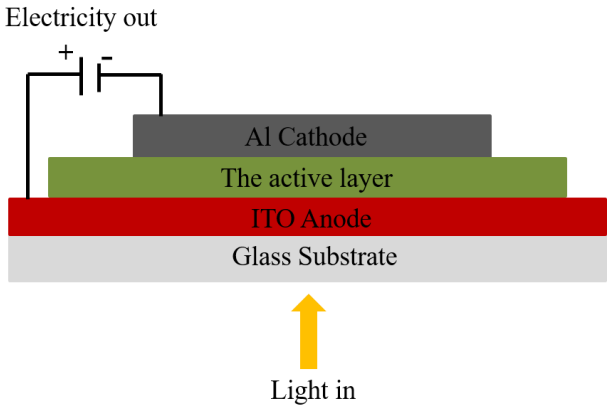

Figure 1.2. Structure of a single solar cell.

The next technological innovation that influenced the functioning of photovoltaic cells was the concept of the bilayer heterojunction (figure 1.3). Bilayer devices have a planar interface where the donor and acceptor materials are stacked on top of each other. The process of separating charges happens at the planar interface, which is facilitated by a huge potential drop between donor and acceptor. To make sure that the process of extracting charges is efficient, the bilayer is slotted between two electrodes that are compatible with the donor (HOMO) and the acceptor (LUMO).[13] In 1986, Tang tested two organic layers slotted in between a semi-transparent metal electrode and a transparent conducting oxide, where the p-type and n-type semiconductor used were phthalocyanine and perylene respectively, and reported an energy conversion efficiency of approximately 1%.[14] Since excitons have limited lifetimes, donor excitons can only diffuse across short distances ranging between 5 and 14 nm. As a result, donor excitons produced at distances further from the heterojunction interface decompose before charge separations resulting in the loss of quantum efficiency as well as absorbed photons. Consequently, the small area of charge-generating interface between the donor and acceptor significantly limits the performance of such devices.[8,10,13]

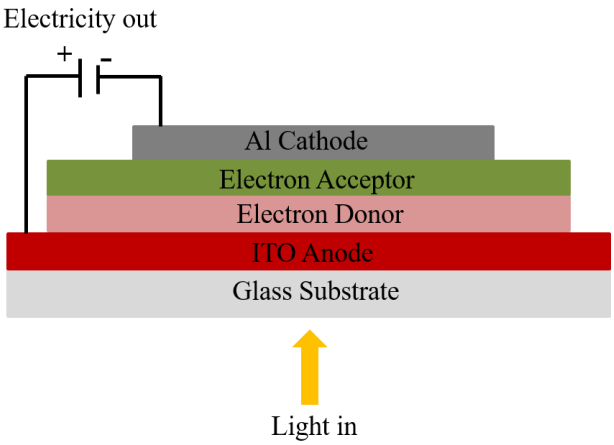

Figure 1.3. Structure of a bilayer solar cell.

To overcome this problem, Yu *et al.* discovered the bulkheterojunction (BHJ) concept, where the donor and acceptor materials are blended together (figure 1.4).[7] The basic component of a polymer solar cell (PSC) in a BHJ configuration is a blend of the conjugated polymers (p-type) and fullerene derivatives (n-type) semiconductors. There are two advantages of an interpenetrated BHJ network. Firstly, it reduces the traveling distance of excitons to get to the donor - acceptor interface and

simultaneously increases the D-A interfacial area, thus ensuring production of extensive free charge carriers because of the dissociation of the excitons at the D-A interface. Secondly, it provides pathways through which charges can be transported thus easing the process of collecting charges at the electrodes. As a result, the photon energy will be converted to electrical energy.[6,8,10]

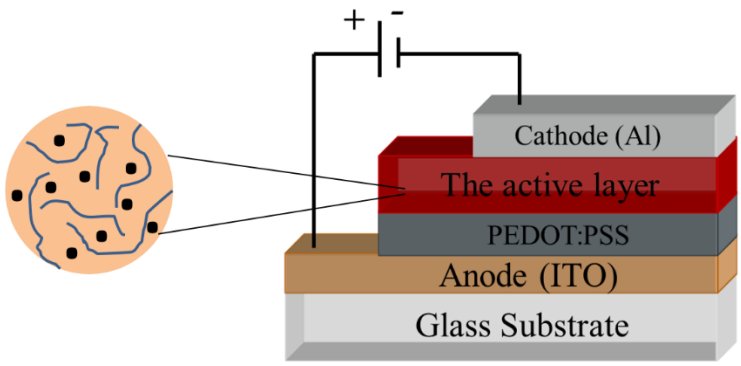

Figure 1.4. Structure of a BHJ photovoltaic device.

In the bulk heterojunction concept, the efficiency of solar cells was immensely improved due to an increase in the interfacial area between the D and A phases. Unlike bilayer heterojunctions, where the donor and acceptor phases are detached from one another and contact the cathode and anode, the donor and acceptor phases in BHJ are closely blended.[10]

The active layer, in an ideal BHJ is slotted between a metallic cathode and an anode made of a transparent material (ITO).[6] The transparent layer serves two purposes. Firstly, it serves as a transparent layer through which light can pass and secondly, it serves as an anode where photogenerated holes are collected.[15] In 2005, Jing *et al.* stated that the components of the anode may spread out into the active layer resulting in the degradation of the BHJ device as a result of the creation of the charge trap centres.[16] To avoid this issue, a protective layer (such as, poly 3,4-ethylenedioxythiophene) was inserted between the anode and the active layer.[15]

In the last 20 years, polymer solar cells have undergone numerous improvements in terms of PCE which rose from less than 1% to above 10%. This remarkable achievement can be attributed mainly to developments of conjugated polymers and fullerene derivatives as donor materials and electron acceptors, respectively. Owing to the restricted solubility of buckminsterfullerene (C60) in most organic solvents, the use of fullerenes derivatives was necessary.[6,17]

A solar cell should be designed in a manner that allows harvesting energy from the solar spectrum as much as possible particularly in the wavelength range between 400–900 nm.[15] It is, therefore, necessary to design polymers that absorb light throughout the visible spectrum in order to harvest high and low energy photons.

1.3. Operation principles of organic photovoltaic devices

The characteristics of organic and inorganic semiconducting materials are significantly different and hence their photovoltaic device configurations are different. Inorganic semiconductors have the ability to generate free positive and negative charge carriers upon light absorption due to their low exciton binding energies and high dielectric constants. The resultant positive and negative charges can simply be transported to the corresponding electrodes due to their high charge carriers mobility as well as to the internal field created by the p-n junction. In organic semiconducting materials, photogeneration of free positive and negative charge carriers cannot occur because they possess higher exciton binding energies and a lower dielectric constants when compared to their inorganic semiconductor counterparts.[2,4] Photoexcitation of the organic material leads to the formation of Frenkel exciton, a coulombically bound electron-hole pair.[4,10,18] To address this issue, buckminsterfullerene has been incorporated into the organic solar cells to act as an acceptor and hence photo-induced electron transfer is generated between the conducting polymers, as electron donors, and fullerene derivatives, as electron acceptors.[2,4,7] As a result, the photogeneration of free positive and negative charge carriers is boosted to occur in comparison with the pure conjugated polymers. Figure 1.5 shows the working principles involved in the conversion of sunlight into electric current in organic photovoltaic devices. Four steps must be followed consecutively. (a) Upon absorption of sunlight, (b) an electron from the conjugated polymer (the donor material) undergoes photoexcitation generating an exciton. The photoexcitation occurs from the highest occupied molecular orbital (HOMO) to the lowest unoccupied molecular orbital (LUMO). (c) The exciton produced is then diffused to the donor-acceptor interface within the diffusion length to avoid decomposition and, hence, recombination. (d) After that, the dissociation of the exciton occurs and leads to the formation of fully separated negative and positive charges. (e) Finally, charges are then driven to their respective electrodes, holes to the anode and electrons to the cathode electrodes, to provide a direct current leading to the generation of photocurrent and photovoltage.[13,18] The acceptor materials (the fullerene derivatives) can also undergo a similar

conversion mechanism when they are subject to photoexcitation.[2] However, fullerenes have generally low absorption coefficients and hence most of the light is absorbed by the conjugated polymers in these devices.

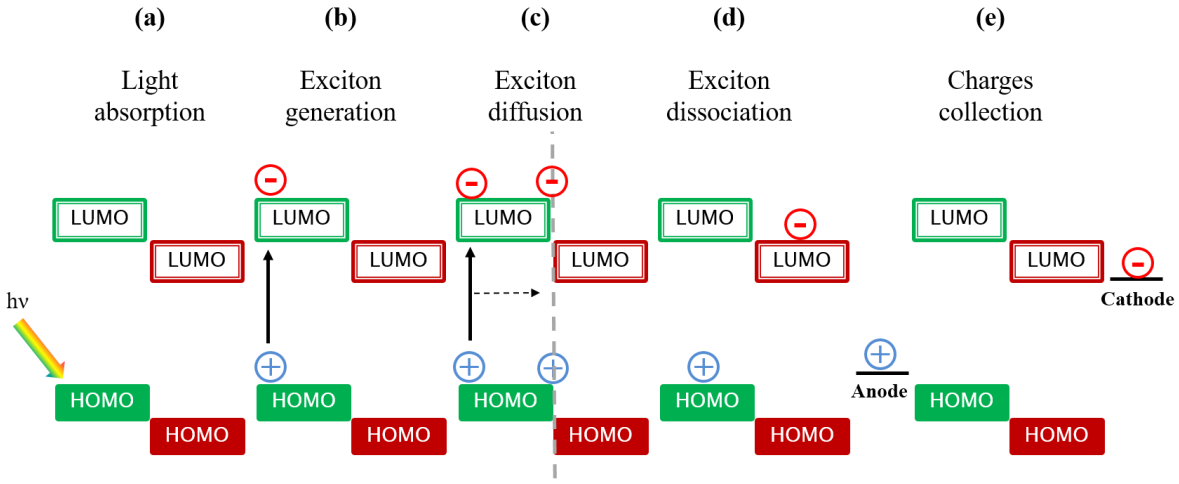

Figure 1.5. Working principle of solar cells.

1.4. Improving the photovoltaic device efficiency

To achieve high power conversion efficiency in BHJ devices based on conjugated polymers, the critical parameters, Open-circuit voltage (V_{oc}), Short-Circuit Current (J_{sc}) and Fill factor (FF), have to be addressed carefully.[6,19,20] The current density-voltage (J-V) curves of an illuminated organic solar cell is shown in figure 1.6. The formula used to calculate the PCE (η) in solar cells is shown below. P_{in} is the power of incident light.

$$\eta = \frac{V_{oc} \times J_{sc} \times \mathrm{FF}}{P_{in}}$$

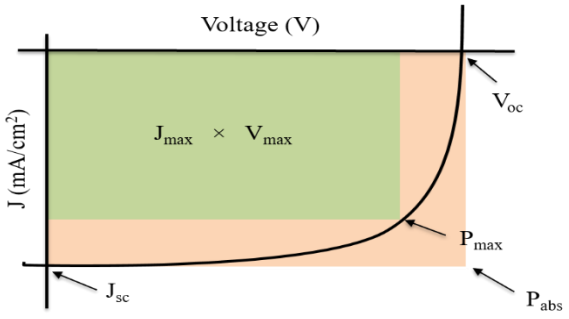

Figure 1.6. The current density-voltage (J-V) curve of an organic photovoltaic device. P_{abs} is the absolute power point and P_{max} is the max power point.

The different crucial parameters that are involved in the operation of solar cells are discussed below.

1.4.1. Open-circuit voltage (V_{oc})

V_{oc} is generally proportional to the difference between the LUMO energy level of the acceptor material (fullerene derivatives, e.g., $PC_{61}BM$) and the HOMO energy level of the donor material. Theoretically, when the HOMO levels of the donor polymers are low-lying the V_{oc} will be higher. The LUMO levels of the donor polymers have also to be considered. They are required to be closer to vacuum level than the LUMO levels of the fullerenes by at least 0.3 eV in order to have efficient excitons separation and, hence, charge dissociation.[6,19]

1.4.2. Short-Circuit Current (J_{sc})

The amount of excitons generated within the period of solar illumination decides the magnitude of short-circuit current in excitonic solar cells. To increase the generation of excitons, absorption of the active layer needs to be matched as much as possible with the solar spectrum. The donor materials work as the main sunlight absorber, as the acceptor materials (fullerene derivatives) have a weak absorption in the solar flux where the visible and near-IR region is positioned. Approximately 70% of the photons energy is found in wavelength regions ranging from 380 to 900 nm. Consequently, an ideal polymer is supposed to have a band gap of between 1.4 and 1.5 eV so as to have maximum solar absorption levels. Polymers with narrow band gaps can absorb more light thus leading into an increase of J_{sc}. Reducing the band gap more leads to the need to raise the HOMO energy level of the donor material which results in the reduction of the V_{oc}.[6,19]

1.4.3. Fill factor (FF)

FF investigates how rectangular the current density-voltage curve is, and it gives an idea about the possibility of extracting photogenerated carriers from a photovoltaic device. Actually, it is impossible for the FF to reach 100%. The highest FF stated for inorganic solar cells, which PCEs that are far larger than OSCs, is approximately 90%. Whereas in organic solar cells, the FF ranges between 50 to 70%.[21]

To maximize the FF, the morphology of the active layer is required to be optimised, as it strongly influences the physical interaction between the conjugated polymer (the donor) and the fullerene (the acceptor). As a result, charge dissociation and, hence, transportation of photogenerated charges is facilitated.[6,19] The formula used to calculate the FF in solar cells is:[21]

$$\mathrm{FF} = \frac{P_{max}}{V_{oc} \times J_{sc}}$$

To summarize, the properties required for an ideal polymer to achieve high performance when used with fullerene derivatives include: a HOMO level of approximately −5.4 eV, a LUMO level of approximately −3.9 eV, a band gap of 1.5 eV, high molecular weight, excellent solubility, optimal morphology in blends with fullerenes, high holes mobility and long-standing stability.[6,19]

1.5. Conjugated polymers (p-type materials)

In the mid-1970s, polymers with an extended π-bond system, known as conjugated polymers, gained research attention. The semiconducting properties of conjugated polymers are derived from their structure of alternating single and double bonds along their backbones. Mobile charge carriers are supported by the delocalized valence and conduction wave functions that are made from the bonding (π) and anti-bonding (π*) orbitals.[22] Prior to that date, interest in polyconjugated systems was very rare. Polyacetylene (PA), the first and simplest conjugated polymer, was presented in 1977 by Heeger, MacDiarmid and Shirakawa.[23] They showed that reaction of PA with bromine or iodine vapours can render PA conductive.[24] In 2000, the Nobel Prize was given to Heeger, MacDiarmid and Shirakawa as a result of their pioneering work in the area. Researchers became more interested in the area of the physics and chemistry of polyconjugated system both in their doped (charged) and undoped (neutral) states.[24,25]

Due to the electron delocalization in continuously overlapping bonding (π) and anti-bonding (π*) orbitals along the polymer chain, a large number of conjugated polymers have interesting electrical and optical properties. These unfamiliar properties in organic materials made polyconjugated systems available for use in many applications such as field effect transistors (FET), organic photovoltaic devices (OPVs) and light emitting diodes (LEDs). However, most of the unfunctionalized conjugated polymers are difficult to process because of their insolubility.[26] In addition, the significant overlap of delocalized π-electrons along the backbone of conjugated polymers is not enough to provide good electrical conductivity. Therefore, reduction and oxidation reactions are required to dope the conjugated polymers. For instance, in the case of oxidation, some of these polymers become good conducting materials. Therefore, conjugated polymers are considered as ionomeric in their conductive states.[27]

Polyacetylene would exhibit a metallic conductive state if the bond lengths of the carbon – carbon were equal.[28] Basically, the carbon – carbon bonds in PA are not equal, they alternate between long and short bonds because of the Peierls distortion. These non-equivalent bonds influence the electronic properties of PA as a band gap is opened between the fully occupied π -band (valence band (VB)) and the empty π*–band (conduction band (CB)).[24]

Electrons need to possess a given energy to occupy a certain band, and also need a higher energy to be promoted from the VB to the CB. Empty bands and full cannot transport electricity; therefore, partially filled bands are needed. Owing to this fact, metals have high conductivities. In terms of insulators, the energy bands are either completely empty or completely full. The valence band of most common saturated polymers is full whereas the conduction band is empty and the energy gap between them is wide. On the other hand, the band gap in conjugated polymers is narrow and the doping process can be performed by removing an electron from the VB or adding an electron to the CB (figure 1.7).[26]

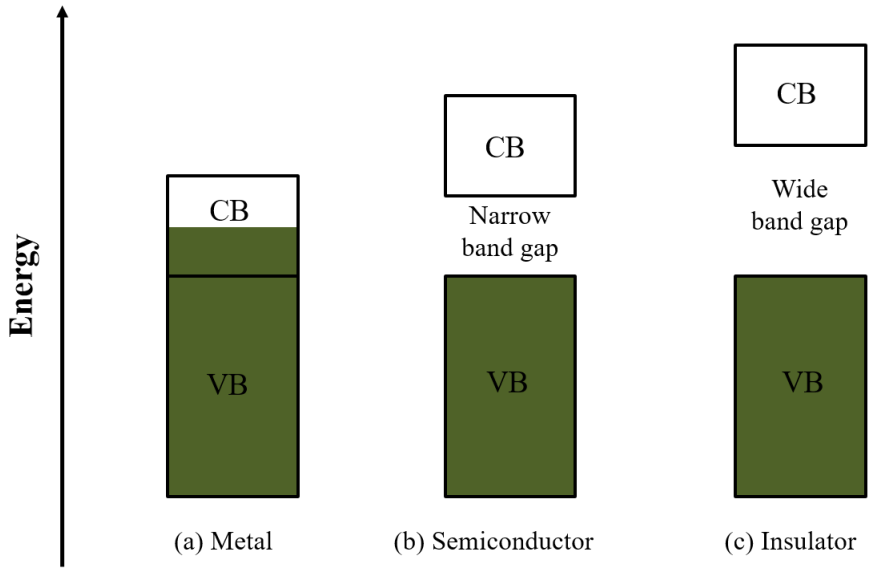

Figure 1.7. A schematic diagram of band gaps in metals, semiconductors and insulators.

Owing to the inability of conjugated polymers to possess intrinsic charge carriers, a doping process is required. There are two types of doping, p-type doping and n-type doping. In p-type doping (oxidative doping) the polymer chain is oxidized by removing an electron using electron acceptors

such as I_2, Br_2 or $FeCl_3$. In n-type doping (reductive doping) the polymer chain is reduced by adding an electron using electron donors such as Na, K, Li, Ca.[25,29]

Doping is not restricted to linear conjugated polymers, it can also be used in polyheterocyclic polymers such as poly(furan), poly(thiophene), poly(pyrrole) and their derivatives by either p-type or n-type doping. For example, removing an electron from a poly(thiophene) will create a radical cation known as a positive polaron. Further oxidation would remove another electron from the poly(thiophene) chain leading to the formation of a positive bipolaron (figure 1.8.a). The same process can be applied to the n-type (reductive) doping to give a negative polaron and a negative bipolaron (Figure 1.8.b).[24]

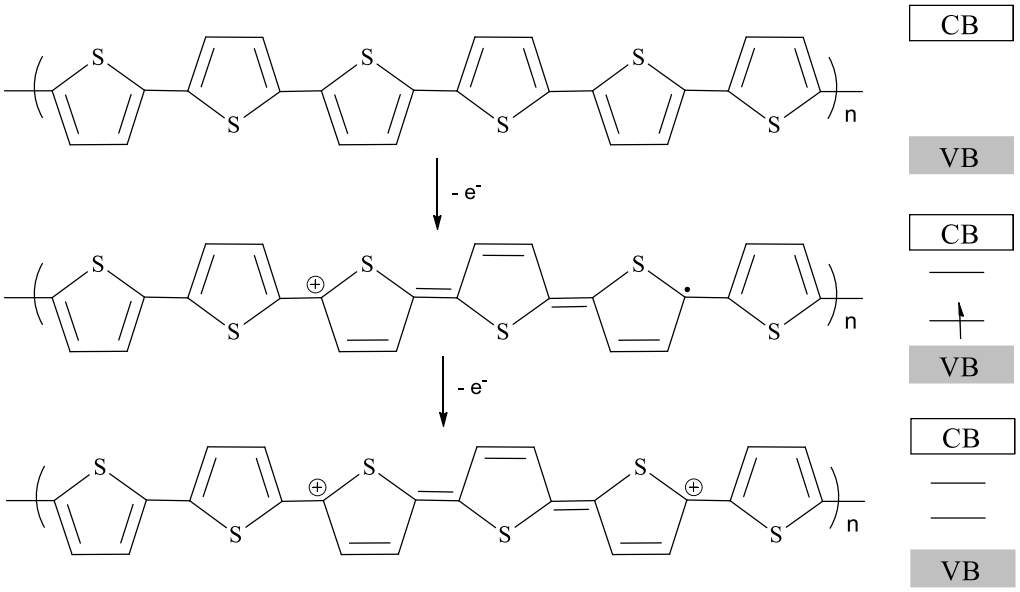

Figure 1.8.a. p-type doping of poly(thiophene) with energy level diagrams.

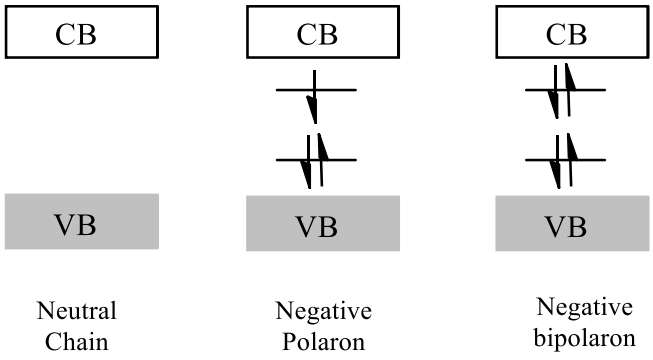

Figure 1.8.b. Energy level diagrams of n-type doping.

1.6. Strategies for Band Gap Engineering

The band gap energy (E_g) is an important element for determining the conducting and electronic properties of conjugated polymers. The band gap is defined as the difference in energy between the highest occupied molecular orbital (HOMO) and the lowest unoccupied molecular orbital (LUMO).[30] In metallic conductors there is no band gap, leading to intrinsic conduction.[31] Structural modification of the polymer backbone can alter the position of the HOMO and LUMO levels, thus, the size of the band gap can be controlled using this knowledge. The gap energy of conjugated polymers is between 1.2 eV to 4 eV, which is the same as inorganic semiconductors. This corresponds to the energy for light harvesting between the near infrared and the visible light regions of the solar spectrum.[32]

Figure 1.9 shows that as the number of monomer units increases, the energy gap between the HOMO and LUMO levels decreases. This results in increased conductivity. The band gap cannot reach zero and behave as a conductor owing to Peierls distortions.[30] Suitable functionalization of conjugated polymers can also vary the value of the optical band gap. Incorporation of an electron-donating group such as alkoxyls, alkyls, thioalkyls and amines would elevate the HOMO energy level. Whereas, attaching electron-withdrawing groups such as fluorine, ketone, alkyne or nitro groups can decrease the LUMO energy level. As a result, the band gap is decreased.[8,24,30] Pei, Qibing, *et al.* reported that poly(3,4-ethylenedioxythiophene) exhibited a low band-gap (1.5 eV), 0.5 eV lower compared to polythiophene which is attributed to the incorporation of electron donating alkoxy groups.[33]

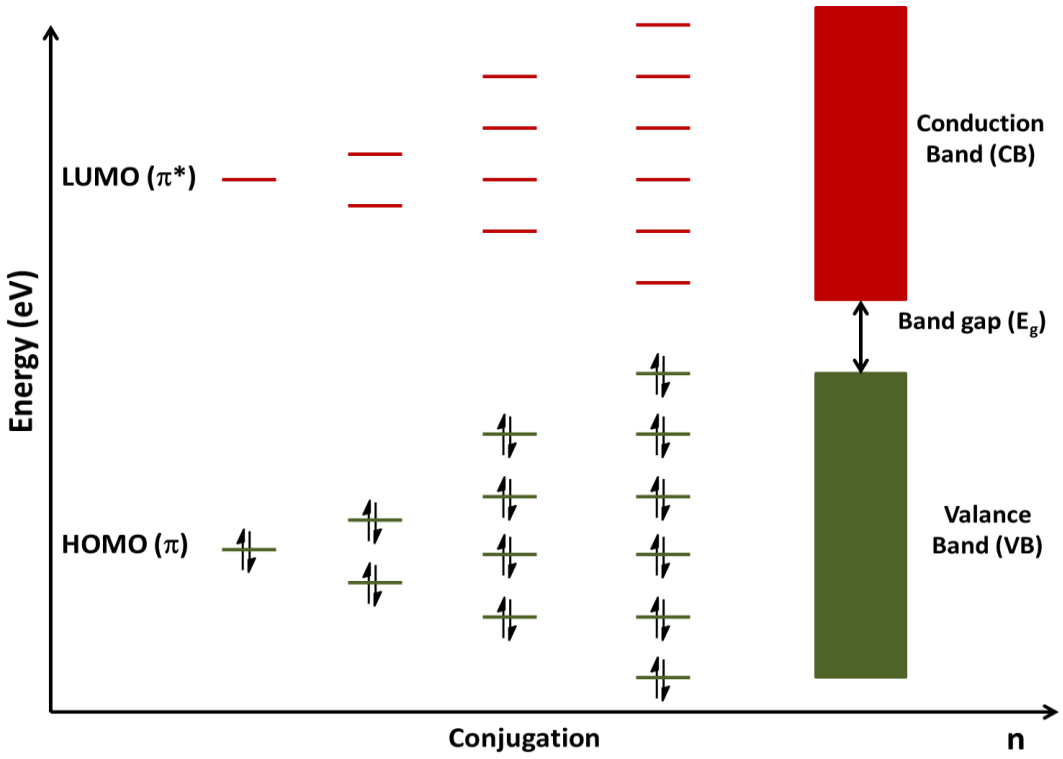

Figure 1.9. A diagram shows the decreasing in the E_g with increasing conjugated monomers.

One of the key elements in reducing the band gap (E_g) is to synthesize copolymers via alternation of electron rich monomers (donors) with electron deficient monomers (acceptors). The bond length alternation can be reduced via the use of this push-pull approach which enhances the electron delocalization. As a result, a quinoid mesomeric structure (D-A → D^+=A^-) is formed along the conjugated polymer chains leading to a reduced band gap. Intramolecular charge transfer (ICT) between the D-A units results in the formation of more double bonds along the repeating units. Consequently, a more coplanar structure is adopted leading to a low band gap. In this unique approach, the HOMO levels of the donor and the acceptor units interact with each other to form two new HOMO levels. Similarly, the LUMO levels of the donor and the acceptor units interact with each other to form two new LUMO levels. This hybridization results in a higher lying HOMO level and a deeper lying LUMO level which leads to a reduced band gap (figure 1.10).[3,6,8]

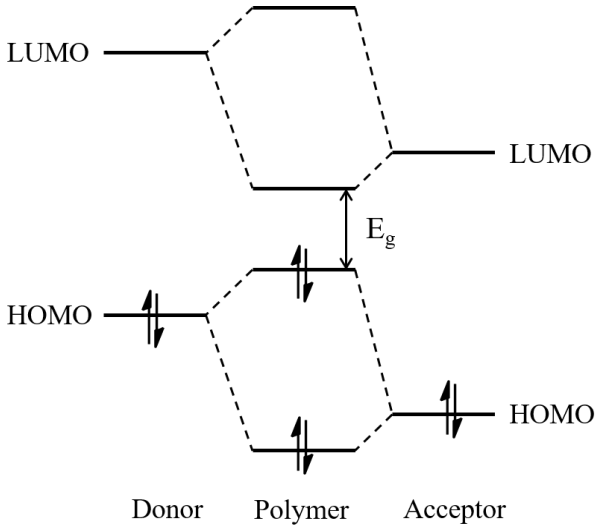

Figure 1.10. Orbital hybridization of electron donor units and electron acceptor units resulting in a narrower energy band gap in donor-acceptor conjugated polymers.

Some examples of the structures of donors and acceptors are presented in figure 1.11. Another approach that has been also adopted to reduce the band gap is the incorporation of heterocyclic compounds or heteroatoms into the monomer backbone.[3,6,8]

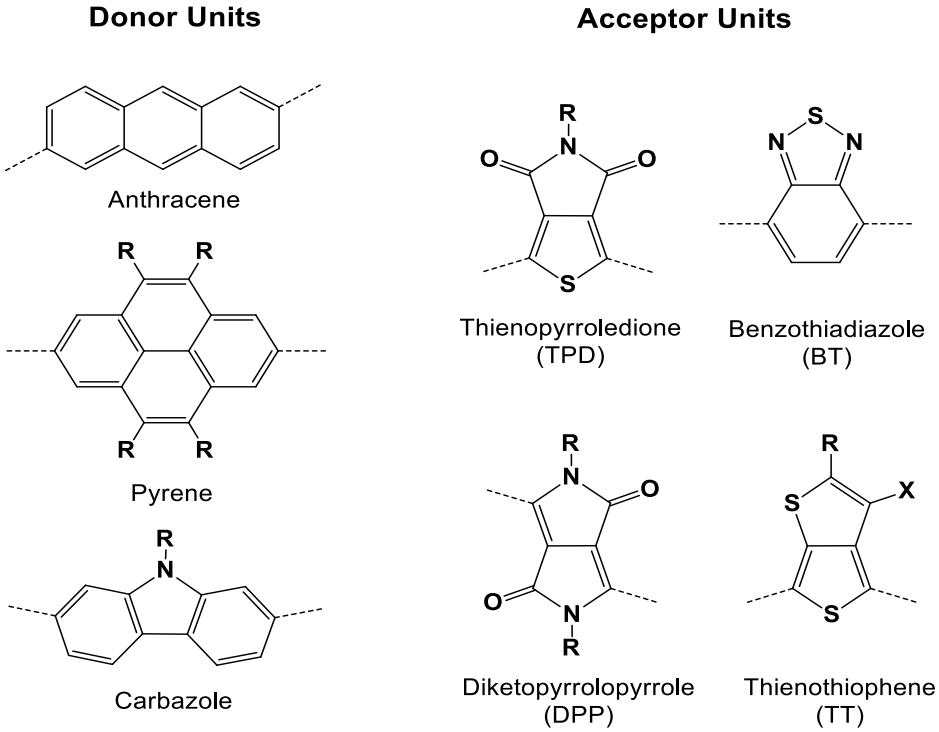

Figure 1.11. Structures of common donor and acceptor units employed in D-A conjugated polymers.

1.7. Solubility

It is very disappointing when a new conjugated polymer is found to be insoluble in common organic solvents such as chloroform and chlorobenzene, as this impedes the use of polymers in devices on processing from solution. Some structural factors govern the degree of solubility of a given conjugated polymer such as backbone rigidity, the degree of polymerization, the length of the aliphatic side chain substituents and also polarity. Improving the solubility of conjugated polymers can be achieved by the introduction of aliphatic side chains. The physical properties of conjugated polymers such as morphology, crystallinity, phase behaviour and interaction with different active components were found to be largely affected by the solubility matter, which eventually define the photovoltaic devices performance. Side chains have a crucial role in defining the interchain interactions at the interfacial area among the conjugated polymer chains. Generally, long alkyl chains will reduce the π−π stacking and hence increase the solubility and processability of the polymers. Actually, the reduction of the π−π stacking can detrimentally affect the device properties, therefore a balance needs to be taken into account. It is worth mentioning that attaching large sized insulating alkyl chains deteriorate the charge carrier mobility function as a consequence of decreasing the amount of hole conductors. The structure of the alkyl chains need to be chosen very carefully. For example, a large and branched alkyl chain will cause large steric hindrance, which would result in disturbing the conjugated backbone. The efficiency of branched alkyl chains for improving solubility is much higher when compared to the analogous linear alkyl chains.[3,8]

1.8. Synthesis of donor-acceptor Polymers

Conjugated polymers can be prepared by different routes such as condensation polymerisation, oxidative preparative and palladium-catalysed cross-coupling. The latter approach is the most extensively used. Different coupling reactions have been reported using the latter technique, however, Suzuki, Stille couplings and more recently direct arylation are the most commonly used and they will be discussed more in detail in the following section. In 2010, the Nobel Prize was given to Heck, Negishi and Suzuki owing to their development in these cross-coupling reactions.[34]

1.8.1. Stille type Cross-coupling

In Stille reactions, functional monomers containing halo- and/or organotin- functionalities are coupled together in the presence of a transition metal and palladium compounds such as tetrakis(triphenylphosphine)palladium ($Pd(PPh_3)_4$) and palladium acetate ($Pd(OAc)_2$). This

method has been widely used owing to its tolerance to different functional groups (such as esters, amines, alcohols and ethers) and its stability to air and humidity. The drawback of using the organotin reagents is the toxicity which in turns limits this method. The Stille reaction usually produces conjugated polymers in high yields.[35,36]

The mechanism of Stille reactions is shown in figure 1.12. Firstly, the palladium catalyst ($Pd(0)L_2$) undergoes oxidative addition when it reacts with an aryl halide to form an organopalladium (II) complex. Then aryltin undergoes a transmetalation process to make a biarylated palladium moiety. Thirdly, the formed biarylated palladium undergoes trans/cis isomerisation. Lastly, a biaryl product (R-R') is produced by reductive elimination and the palladium (0) species is regenerated to close the catalytic cycle.[35,36]

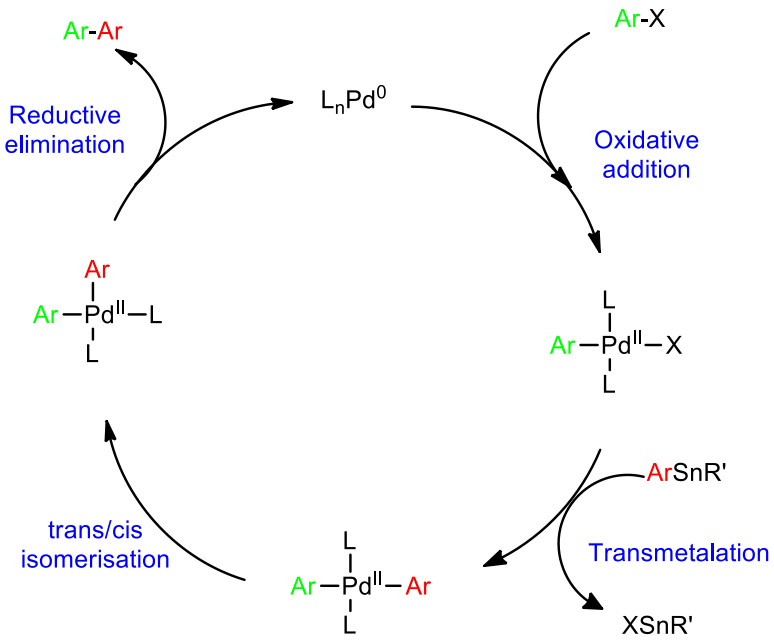

Figure 1.12. Stille cross-coupling mechanism.

1.8.2. Suzuki type cross-coupling

Suzuki coupling reactions features a palladium catalysed cross-coupling between aryl halides with aryl boronic ester/acid derivatives. This method is the most widely used as it involves boronic derivatives in its backbone which offers several advantages such as: tolerance to different functional groups (similar to Stille reactions), ease of handling and finally the reagents used have lower toxicity when compared to organotin compounds. The mechanism of this reaction is shown

in figure 1.13. It is mainly similar to Stille coupling including oxidative addition, transmetalation and reductive elimination sequences. The oxidative addition is considered to be the rate-determining step in the catalytic cycle. The existence of a mineral base is often required for the success of Suzuki reactions.[35,37]

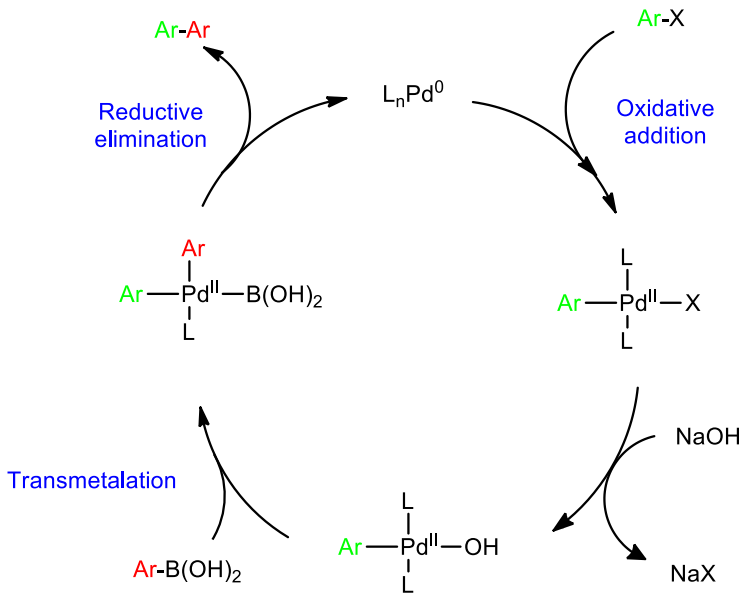

Figure 1.13. Suzuki cross-coupling mechanism.

1.9. Application of conjugated polymers in photovoltaic devices

A huge number of π-conjugated polymers have been synthesized and applied as donor semiconductors in organic photovoltaic devices, either as homopolymers or D-A copolymers. Dialkoxy-substituted poly(*para*-phenylene vinylene)s (**PPV**) and regioregular poly(3-hexylthiophene) (**P3HT**) as homopolymers have been studied most extensively in OPV devices (figure 1.14). Both polymers have a high absorption in the visible region.[38,39] Different strategies have been taken into account to optimize and enhance organic photovoltaic devices based on **PPV** and **P3HT** including film making conditions, thermal annealing of the active layer, electrodes interfacial layers, optical spacer, mixing solvents, additives and employing different organic solar cell architectures.[38] Padinger *et al.* was the first to report a PCE of 3.5% on regioregular **P3HT:PC61BM** at elevated temperature.[40] After this report, intensive research from many groups focusing on processing of the active layer and on optimizing the chemical properties of regioregular **P3HT** have been published, boosting the efficiency to around 5%.[39]

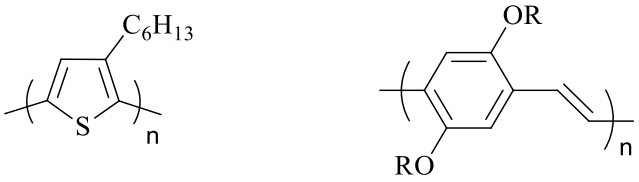

P3HT **PPV**

Figure 1.14. Molecular structures of **P3HT** and **PPV**.

Studies on **PPV** and **P3HT** polymers have facilitated understanding how BHJ photovoltaic devices work and what criteria are needed to improve the stability and efficiency as well as leading researchers to design new classes of conjugated polymers. Recently, different π-conjugated polymers comprising alternating donor and acceptor units have been synthesized and used as promising donor materials in BHJ photovoltaic devices. Fluorene, carbazole, cyclopentadithiophene and dithiophene are examples of the donating repeat units used, while diketo-pyrrolo-pyrrole (**DPP**), benzothiadiazole (**BT**), thieno[3,4-c]pyrrole-4,6-dione (**TPD**) and quinoxaline are examples of the electron acceptors.[38] The advantages of combining donor and acceptor units along polymer chains have been already covered in this chapter. Recently, Guo *et al.* reported the synthesis of a series of polymers using benzodithiophene (**BDT**) as the electron rich units and diketopyrrolopyrroles (**DPP**) as the electron deficient units. **PBDTT-TTDPP** exhibited a high PCE of 4.74 % with a high V_{oc} of 0.88 V, a J_{sc} of 10.63 mA cm^{-2} and a FF of 51.0 %.[41] Stuart *et al.* synthesized three corresponding copolymers **PBnDT-DTBT**, **PBnDT-DTfBT** and **PBnDT-DTffBT**, but with different number of fluorine atoms on the **BT** unit (figure 1.15).[42] All polymers were blended with $PC_{61}BM$ in a weight ratio of 1:1. The polymer with two fluorine atoms, **PBnDT-DTffBT**, displayed the highest efficiency (7.16 %) in the three polymers with the highest values of V_{oc} (0.90) V, FF (62.1 %) and J_{sc} (12.2 mA/cm^2).[42]

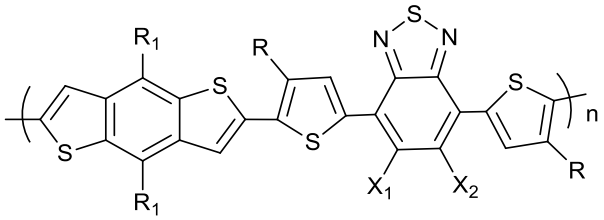

X_1= H, X_2= H: **PBnDT-DTBT**

X_1= H, X_2= F: **PBnDT-DTfBT**

X_1= F, X_2= F: **PBnDT-DTffBT**

Figure 1.15. Molecular structures of **PBnDT-DTBT**, **PBnDT-DTfBT** and **PBnDT-DTffBT**.

Another example of a donor-acceptor polymer was reported by Lee *et al*. The polymer is based on carbazole as the donor and quinoxaline as the acceptor moiety. The photovoltaic performance of the polymer was investigated using BHJ solar cells. Poly[*N*-9''-heptadecanyl-2,7-carbazole-*alt*-5,5-(5',8'-di-2-thienyl-2,3-bis(4-octyloxyl)phenyl)quinoxaline (figure 1.16) was blended with $PC_{71}BM$ yielding a good performance with a V_{oc} of 0.82 V, FF of 0.49, J_{sc} of 9.96 mA/cm^2 and a PCE of 4.0 %.[43] The researchers ascribed this good performance to the small-sized polymer:$PC_{71}BM$ domains in blends which could result in a high bicontinuous interpenetrating network.[43]

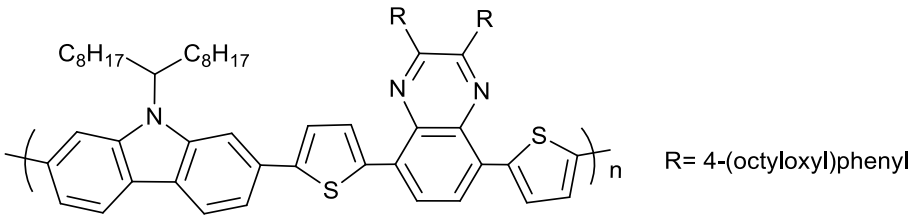

Figure 1.16. Molecular structure of poly[*N*-9''-heptadecanyl-2,7-carbazole-*alt*-5,5-(5',8'-di-2-thienyl-2,3-bis(4-octyloxyl)phenyl)quinoxaline.

1.10. Materials used in organic solar cells

1.10.1. Pyrene-based conjugated polymers

The pyrene moiety, a member of polycyclic aromatic hydrocarbons (PAHs), has been scarcely explored in OPV materials when compared to other PAHs such as phenanthrene, anthracene and naphthalene, however, pyrene has unique electronic and photophysical properties. Pyrene was discovered in 1837 by French chemist Laurent via the distillation of coal tar. In 1871 Gräbe determined the chemical formula of pyrene where in 1887 its structure was figured out by Bamberger and Philip.[44] Since that time pyrene has appeared to be an attractive material for the fabrication of new organic semiconductors in various fields. It has also been a promising building block for organic solar cells due to its ability to extend the π-conjugated systems.[44,45] Few literature sources reported the use of the pyrene moiety as an electron donor in organic photovoltaic devices; due to the difficulty of functionalizing the pyrene unit.[46] Although the chemical structure of pyrene is well-known, there are significant difficulties regarding purification of its derivatives.

The structure of pyrene can be split into four parts as it possesses three mirror planes leading to the existence of three different positions (figure 1.17 (a)). Each position shows a significant difference in terms of the chemical reactivity. The majority of pyrene derivatives reported in the literature concern pyrene with substitution at "1,3,6,8", "2,7" or "4,5,9,10" positions (figure 1.17 (b)). The latter one is known as the K-region.[45,46]

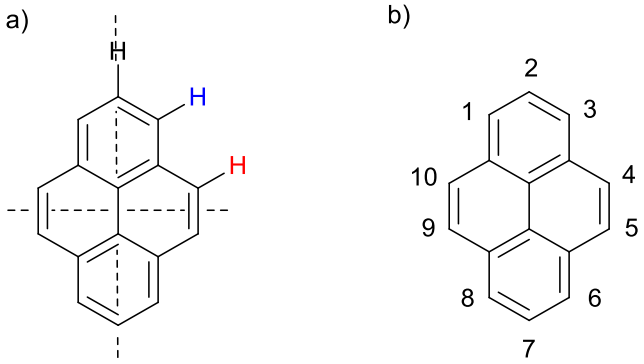

Figure 1.17. (a) Three mirror planes displaying three different chemically positions, (b) Pyrene with positions numbered.

The 1,3,6,8-positions have the most electron density resulting in their high reactivity towards electrophilic aromatic substitution, because the orbital coefficients of the four carbon are large.[47,48] Mono-substituted pyrene is the most commonly synthesised.[47] Ogino first reported the synthesis of 1,3,6,8-tetracyanated and -halogenated pyrenes.[49] In 1937, Vollmann *et al.* described the synthesis of mono-, di-, tri- and tetra-bromopyrene using bromine. 1,3,6,8-Tetrabromopyrene was synthesised using nitrobenzene as a solvent at high temperature (160 °C). The product was obtained in 90% yield and was produced in gram scales. The ease of preparation of 1,3,6,8-tetrabromopyrene created new routes for introducing various building blocks via Stille, Sonogashira or Suzuki coupling reactions (figure 1.18).[44,47,50]

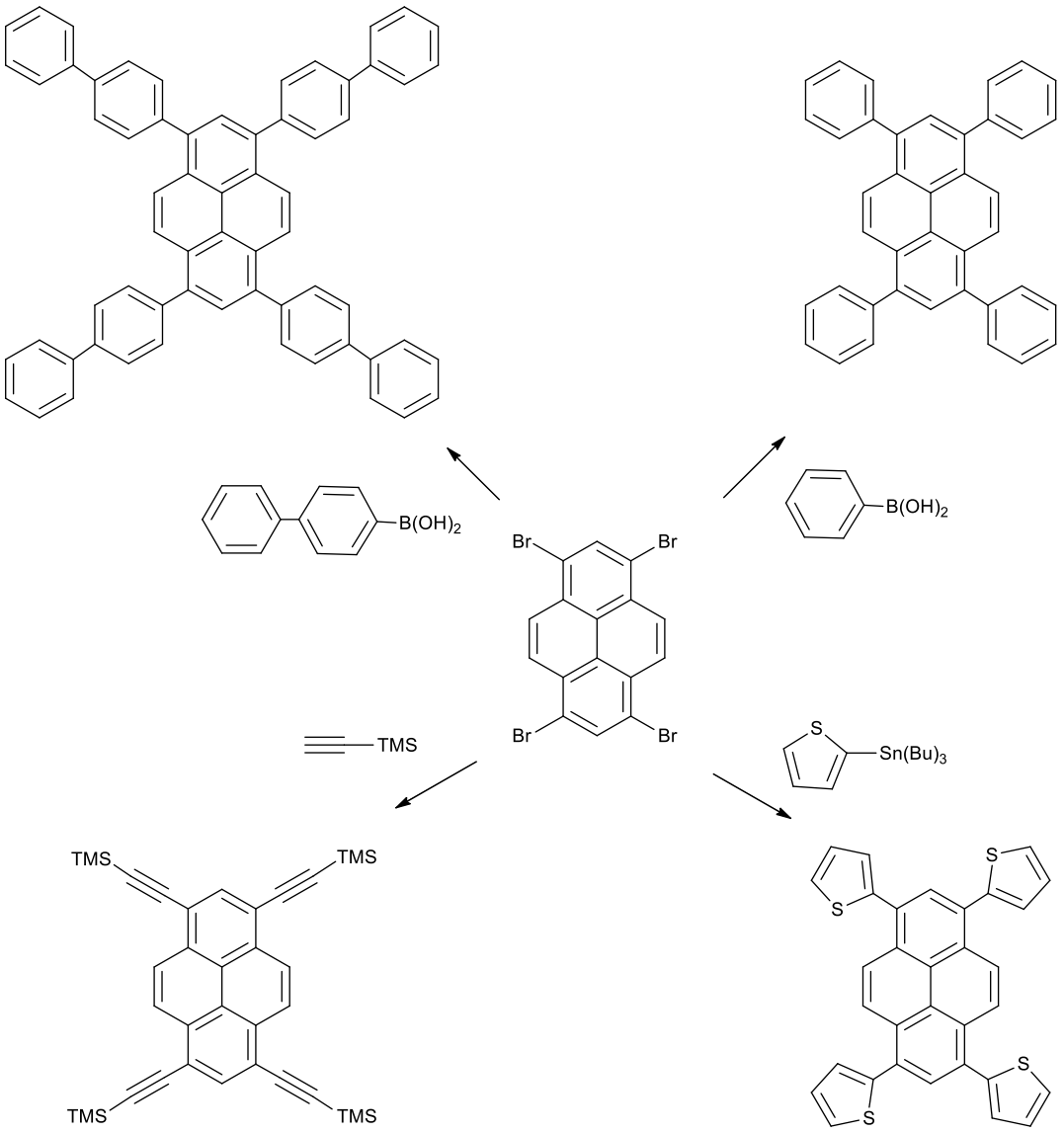

Figure 1.18. Synthesis of tetrasubstituted pyrenes using Stille, Sonogashira or Suzuki coupling.

Functionalization of the 2,7-positions of pyrene is a big challenge as there is no straight forward access by electrophilic aromatic substitution. In fact, the 2- and 7-positions exhibit lower reactivity towards electrophilic substitution compared to 1,3,6,8-positions.[44,47] There are only two examples that have been reported up to now where 2- and 7-positions reacted selectively in one step employing a bulky electrophile. The first one was published in 1993 by Yamato *et al.* who synthesised 2- and 2,7-di-*tert*butyl pyrene using *tert*-butyl chloride in the presence of Lewis acid aluminum chloride ($AlCl_3$) (figure 1.19 (a)).[51] The second breakthrough was reported in 2005 by Coventry *et al.* who used a bulky iridium-based catalyst with bis(pinacolato)diboron to synthesis

2- and 2,7- borylated pyrenes in a high yield (figure 1.19 (b)). The sterically bulky nature of the intermediate complex [Ir(bpy)(Bpin)$_3$] is believed to be the main factor in activation of C-H bonds at the 2,7-positions of pyrene.[52] Since the publication of Coventry *et al.*, borylated pyrenes have been employed as a starting material to synthesize new derivatives and also to introduce various building blocks via Stille, Sonogashira or Suzuki coupling reactions.

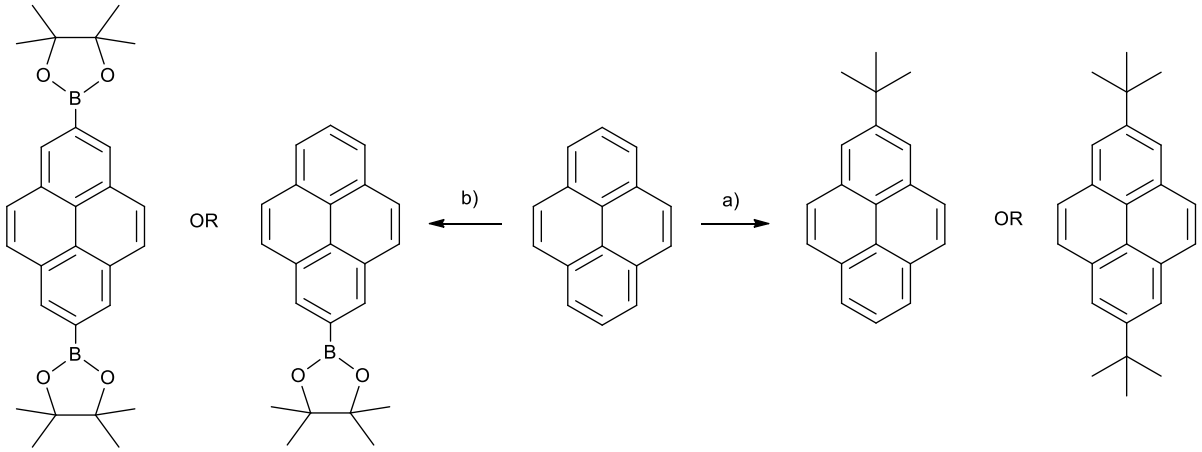

Figure 1.19. 2,7-Functionalization of pyrene via (a) Friedel-Craft alkylation or (b) borylation using iridium-based catalyst.

An indirect approach was proposed to facilitate access to the 2,7-positions of pyrene by electrophilic aromatic substitution via reduction of the 4,5,9,10-positions of pyrene using H_2/Pd/C to produce 4,5,9,10-tetrahydropyrene followed by electrophilic substitution and finally re-aromatization (figure 1.20).[44,47,53] The utility of this approach was first reported in 1964 by Bolton who synthesised a 2-substituted pyrene such as 2-benzoyl-, 2-nitro- and 2-acetylpyrene in two steps and in a good yield.[54] These compounds have been used as starting materials for different subsequent pyrene derivatives. 2,7-Disubstitution of 4,5,9,10-tetrahydropyrene is an issue, therefore some conditions should be modified to avoid it.[47] Disubstitution is usually the main product even if one equivalent of a reagent was used, producing a mixture that is difficult to purify. Harvey *et al.* described that choosing the appropriate solvent with the required amount of the reagent, as well as temperature play an important role in controlling the reaction.[55] For example, carbon disulfide produces monoacetylation whereas DCM leads to diacetylation.[47,55]

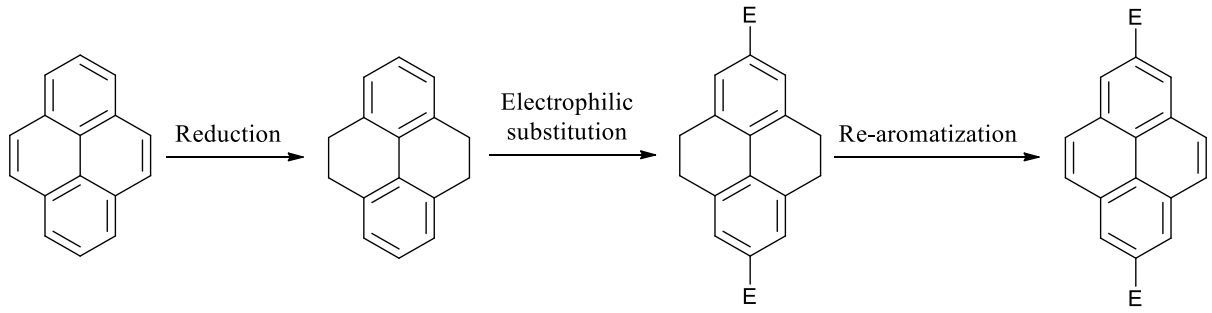

Figure 1.20. Functionalization of 2,7-positiones of pyrene via reduction of the K-region.

The 4,5,9,10-positions (or the K-region) of pyrene moiety have been most investigated owing to its capability in extending the π-conjugated systems via introducing different kind of building blocks. Similar to 2,7-positions, these four positions have no straight access to be functionalised.[44] A number of strategies have been carried out to synthesize 4,5-di- and 4,5,9,10-tetraketopyrene.

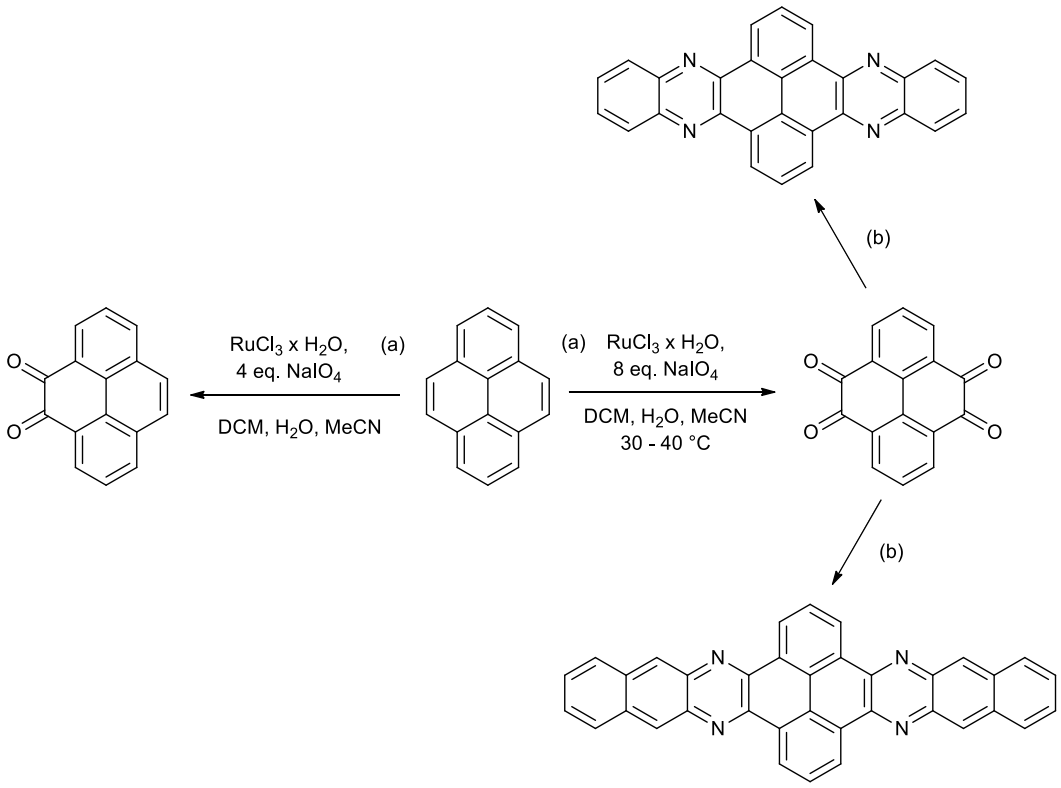

Figure 1.21. (a) Oxidation of 4,5- or 4,5,9,10-positiones of pyrene and (b) extending the conjugated system.

In 2005, Jie Hu *et al.* reported the most promising way for preparation of the di- and tetraketopyrene in one step using ruthenium chloride and sodium periodate in DCM, water and CH_3CN. It was found that pyrene-4,5-dione and pyrene-4,5,9,10-tetraone can be selectively obtained by varying the amount of the catalyst used as well as the reaction temperature (figure 1.21 (a)).[56] This strategy created several routes to increase the aromatic system of the pyrene through the means of cyclocondensation by using, for example, 1,2-phenylenediamine and 2,3-diaminonaphthalene (figure 1.21 (b)).[57,58,59]

The second approach to reach these four positions is via indirect method by adding two *tert*-butyl group at the 2,7-positions to produce 2,7-di-*tert*butyl pyrene which in turns would block the most electron rich 1,3,6,8-positions and activate the 4,5,9,10-positions towards electrophilic aromatic substitution.[44,47] In 1997, Yamato *et al.* reported the synthesis of 4,5,9,10-tetrabromo-2,7-di-tert-butylpyrene in a high yield (90%) via adding 6.0 mol. equivalent of Br_2 as well as iron powder to 2,7-di-*tert*butylpyrene (figure 1.22).[48]

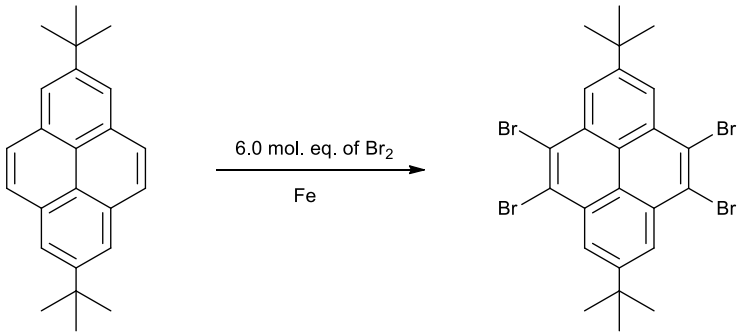

Figure 1.22. Bromination of 4,5,9,10-positions of pyrene.

1.10.2. Fullerenes (n-type materials)

In recent years, intensive research has been done in organic photovoltaics focusing on the development of new conjugated polymers (the p-type materials). However, the fullerene derivatives (the n-type materials) are still the dominant acceptors used in BHJs up to date owing to their exceptional electron accepting and transporting properties.[8,60,61] The main disadvantage of fullerene derivatives is their poor absorption in the visible and near-IR region.[8] In 1995, Hummelen *et al.* provided the first report of using PCBM in organic photovoltaic device applications.[7] Buckminsterfullerene (C_{60}) (figure 1.23 (a)) showed restricted solubility in common organic solvents, and therefore, [6,6]- phenyl-C61-butyric acid methyl ester ($PC_{60}BM$) (figure 1.23 (b))

was produced with a solubilizing group.[6,60] $PC_{61}BM$ has several advantages alongside the good solubility such as high electron-affinity and –mobility; but it has a relatively low-lying LUMO level which in turns affects the J_{SC} of the photovoltaic device and also limit the needed energy level for the donor materials to achieve high V_{OC} value.[60] The photo-induced electron/hole transfer between the donor materials and fullerene derivatives happens quantitatively on a time scale of sub-picosecond. It was observed that the charge transfer process is thousand times quicker compared to radiative decay of photoexcitations.[6,7] Replacing $PC_{61}BM$ with $PC_{71}BM$, C70 derivatives, has proven to improve the efficiency as a result of having a lower symmetry compared to its C60 counterpart.[6,60] $PC_{71}BM$ has higher optical transitions leading to stronger absorption in the visible region and hence greater J_{SC} values. $PC_{71}BM$ has been commonly used with different types of low band gap conjugated polymers, and it exhibited improvement in devices performance.[60] Adjusting the LUMO level of the acceptor materials, fullerenes, relative to the donor materials LUMO levels is the biggest challenge; as this approach would result in decreasing the thermalization losses.[60,61] He *et al.* exploit this approach and reported the use of indene-C60 bis-adduct (ICBA), which has a higher LUMO level relative to $PC_{61}BM$. ICBA has several advantages relative to $PC_{61}BM$ and $PC_{71}BM$ such as solubility and ease of preparation.[62]

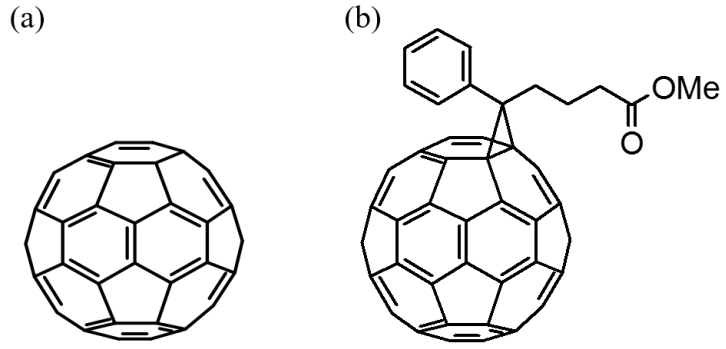

Figure 1.23. The structure of: (a) **C60** and (b) **$PC_{61}BM$**.

1.11. Project aims

Inorganic solar cells exhibit good power conversion efficiencies from 8 to 29%.[2,3] However, the high cost of these devices has impeded their widespread usage. Intensive research efforts are underway in order to find different approaches to explore less expensive materials to maintain a technology path for solar cells. Organic solar cells based on conjugated polymers have gained a large amount of attention from researchers and academics because of their potential characteristics when compared with inorganic solar cells.

The aim of this project is mainly to synthesize and develop donor-acceptor conjugated polymers with high performance for application in bulk heterojunction solar cells. The conjugated polymers will be synthesised via palladium catalysed cross-coupling reactions such as Stille or direct arylation. In this dissertation, the pyrene moiety will be used as the main electron donor in all donor-acceptor polymers owing to its unique properties as mentioned before.

Benzothiadiazole based donor-acceptor copolymers have gained a large amount of attention from the researchers and academicians community. High efficiencies have been reported for BHJ solar cells fabricated from benzothiadiazole based copolymers. Therefore, one of the objectives of the dissertation is to synthesise a series of alternating copolymers comprising pyrene as the electron donor unit and benzothiadiazole as the electron acceptor moiety and investigate their thermal, optical and electrochemical properties in the solid state. Also, their molecular organisation and photovoltaic properties in thin film will be investigated. The hydrogen atoms on the 5,6-positions of the benzothiadiazole unit will be replaced with fluorine atoms. Previous literature reported that introducing fluorine atoms to the benzothiadiazole moiety produces polymers with poor solubility and low molecular weight. To address this issue, different branched alkyl chains such as 2-ethylhexyl or 2-hexyldecyl will be attached to the 4,5,9,10-positions of the pyrene moiety in order first to enhance solubility and also to increase the molecular weight of the resultant polymers. The structures of the suggested polymers are presented in figure 1.24.

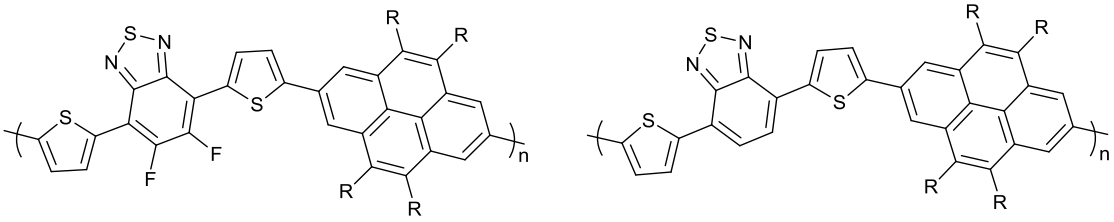

Figure 1.24. The chemical structures of the proposed pyrene-*alt*-benzothiadiazole polymers.

In order to explore more the potential of pyrene-*alt*-benzothiadiazole copolymers, octyloxy substituents will be attached at the 5,6-positions of benzothiadiazole to increase the solubility as well as to aid the formation of processable polymer materials with high molecular weight. Additionally, it is believed that increasing the conjugated length can noticeably enhance the absorption and electronic properties of the resultant polymers. Therefore, the backbone of the conjugated polymers will be extended by replacing thiophene spacers between pyrene and benzothiadiazole alternating units with bithiophene spacers. The thermal, optical and electrochemical properties of these substitution on the properties of the resulting polymers in the solid state will be analysed. Also, their molecular organisation and photovoltaic properties in thin film will be characterised. The structures of these two polymers are presented in figure 1.26.

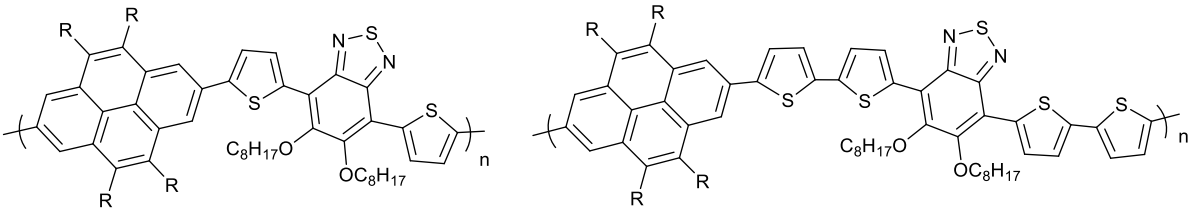

Figure 1.26. The structures of the suggested pyrene-*alt*-benzothiadiazole polymers.

Recently, the thiecno[3,4-c]pyrrole-4,6-dione (TPD) based donor-acceptor polymers has been widely explored for use in BHJ solar cells owing to its high degree of structural symmetry and planarity, which would boost the electronic delocalisation along the conjugated polymer backbone. The TPD moiety can be functionalised by attaching different solubilising groups to the nitrogen of the imide group. Therefore, a series of polymers based on the pyrene unit as the electron donor and TPD moiety as the electron acceptor will be synthesised. To the best of our knowledge, pyrene-*alt*-TPD polymers have not been reported before in the literature. Coupling pyrene with TPD will be fascinating to evaluate the suitability of pyrene in these donor-acceptor polymers. Pyrene-*alt*-TPD based conjugated polymers are expected to show a narrow energy gap and efficient solar

spectrum harvesting. Solubilizing groups (octyl or hexylphenyl) will be attached to the TPD unit through the nitrogen of the imide group to boost solubility and to facilitate the formation of high molecular weight conjugated polymers. Their influence on the optical, electrochemical, thermal and photovoltaic properties of the prepared polymers will be investigated. Previous work in the Iraqi group was carried out on the anthracene-*alt*-TPD based polymers and showed that the solubilizing groups introduced a large amount of steric repulsion which led to reduced electronic conjugation and low planarity. To avoid this issue, a thiophene group or bithiophene unit will be introduced as a spacer between the pyrene and TPD units. Moreover, the impact of these additions on the properties of the resulting polymers will also be considered. Finally, it seems to be that TPD moiety has promising features. Therefore, further studies are needed to evaluate their performance in organic photovoltaic devices. The structures of the suggested polymers are presented in figure 1.25.

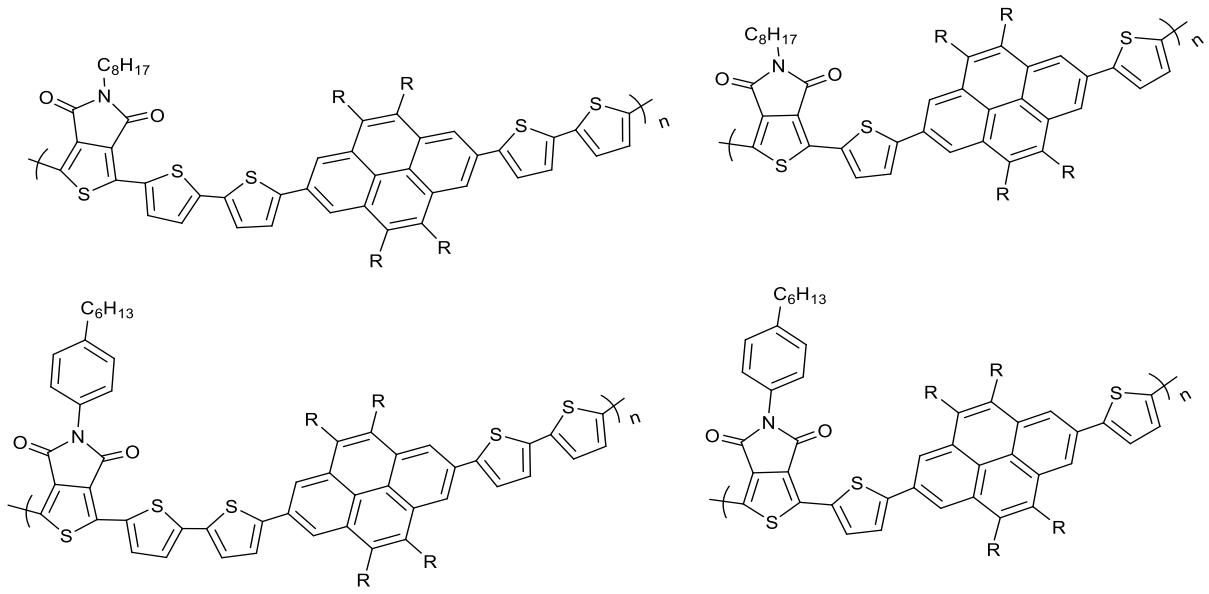

Figure 1.25. The chemical structures of the proposed pyrene-*alt*-TPD polymers.

1.12. References

1 A. Mohajeri and A. Omidvar, *Phys. Chem. Chem. Phys.*, 2015, **17**, 22367–22376.

2 K. I. Jayawardena, L. J. Rozanski, C. A. Mills, M. J. Beliatis, N. A. Nismy and S. R. P. Silva, *Nanoscale*, 2013, **5**, 8411-8427.

3 L. Lu, T. Zheng, Q. Wu, A. M. Schneider, D. Zhao and L. Yu, *Chem. Rev.*, 2015, **115**, 12666–12731.

4 B. A. Gregg, *J. Phys. Chem.* 2003, 4688–4698.

5 T. Ameri, G. Dennler, C. Lungenschmied and C. J. Brabec, *Energy Environ. Sci.*, 2009, **2**, 347-363.

6 H. Zhou, L. Yang and W. You, *Macromolecules*, 2012, **45**, 607–632.

7 G. Yu, J. Gao, J. C. Hummelen, F. Wudl and A. J. Heeger, *Science*, 1995, **270**, 1789–1791.

8 Y. Cheng, S. Yang and C. Hsu, *Chem. Rev.*, 2009, **109**, 5868–5923.

9 B. C. J. Brabec, N. S. Sariciftci and J. C. Hummelen, *Adv. Funct. Mater.*, 2001, **11**, 15–26.

10 S. Gu, H. Neugebauer and N. S. Sariciftci, *Chem. Rev.*, 2007, **107**, 1324–1338.

11 M. A. Topinka, *Nature Mater.*, 2006, **5**, 675–676.

12 J. Nelson, *Curr. Opin. Solid State Mater. Sci*., 2002, **6**, 87–95.

13 H. Hoppe and N. S. Sariciftci, *J. Mater. Res.*, 2004, **19**, 1924-1945.

14 C. W. Tang, *Appl. Phys. Lett.*, 1986, **48**, 183-185.

15 P. Taylor, O. A. Abdulrazzaq, V. Saini, S. Bourdo, E. Dervishi and S. Alexandru, *Part. Sci. Technol.*, 2013, **31**, 427–442.

16 X. Jing, D. Zhenbo, L. Chunjun, X. Denghui, X. Ying and G. Dong, *Physica E: Low-dimensional Systems and Nanostructures*, 2005, **28**, 323-327.

17 T. Ameri, P. Khoram, J. Min and C. J. Brabec, *Adv. Mater.*, 2013, **25**, 4245–4266.

18 Y. Su, S. Lan and K. Wei, *Mater. Today*, 2012, **15**, 554–562.

19 H. Zhou, L. Yang, S. Stoneking and W. You, *ACS Appl. Mater. Interfaces*, 2010, **2**, 1377–1383.

20 Z. He, C. Zhong, X. Huang, W. Wong and H. Wu, *Adv. Mater.*, 2011, **23**, 4636–4643.

21 B. Qi, J. Wang, *Phys. Chem. Chem. Phys.*, 2013, **15**, 8972–8982.

22 R. H. Friend, R. W. Gymer, A. B. Holmes, J. H. Burroughes, R. N. Marks, C. Taliani, D. D. C. Bradley, M. Lo, W. R. Salaneck, D. A. Dos Santos and J. L. Bre, *Nature*, 1999, **397**, 121–128.

23 H. Shirakawa, E. J. Louis, A. G. MacDiarmid, C. K. Chiang and A. J. Heeger, *J. Chem. Soc., Chem. Commun.*, 1977, 578-580.

24 A. Pron, P. Rannou, *Prog. polym. sci.*, 2002, 27, 135–190.

25 M. Kuik, G. A. H. Wetzelaer, H. T. Nicolai, N. I. Craciun, D. M. De Leeuw and P. W. M. Blom, *Adv. Mater.* 2014, **26**, 512–531.

26 L. Dai, *Intelligent macromolecules for smart devices: From Materials Synthesis to Device Applications. London:, Springer-Verlag*, 2004, 41-80.

27 M. F. Suarez-Herrera, Electrochemistry, Conducting polymers, 2009.

28 A. J. Heeger, *Angew. Chem. Int. Ed.*, 2001, **40**, 2591-2611.

29 A. J. Epstein, *MRS Bulletin*, 1997, **22**, 16-23.

30 A. Ajayaghosh, *Chem. Soc. Rev.*, 2003, **32**, 181–191.

31 R. Kroon, M. Lenes, J. A. N. C. Hummelen, P. W. M. Blom and B. D. E. Boer, *Polym. Rev.*, 2008,**48**, 531-582.

32 Strobl, Gert R. *The Physics of Polymers: Concepts for Understanding Their Structures and Behavior. Berlin: Springer*, 2007, 287-301.

33 Q. Pei, G. Zuccarello, M. Ahlskogt and O. Ingan, *Polymer*, 1994, **35**, 1347–1351.

34 C. C. C. J. Seechurn, M. O. Kitching, T. J. Colacot and V. Snieckus, *Angew. Chem. Int. Ed.*, 2012, **51**, 5062–5085.

35 J. Hassan, M. Se, C. Gozzi, E. Schulz and M. Lemaire, *Chem. Rev.*, 2002, **102**, 1359-1469.

36 Z. Bao, W. Chan, and L. Yu, *Chem. Mater.*, 1993, **5**, 2–3.

37 N. Miyaura, A. Suzuki and W. January, *Chem. Rev.*, 1995, **95**, 2457-2483.

38 A. Facchetti, *Chem. Mater.*, 2011, **23**, 733–758.

39 C. L. Chochos and S. A. Choulis, *Prog. Polym. Sci.*, 2011, **36**, 1326–1414.

40 F. Padinger, R. S. Rittberger and N. S. Sariciftci, *Adv. Funct. Mater.*, 2003, **13**, 85-88.

41 H. Guo, C. Weng, G. Wang, B. Zhao and S. Tan, *Dye. Pigment.*, 2016, **133**, 16–24.

42 A. C. Stuart, J. R. Tumbleston, H. Zhou, W. Li, S. Liu, H. Ade, and W. You., *J. Am. Chem. Soc.*, 2013, **135**, 1806−1815.

43 S. K. Lee, W. Lee, J. M. Cho, S. J. Park, J. Park, W. S. Shin, J. Lee, I. Kang and S. Moon, *Macromolecules*, 2011, **44**, 5994–6001.

44 T. M. Figueira-Duarte and K. Müllen, *Chem. Rev.*, 2011, **111**, 7260–7314.

45 S.-Y. Liu, W.-Q. Liu, J.-Q. Xu, C.-C. Fan, W.-F. Fu, J. Ling, J.-Y. Wu, M.-M. Shi, A. K.-Y. Jen and H.-Z. Chen, *ACS Appl. Mater. Interfaces*, 2014, **6**, 6765–6775.

46 L. Zöphel, D. Beckmann, V. Enkelmann, D. Chercka, R. Rieger and K. Müllen, *Chem. Commun.*, 2011, **47**, 6960–6962.

47 J. M. Casas-Solvas, J. D. Howgego and A. P. Davis, *Org. Biomol. Chem.*, 2013, **12**, 212–232.

48 Yamato, T., Fujimoto, M., Miyazawa, A. and Matsuo, K., *J. Chem. Soc.*, 1997, **1**, 1193-1200

49 K. Ogino, S. Iwashima, H. Inokuchi and Y. Harada, *Bull. Chem. Soc. Jpn.*, 1965, **38**, 473-477.

50 W. Kuznik, J. Frydel, T. Licha and T. Ratajczyk, *Phys. Chem. Chem. Phys.*, 2015, **17**, 22758–22769.

51 T. Yamato, A. Miyazawa, and M. Tashiro, *J. Chem. Soc.*, 1993, **24**, 3127–3137.

52 D. N. Coventry, A. S. Batsanov, E. Goeta, J. A. K. Howard, B. Marder and R. N. Perutz, *Chem. Commun.*, 2005, 2172–2174.

53 D. M. Connor, S. D. Allen, D. M. Collard, C. L. Liotta, D. A. Schiraldi, *J. Org. Chem.*, 1999, **64**, 6888–6890.

54 R. Bolton, *J. Chem. Soc.*, 1964, 4637–4638.

55 R. G. Harvey, M. Konieczny and J. Pataki, *J. Org. Chem.*, 1983, **48**, 2930–2932.

56 J. Hu, D. Zhang and F. W. Harris, *J. Org. Chem.*, 2005, **70**, 707–708.

57 R. M. Moustafa, J. A. Degheili, D. Patra and B. R. Kaafarani, *J. Phys. Chem. A*, 2009, **113**, 1235–1243.

58 N. Kulisic, S. More and A. Mateo-Alonso, *Chem. Commun.*, 2011, **47**, 514–516.

59 S. More, R. Bhosale, S. Choudhary and A. Mateo-Alonso, *Org. Lett.*, 2012, **14**, 4170-4173.

60 C. Soc, K. A. Mazzio and C. K. Luscombe, *Chem. Soc. Rev.*, 2014, **44**, 78–90.

61 B. C. J. Brabec, S. Gowrisanker, J. J. M. Halls, D. Laird, S. Jia and S. P. Williams, *Adv. Mater.*, 2010, **22**, 3839–3856.

62 B. G. Dennler, M. C. Scharber and C. J. Brabec, *Adv. Mater.*, 2009, **21**, 1323–1338.

Chapter II:

Pyrene-Benzothiadiazole Based Copolymers for Application in Photovoltaic Devices

Pyrene-Benzothiadiazole Based Copolymers for Application in Photovoltaic Devices

Abstract

The preparation and characterization of four narrow band gap pyrene–benzothiadiazole-based alternating copolymers are presented. An investigation of the impact of attaching different solubilizing groups to the pyrene repeat units on the optical, electrochemical, and thermal properties of the resulting materials was undertaken along with studies on the aggregation of polymer chains in the solid state. Unsurprisingly, polymers which had the smaller 2-ethylhexyl chains attached to the pyrene units **(PP$_{EH}$-DTBT** and **PP$_{EH}$-DTffBT**) displayed lower molecular weights relative to polymers with larger 2-hexyldecyl substituents (**PP$_{HD}$-DTBT** and **PP$_{HD}$-DTffBT**). Despite this, the 2-ethylhexyl substituted polymers displayed narrower optical band gaps relative to their analogous 2-hexyldecyl substituted polymers. Of all polymers synthesized, **PP$_{EH}$-DTBT** displayed the lowest optical band gap (1.76 eV) in the series. All of the polymers displayed degradation temperatures in excess of 300 °C. Polymers with smaller alkyl chains on the pyrene units display shallower highest occupied molecular orbital levels, which could be due to increased intramolecular charge transfer between the donor and acceptor units. Preliminary investigations on bulk heterojunction solar cells with a device structure indium tin oxide/poly(3,4-ethylenedioxythiophene) : polystyrene sulfonate /Polymer : $PC_{70}BM$/Ca/Al were undertaken. Polymer/$PC_{70}BM$ blend ratios of one third were used in these studies and have indicated that **PP$_{EH}$-DTBT** displayed the highest efficiency with a power conversion efficiency of 1.86%.

2.1. Introduction

Organic semiconductors have gained a tremendous amount of attention from researchers in recent years owing to the advantages they possess over their inorganic counterparts. These advantages include high absorption coefficients, non-toxic and recyclable materials, and can be manufactured on lightweight, flexible substrates via low-cost solution processing methods. These unique electrical and optical properties make organic semiconductors promising candidates for use in organic photovoltaic (OPV) cells, organic light-emitting diodes, and organic field effect transistors.[1-4]

Bulk heterojunction (BHJ) photovoltaic devices based on conjugated polymers as p-type organic semiconductors, and fullerene derivatives as n-type organic semiconductors, have been intensively studied in recent years. This has resulted in the efficiency of OPV BHJ devices rising from less than 1 % to over 10 %. The high rise in efficiencies can be attributed to the development of conjugated polymers and the improvement in the morphology of the photoactive layer of BHJ solar cells.[5-7] Previous literature reports have shown that BHJ solar cells fabricated from donor-acceptor (D-A) conjugated polymers yield the best efficiencies. In the D-A approach, an electron-poor acceptor unit is copolymerized with an electron-rich donor unit. A fraction of electronic charge is transferred between the electron-rich and electron-poor units along polymer chains, leading to intramolecular charge transfer (ICT) and a narrow optical band gap, allowing the polymer to absorb large portions of light from the visible spectrum.[8-10]

Benzothiadiazole (BT)-based copolymers have received a large amount of attention from the academic community. High efficiencies have been reported for BHJ solar cells fabricated from BT-based D-A copolymers.[9] Recently, Liu *et al.* reported the synthesis of highly efficient BHJ solar cells based on BT-thiophene alternate copolymers.[11] Efficiencies of 10.8% were achieved when the polymer, **PffBT4T-2OD**, was blended with the fullerene acceptor **TC$_{71}$BM**. High efficiencies were still achieved when thick-film (250-300 nm) polymer solar cells were fabricated. Other efficient BT-based polymers include **BDT-DTBTff** synthesised by You and co-workers, which achieved an efficiency of 7.2 % when fabricated into BHJ solar cells.[10,12-14]

Polycyclic aromatic hydrocarbons have found widespread use in OPV and organic light-emitting diode devices.[15] When compared with other polycyclic aromatic hydrocarbons such as naphthalene and anthracene,[16-18] pyrene-based conjugated polymers have received little attention from to date.

Pyrene is a planar, symmetrical, electron rich unit that possesses an extended π-conjugated system. Thus, pyrene molecules may exhibit strong π-π stacking and a high degree of crystallinity which could promote charge carrier mobility. Furthermore, the electron rich nature of pyrene means that the pyrene-unit can be polymerised with electron-deficient units forming the advantageous D-A arrangement discussed earlier. The pyrene unit can be polymerised through the 2,7-positions.[19,20] Furthermore, the optical and electronic properties of pyrene units can be altered by functionalising the 4,5,9,10-positions of pyrene with different substituents. Yang and co-workers synthesised a series pyrene-diketopyrrolopyrrole based copolymers for use in organic field effect transistors. **P[DTDPP-*alt*-(2,7)PY]** displayed a narrow optical band gap of 1.65 eV and hole mobilities of 0.23 cm^2 V^{-1} s^{-1}.[21] Hwang *et al.* reported the synthesis of pyrene-based alternate copolymers.[22] BHJ solar cells fabricated from these polymers displayed efficiencies up to 5.04%. They synthesised a terpolymer, **PBDTDTBT** that comprised carbazole, BT and pyrene repeat units. **PBDTDTBT** was compared to the well-studied polymer, **PCDTBT**. The researchers found that **PBDTDTBT** displayed higher charge transport abilities when compared with **PCDTBT**, a consequence of incorporating pyrene units. Solar cells based on **PBDTDTBT** displayed efficiencies of 3.34%, which is higher than that of solar cells fabricated from **PCDTBT** by using similar conditions. Furthermore, the introduction of pyrene resulted in the polymers displaying higher open circuit voltages.[22]

Herein, we report the preparation of four D-A polymers comprising pyrene-BT repeat units. Poly{4,5,9,10-tetrakis[(2-hexyldecyl)oxy]-pyrene-2,7-diyl-*alt*-[4,7-dithiophen-2-yl]-2',1',3'-BT-5,5-diyl} **(PP_{HD}-DTBT)**, poly{4,5,9,10-tetrakis[(2-hexyldecyl)oxy]pyrene-2,7-diyl-*alt*-[5,6-difluoro-4,7-di(thiophen-2-yl)-2',1',3'-BT-5,5-diyl]} **(PP_{HD}-DTffBT)**, poly{4,5,9,10-tetrakis[(2-ethylhexyl)oxy]pyrene-2,7-diyl-*alt*-[4,7-dithiophen-2-yl]-2',1',3'-BT-5,5-diyl} **(PP_{EH}-DTBT)** and poly{4,5,9,10-tetrakis[(2-ethylhexyl)oxy]pyrene-2,7-diyl-*alt*-[5,6-difluoro-4,7-di(thiophen-2-yl)- 2',1',3'-BT-5,5-diyl]} **(PP_{EH}-DTffBT)** were synthesised by Stille polymerisation (figure 2.1). The properties of the polymers were investigated and their performance in BHJ photovoltaic devices was assessed. Polymers that had smaller alkyl chains attached to the pyrene unit displayed narrower optical band gaps, shallower highest occupied molecular orbital (HOMO) levels and improved π-π stacking in solid state. BHJ solar cells fabricated from **PP_{HD}-DTBT**, **PP_{EH}-DTBT**, **PP_{HD}-DTffBT** and **PP_{EH}-DTffBT** displayed efficiencies of 0.98, 1.86, 0.66 and 0.83%, respectively.

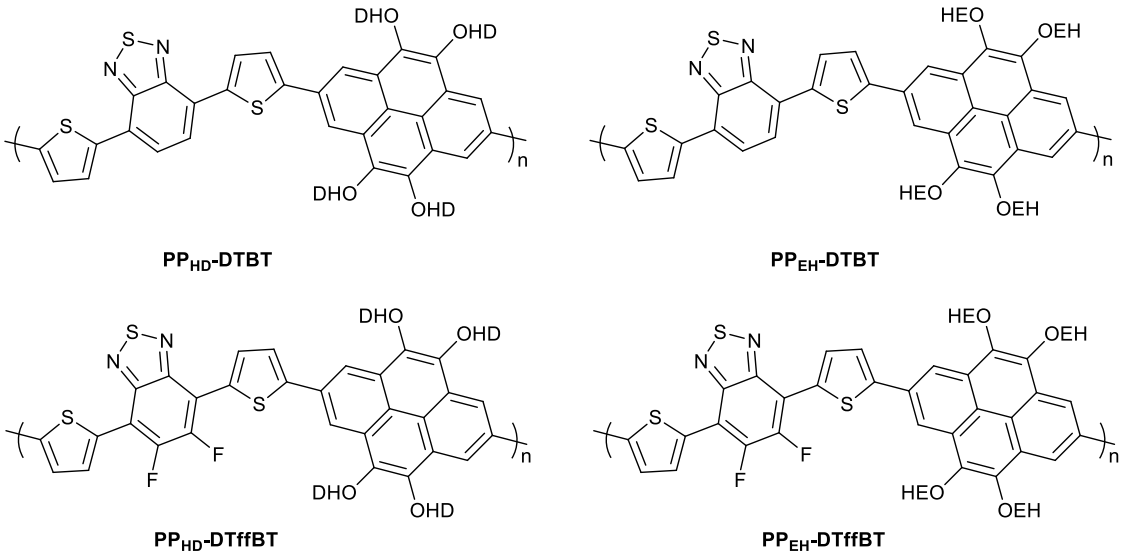

Figure 2.1. The structures of **PP$_{HD}$-DTBT**, **PP$_{EH}$-DTBT**, **PP$_{HD}$-DTffBT** and **PP$_{EH}$-DTffBT**.

2.2. Results and Discussion

2.2.1. Monomer synthesis

The preparation of monomers 2,7-dibromo-4,5,9,10-tetrakis((2-hexyldecyl)oxy)pyrene (**M1**) and 2,7-dibromo-4,5,9,10-tetrakis((2-ethylhexyl)oxy)pyrene (**M2**) is depicted in Scheme 2.1. Synthetic procedures are described in the experimental part.

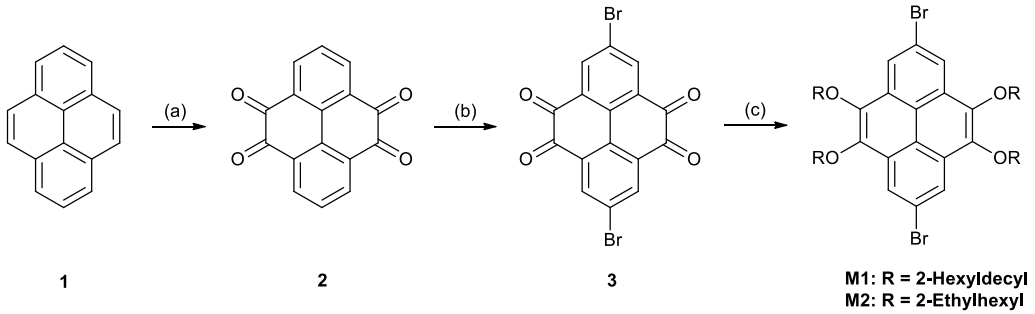

Scheme 2.1. (a) $RuCl_3.xH_2O$, $NaIO_4$, DCM, H_2O, MeCN; (b) NBS, H_2SO_4; (c) $Na_2S_2O_4$, *t*-Bu_4NBr, KOH, THF, H_2O, R-Br.

Both pyrene monomers were synthesised starting from the commercially available pyrene (**1**). The pyrene was oxidised at the 4,5,9,10-positions using ruthenium (III) chloride ($RuCl_3xH_2O$) as an oxidant reagent and sodium *meta*-periodate ($NaIO_4$) as a co-oxidant reagent to produce pyrene-4,5,9,10-tetraone (**2**). The reaction mechanism is not well known; however, it is suggested that the

two oxidant reagents firstly react with each other to form ruthenium tetroxide (RuO_4) *in situ* which is considered to be an aggressive oxidant reagent. A suggested mechanism for the reaction is shown in scheme 2.2.

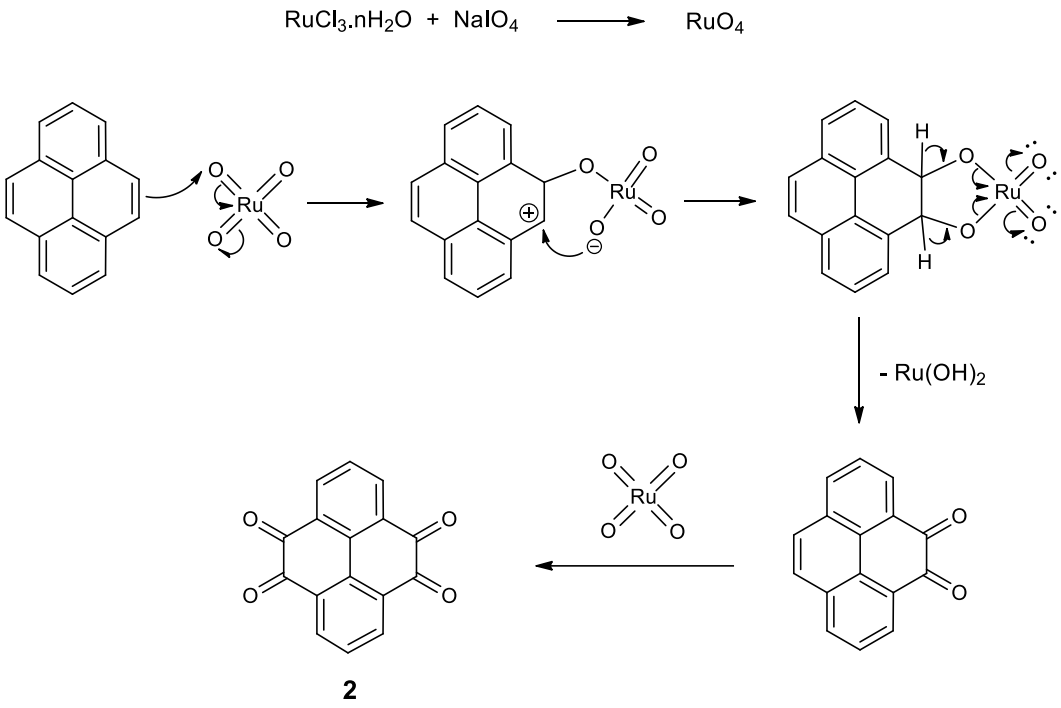

Scheme 2.2. Suggested mechanism for the preparation of pyrene-4,5,9,10-tetraone.

Intermediate **2** was then brominated at the 2,7-positions using *N*-bromosuccinimide (NBS) to yield 2,7-dibromopyrene-4,5,9,10-tetraone (**3**). Compound **3** was prepared *via* an electrophilic aromatic substitution. The bromination process occurs at 2,7-positions of the pyrene rather than 1,3,6,8-positions due to the presence of steric hindrance of NBS with the tetraketone groups.

The final step of the synthesis involved attaching the solubilising alkyl chains to the 4,5,9,10 positions. In this step sodium dithionite ($Na_2S_2O_4$) was used to reduce compound **3** in the presence of H_2O to produce 2,7-dibromopyrene-4,5,9,10-tetraol (**a**) as an intermediate. After that, the alcohol groups were deprotonated by an aqueous solution of KOH in the presence of tetra-*n*-butylammonium bromide (*t*-BuNBr) followed by alkylation using 1-bromo-2-hexyldecane or 1-bromo-2-ethylhexane to produce the desired monomers, 2,7-dibromo-4,5,9,10-tetrakis((2-hexyldecyl)oxy)pyrene (**M1**) or 2,7-dibromo-4,5,9,10-tetrakis((2-ethylhexyl)oxy)pyrene (**M2**),

respectively. The mechanism of the reaction is not fully well known. However, a proposed mechanism is shown in scheme 2.3.

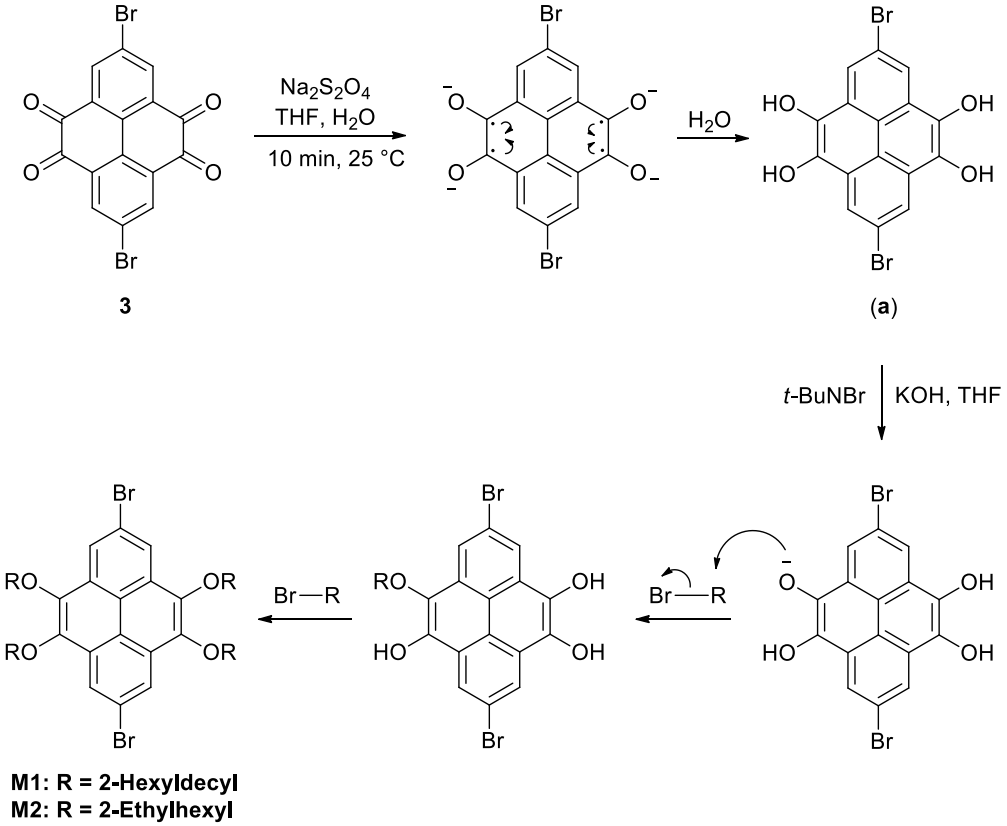

Scheme 2.3. Suggested reaction mechanism for the formation of **M1** and **M2**.

The structures of the two monomers were confirmed by ^{1}H NMR spectroscopy. The ^{1}H NMR spectra of **M1** and **M2** are depicted in figure 2.2 and figure 2.3, respectively. The two monomers showed a singlet resonance at 8.54 ppm which corresponds to the four protons on the pyrene unit. The resonances positioned below 4.20 ppm correspond to the protons located on the alkyl chains. It is observed that the resonance in the aromatic region was slightly shifted downfield when compared to the ^{1}H NMR spectrum of compound **3**, confirming that the desired product had been formed.

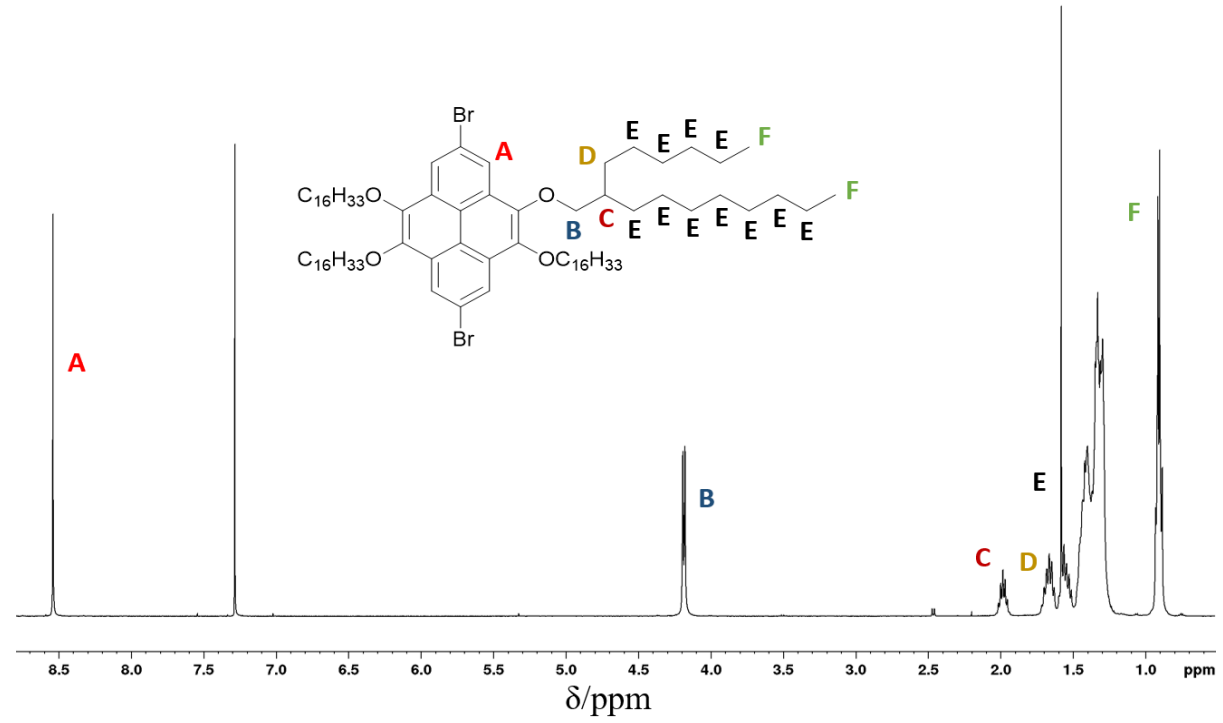

Figure 2.2. ^{1}H NMR spectrum of **M1** in $CDCl_3$.

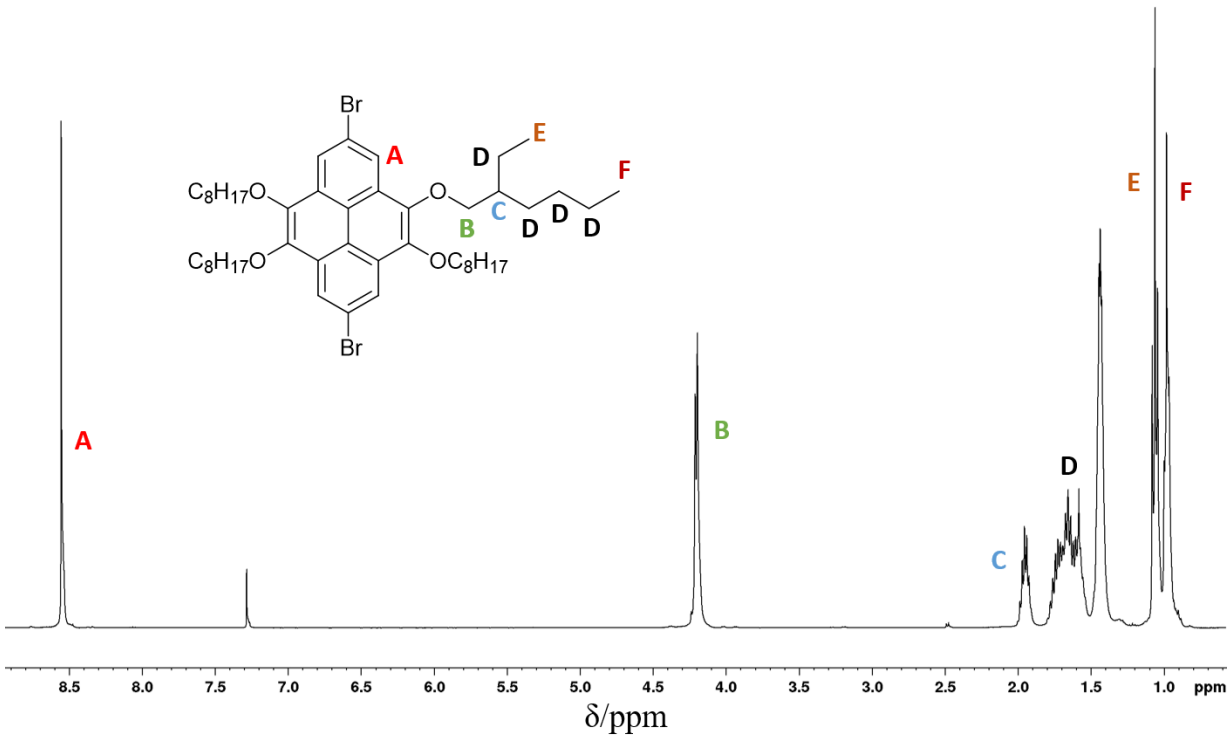

Figure 2.3. ^{1}H NMR spectrum of **M2** in $CDCl_3$.

The synthetic routes towards the preparation of 4,7-bis(5-(trimethylstannyl)thiophen-2-yl)benzo[c][1,2,5]thiadiazole (**M3**) is presented in scheme 2.4. Synthetic procedures are described in the experimental part.

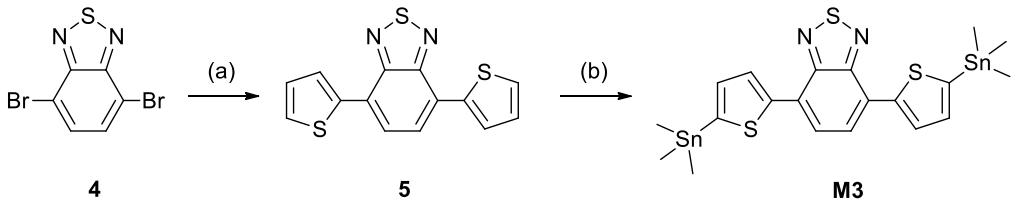

Scheme 2.4. Synthesis of **M3**: *(a)* 2- (tributylstannyl)thiophene, $Pd(PPh_3)_2Cl_2$, toluene; and (*b*) 2,2,6,6-tetramethylpiperdine, *n*-BuLi, trimethyltin chloride, THF.

Stille coupling of 4,7-dibromobenzo[c][1,2,5]thiadiazole (**4**) using 2-(tributylstannyl)thiophene and $Pd(PPh_3)_2Cl_2$ as a catalyst produced 4,7-di(thiophen-2-yl)benzo[c][1,2,5]thiadiazole (**5**) in a yield of 86% as orange needles. The final step involved the reaction of 2,2,6,6-tetramethylpiperdine with *n*-BuLi to produce lithium 2,2,6,6- tetramethylpiperdine *in situ* which in turns was employed to deprotonate compound **5** at the 4,7-positions. Metalation of compound **5** using trimethyltin chloride (Me_3SnCl) produced 4,7-bis(5-(trimethylstannyl)thiophen-2-yl)benzo[c][1,2,5]thiadiazole (**M3**). The product was prepared via a nucleophilic aromatic substitution (S_N2) and was obtained in a good yield (70 %) as red needle-like crystals. The mechanism of the reaction is shown in scheme 2.5.

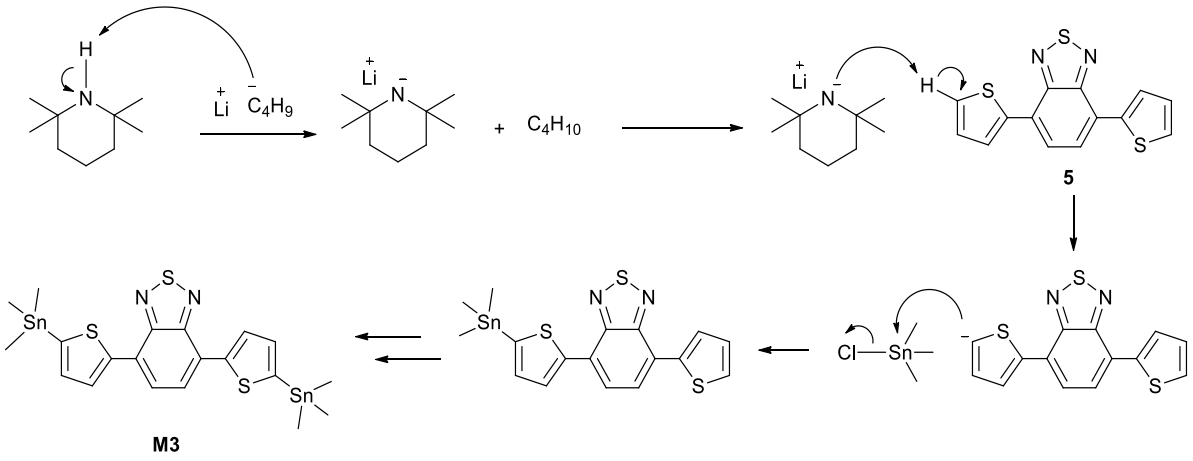

Scheme 2.5. Reaction mechanism of the production of **M3**.

The structure of the monomer was confirmed by ^{1}H NMR spectroscopy (figure 2.4). The aromatic region showed three resonances at 8.20, 7.90 and 7.32 ppm, respectively. The two resonances at 8.20 and 7.32 are doublets and correspond to the protons on the thiophene rings, whereas the resonance at 7.90 is a singlet and correspond to the proton on the benzothiadiazole unit. The absence of a doublet resonance in the aromatic region and the appearance of a singlet resonance at 0.46 ppm which assign to the protons on the methyl groups compared to compound **5**, indicates the formation of **M3**.

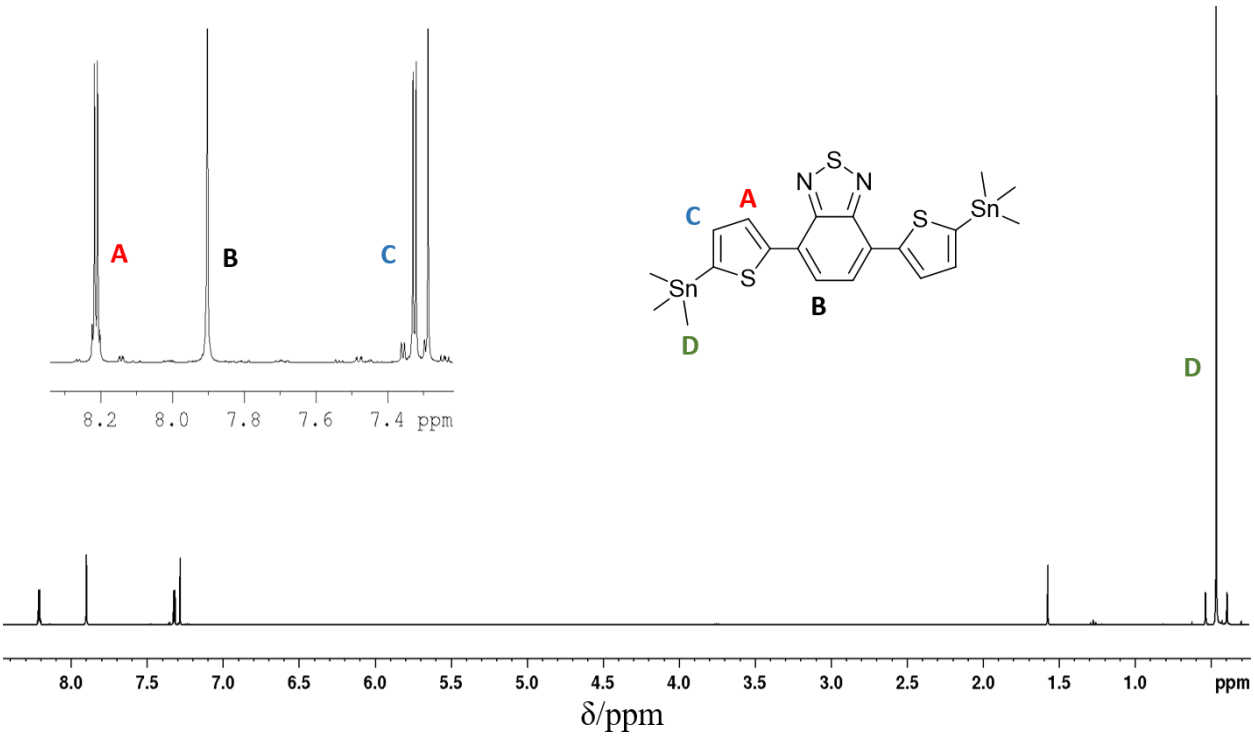

Figure 2.4. ^{1}H NMR spectrum of **M3** in $CDCl_3$.

2.2.2. Polymer Synthesis

All polymers were prepared via Stille coupling using $Pd(OAc)_2$ and tri(*o*-tolyl)phosphine as the catalyst and toluene as the solvent. All polymerisations, with the exception of **PP$_{EH}$-DTffBT**, were conducted over 48 hours. Polymerisation of **PP$_{EH}$-DTffBT** was stopped after 2 hours, as after this time, polymer precipitation was observed as a result of its lower solubility. The crude polymers were purified via Soxhlet extraction by using methanol, acetone, hexane, toluene and chloroform. The methanol, acetone and hexane fractions removed catalyst residues, inorganic impurities and low molecular weight oligomers/polymers. The toluene fractions were collected for **PP$_{HD}$DTBT**

and **PP$_{HD}$-DTffBT**. In contrast, the chloroform fraction was collected for **PP$_{EH}$-DTBT**, and **PP$_{EH}$-DTffBT**, a consequence of the smaller alkyl chain on the pyrene repeat units that provide lower solubility in toluene fractions on Soxhlet extraction. The number-average molecular weights (M_n) and weigh-average molecular weighs (M_w) were determined *via* gel permeation chromatography (GPC) at 140 °C by using 1,2,4-trichlorobenzene as the eluent. A series of polystyrene standards were used as the internal standards, and the results are outlined in table 2.1. Unsurprisingly, polymers that are substituted with the short 2-ethylhexyl chains displayed lower molecular weights relative to polymers that are substituted with the larger 2-hexyldecyl alkyl chains. Clearly, the incorporation of larger alkyl chains on the pyrene units inhibits intermolecular interactions between polymer chains aiding the formation of processable polymer materials with higher molecular weight. Interestingly, **PP$_{EH}$-DTffBT** displayed a lower M_n (5,300 Da) relative to its non-fluorinated analogue, **PP$_{EH}$-DTBT** (12,800 Da). Previous literature has shown that the incorporation of fluorine on the BT unit results in stronger π-π stacking interactions and aggregation of polymers chains, which limits the final molecular weight of the polymer.[23,24] However, **PP$_{HD}$-DTffBT** (20,700 Da) did not display a lower M_n value relative to its non-fluorinated analogue, **PP$_{HD}$-DTBT** (20,500 Da). It is speculated that the large 2-hexyldecyl chains are long enough to break these additional interactions, in solution, facilitating the formation of a high molecular weight material.

Table 2.1. GPC, UV-vis absorption and electrochemical data for **PP$_{HD}$-DTBT**, **PP$_{EH}$-DTBT**, **PP$_{HD}$-DTffBT** and **PP$_{EH}$-DTffBT**.

Polymer	M_n (Da)[c]	M_w (Da)[c]	PDI	λ_{max} (nm)		$E_{g\ opt}$ (eV)[d]	HOMO (eV)[e]	LUMO (eV)[f]	E_g^{elec} (eV)[g]
				Solution	Film				
PP$_{EH}$-DTBT[a]	12,800	22,000	1.72	538	585	1.76	-5.45	-3.55	1.90
PP$_{EH}$-DTffBT[a]	5,300	6,300	1.19	521	564	1.81	-5.53	-3.55	1.98
PP$_{HD}$-DTBT[b]	20,500	30,200	1.47	531	571	1.79	-5.50	-3.28	2.22
PP$_{HD}$-DTffBT[b]	20,700	40,400	1.95	526	562	1.84	-5.60	-3.28	2.32

[a] Measurements conducted on the chloroform fraction of the polymers. [b] Measurements conducted on the toluene fraction of the polymers. [c] GPC conducted in 1,2,4-trichlorobenzene at 140 °C using a differential refractive index (DRI) method. [d] Optical band gap determined from the onset of the absorption band in thin film. [e] HOMO level determined from the onset of oxidation. [f] LUMO level determined from the onset of reduction. [g]Electrochemical band gap.

2.2.3. UV-vis absorption spectroscopy

The optical properties of all polymers were investigated by UV-vis spectroscopy in dilute chloroform solutions (Fig. 2.5.a) and film states (Fig. 2.5.b). The optical band gaps of the polymers were calculated from their onsets of absorption in films. The data are summarised in Table 1. All UV-vis spectra display two main absorption bands. The band at shorter wavelengths can be attributed to π-π* transitions, whereas the absorption bands at longer wavelengths can be attributed to ICT between the electron-rich pyrene units flanked by thiophene rings and the electron deficient BT units. In solutions, the ICT absorption maxima are located at 531, 538, 526 and 521 nm for **PP_{HD}-DTBT**, **PP_{EH}-DTBT**, **PP_{HD}-DTffBT** and **PP_{EH}-DTffBT**, respectively. When cast into films, these maxima are redshifted to 571, 585, 562 and 564 nm for **PP_{HD}-DTBT**, **PP_{EH}-DTBT**, **PP_{HD}-DTffBT** and **PP_{EH}-DTffBT**, respectively. The bathochromic shifts can be attributed to the polymers adopting more planar conformations in the solid state, which extends the electronic conjugation along the backbone of polymers. When cast into films, polymers with shorter alkyl chains, **PP_{EH}-DTBT** and **PP_{EH}-DTffBT**, display more redshifted absorption maxima relative to their analogous polymers, **PP_{HD}-DTBT** and **PP_{HD}-DTffBT**. Furthermore, all fluorinated polymers display a hypsochromic shift relative to their non-fluorinated polymers. This phenomenon has been reported in previous literature.[24]

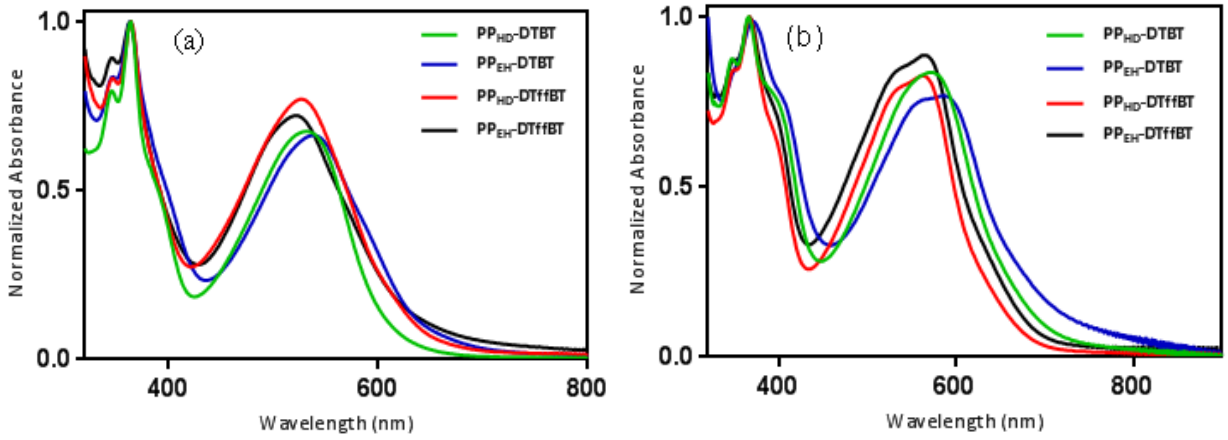

Figure 2.5. Normalised absorption spectra of **PP_{HD}-DTBT**, **PP_{EH}-DTBT**, **PP_{HD}-DTffBT** and **PP_{EH}-DTffBT** in: (*a*) chloroform solutions; and (*b*) thin films.

A very small shoulder appeared at shorter wavelength for all polymers. This was located at 346 and 348 nm in solution and film states, respectively. This phenomenon has been observed in most D-A conjugated polymers containing DTBT units.[10] The UV-vis spectra of **PP$_{HD}$-DTffBT** and **PP$_{EH}$-DTffBT** both display a small shoulder peak at ~500 nm in solid state. **PP$_{EH}$-DTBT** also displays a shoulder peak in this region, however, it is not as pronounced. Interestingly, this shoulder peak is completely absent in **PP$_{HD}$-DTBT**. Previous work has speculated that the incorporation of fluorine substituents yield additional intermolecular interactions between fluorine substituents with neighbouring aromatic chains. Thus, the polymer adopts a more planar conformation with improved stacking between polymer chains.[24] It is possible that the short 2-ethylhexyl chains in **PP$_{EH}$-DTBT** allow a similar π-π stacking of polymer chains to occur all be it to a much reduced level. In contrast, the large alkyl chains attached to **PP$_{HD}$-DTBT** disrupt intermolecular interactions, resulting in a higher degree of structural and electronic disorder, which is displayed in the broad, ill-resolved absorption bands.

The optical band gaps of **PP$_{HD}$-DTBT**, **PP$_{EH}$-DTBT**, **PP$_{HD}$-DTffBT** and **PP$_{EH}$-DTffBT** were estimated to be 1.77, 1.74, 1.84 and 1.81 eV, respectively. **PP$_{EH}$-DTBT** and **PP$_{EH}$-DTffBT** displayed narrower optical band gaps relative to their analogous polymers, **PP$_{HD}$-DTBT** and **PP$_{HD}$-DTffBT**. The rational for this can be linked to the size of the solubilising chain attached to the pyrene donor units on the respective polymers. It is also noted that the band gaps of the non-fluorinated polymers (**PP$_{HD}$-DTBT** and **PP$_{EH}$-DTBT**) are narrower than those of their fluorinated analogues (**PP$_{HD}$-DTffBT** and **PP$_{EH}$-DTffBT**) as a consequence of deeper HOMO levels in the fluorinated polymers (see below).

PP$_{HD}$-DTBT, **PP$_{EH}$-DTBT**, **PP$_{HD}$-DTffBT** and **PP$_{EH}$-DTffBT** are analogous polymers to the BT-anthracene-based polymer **PPATBT** synthesised by Almeataq *et al*.,[18] which uses an anthracene functionalised with 4-dodecyloxybenzene as the donor polyaromatic hydrocarbon unit, instead of pyrene, and which has an optical band gap of 1.84 eV, or to the fluorinated BTT-anthracene-based polymer **PTATffBT** synthesised by Cartwright and co-workers,[25] which has a band gap of 1.92 eV. It is speculated that the additional cyclic aromatic ring in pyrene units for polymers described in this study extends the electron conjugation, yielding more planar polymer backbones that improves π-π stacking in the solid state.

2.2.4. Thermal Properties

Thermogravimetric analysis (TGA) was used to investigate the thermal properties of the polymers synthesised within this report (figure 2.6). All polymers display degradation temperatures (5% weight loss) in excess of 320 °C. **PP_{HD}-DTBT**, **PP_{EH}-DTBT, PP_{HD}-DTffBT** and **PP_{EH}-DTffBT** displayed degradation temperatures of 328, 322, 328 and 320 °C, respectively. All initial weight losses can be attributed to the loss of alkyl chains from the pyrene donor unit. **PP_{EH}-DTBT** and **PP_{EH}-DTffBT** both display second weight loss peaks at 530 and 513 °C, respectively. This second weight loss peak corresponds to degradation of the polymer backbone. Interestingly, this second weight loss peak is absent in both **PP_{HD}-DTBT** and **PP_{HD}-DTffBT**. It is speculated that the larger 2-hexyldecyl chain is significantly less volatile, when combusted, relative to the 2-ethylhexyl chain. Thus, as **PP_{HD}-DTBT** and **PP_{HD}-DTffBT** degrade, a char layer is formed over the virgin polymer that acts as a thermal insulator owing to its low thermal conductivity. Consequently, the char layer reduces the heat flux reaching the virgin polymer. Furthermore, as the surface temperature of the char increases, there will be a significant increase in re-radiation losses. Both of these processes retard thermal degradation of the polymer.[26]

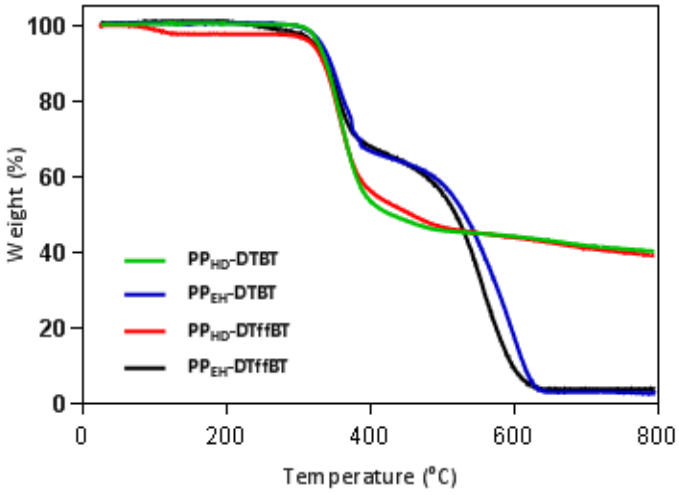

Figure 2.6. TGA curves of **PP_{HD}-DTBT**, **PP_{EH}-DTBT**, **PP_{HD}-DTffBT** and **PP_{EH}-DTffBT**.

2.2.5. Cyclic Voltammetry

Cyclic voltammetry was used to characterise the frontier energy levels of **PP_{HD}-DTBT**, **PP_{EH}-DTBT**, **PP_{HD}-DTffBT** and **PP_{EH}-DTffBT**. Studies were carried out on drop-cast polymer films in acetonitrile and tetrabutylammonium perchlorate as the electrolyte (Fig. 2.7). The onsets of oxidation and reduction were used to assess the HOMO and lowest unoccupied molecular orbital (LUMO) energy levels of the polymers. The values of these (*versus vacuum*) along with the electrochemical energy band gaps calculated from the difference of their HOMO and LUMO levels are shown in Table 2.1.

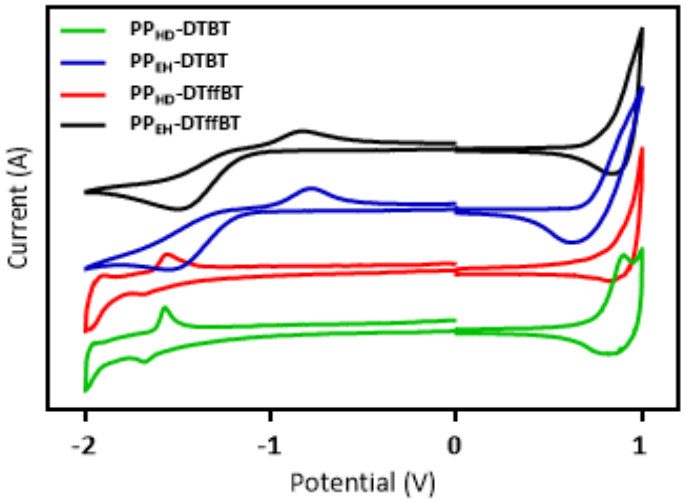

Figure 2.7. Cyclic voltammograms of thin films **of PP_{HD}-DTBT**, **PP_{EH}-DTBT**, **PP_{HD}-DTffBT** and **PP_{EH}-DTffBT** on platinum disc electrodes (area 0.031 cm^2) at a scan rate of 100 mV s^{-1}.

All fluorinated polymers display deeper HOMO levels relative to their non-fluorinated counterparts, a consequence of attaching electron-withdrawing substituents to the BT unit. This phenomenon has been observed in previous literature.[27,28] It is speculated that the lower HOMO levels of fluorinated polymers should result in a higher open circuit voltage (V_{oc}) in photovoltaic devices. Furthermore, the polymers should display better oxidative stability relative to their non-fluorinated counterparts. The HOMO/LUMO levels of **PP_{HD}-DTffBT** and **PP_{EH}-DTffBT** were positioned at -5.60/-3.28 eV and -5.53/-3.55 eV, respectively. Clearly, the LUMO level of **PP_{EH}-DTffBT** is positioned further from the vacuum level than that of **PP_{HD}-DTffBT**. It is speculated that this is a consequence of attaching larger alkyl chains to the pyrene units that lead to lower electronic delocalisation. The shallower HOMO level of **PP_{EH}-DTffBT** is a consequence of

attaching shorter 2-ethyl hexyl chains to the pyrene units. It is hypothesised that the shorter alkyl chains in **PP$_{EH}$-DTffBT** facilitate improved intermolecular interactions and a more planar polymer backbone which facilitates ICT between the electron-deficient and electron-donating units. This phenomenon is repeated in the non-fluorinated polymers **PP$_{HD}$-DTBT** and **PP$_{EH}$-DTBT**. Their HOMO/LUMO levels are positioned at -5.50/-3.28 eV and -5.45/-3.55, respectively. The electrochemical band gaps of **PP$_{HD}$-DTBT**, **PP$_{EH}$-DTBT**, **PP$_{HD}$-DTffBT** and **PP$_{EH}$-DTffBT** were estimated to be 2.22, 1.90, 2.32 and 1.98 eV, respectively. The electrochemical band gaps are significantly larger than the optical band gaps. Previous literature has shown this is a consequence of an additional interfacial barrier between the polymer films and electrode surface.[29]

2.2.6. Powder X-ray diffraction

The molecular organization of **PP$_{HD}$-DTBT**, **PP$_{EH}$-DTBT**, **PP$_{HD}$-DTffBT** and **PP$_{EH}$-DTffBT** in the solid state were probed via powder X-ray diffraction patterns (PXRD) (figure 2.8). The PXRD pattern of **PP$_{HD}$-DTBT** and **PP$_{HD}$-DTffBT** both display broad, diffuse features in the wide angle region at 20.7° and a poorly resolved peak in the small angle region at 3.67°. These correspond to a π-π stacking distance of 4.29 Å and a lamellar distance of ~24.0 Å, respectively.[24]

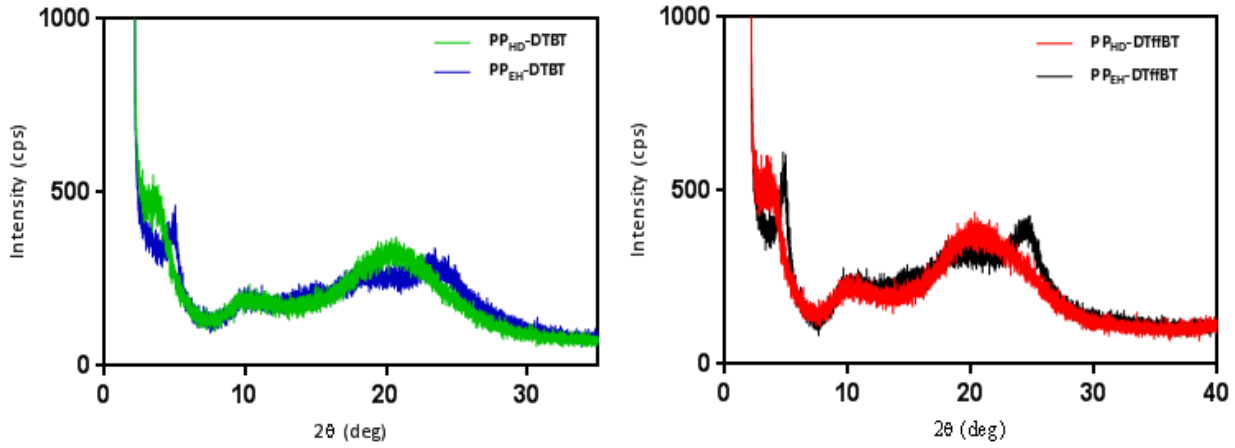

Figure 2.8. PXRD patterns of **PP$_{HD}$-DTBT**, **PP$_{EH}$-DTBT**, **PP$_{HD}$-DTffBT** and **PP$_{EH}$-DTffBT**.

Previous literature reports have shown that fluorination of the BT unit yields a decrease in the π-π stacking distance.[23-25] **PP$_{HD}$-DTffBT** does not follow this reported trend. It is speculated that the large 2-hexyldecyl negate the effects that fluorination has on the π-π stacking properties of the polymer in the solid state. Thus, **PP$_{HD}$-DTffBT** possesses the same number and extent of intermolecular interactions as **PP$_{HD}$-DTBT**. **PP$_{EH}$-DTBT** and **PP$_{EH}$-DTffBT** display lamellar

stacking distances of 18.0 and 17.9 Å, respectively, and π-π stacking distances of 3.81 and 3.59 Å, respectively. Unsurprisingly, polymers that have 2-ethylhexyl chains attached to the pyrene unit possess smaller lamellar stacking distances relative to polymers that have 2-hexyldecyl chains attached to the pyrene unit. The smaller π-π stacking distance of **PP_{EH}-DTffBT**, relative to **PP_{EH}-DTBT**, can be attributed to the incorporation of fluorine. Previous literature has reported this phenomenon.[24] The smaller stacking distance and more resolved peaks in **PP_{EH}-DTffBT** relative to **PP_{EH}-DTBT** suggest the polymer adopts a more crystalline structure in the solid state. [23-25]

2.2.7. Photovoltaic properties

Preliminary studies on the photovoltaic properties of the four polymers were undertaken. BHJ solar cells were fabricated with a device architecture of Glass/indium tin oxide (ITO)/ poly(3,4-ethylenedioxythiophene) (PEDOT) : polystyrene sulfonate (PSS)/ Polymer : $PC_{70}BM$/Ca/Al by using a mixture of Polymer:$PC_{70}BM$ in a weight ratio of 1:3 in chlorobenzene as the processing solvent. A detailed device fabrication is outlined in the experimental section. The current density-voltage (J-V) characteristic curves from these devices are displayed in figure 2.9. The device parameters are depicted in Table 2.2. The V_{oc} values for polymers with 2-hexyldecyl substituents **PP_{HD}-DTBT** and **PP_{HD}-DTffBT** are found to be higher (0.90 and 0.93 V, respectively) than those of polymers with the smaller 2-ethylhexyl substituents **PP_{EH}-DTBT** and **PP_{EH}-DTffBT** (0.74 and 0.79 V, respectively). This can be partly explained with their deeper HOMO energy levels (-5.50 and -5.60 eV for **PP_{HD}-DTBT** and **PP_{HD}-DTffBT**, respectively, *versus* -5.45 and -5.53 eV for **PP_{EH}-DTBT** and **PP_{EH}-DTffBT**, respectively). All polymers exhibit modest efficiencies. **PP_{EH}-DTBT** boasted the highest efficiency in this series of polymers with a power conversion efficiency (PCE) of 1.86 %, fill factor (FF) of 60.58 % and a J_{sc} of 4.14 mA/cm^2. In contrast, the equivalent polymer, which has the larger 2-hexyldecyl chains attached to the pyrene units **PP_{HD}-DTBT**, demonstrated a PCE of 0.98 %, a FF of 45.81 % and a J_{sc} of 2.38 mA cm^{-2}. The higher J_{sc} and FF of **PP_{EH}-DTBT**, relative to those of **PP_{HD}-DTBT**, are presumably a result of the smaller 2-ethylhexyl substituents attached to its pyrene repeat units. As shown from the X-ray diffraction studies, the smaller alkyl chains yield a smaller amount of steric hindrance, which should improve the packing of polymer chains in the photoactive layer of the photovoltaic device. The improved stacking should yield improved charge mobility and extraction in photovoltaic devices fabricated from **PP_{EH}-DTBT**, relative to those fabricated form **PP_{HD}-DTBT**. It is worth noting that a similar

phenomenon was observed when comparing the two analogous polymers, **PP$_{HD}$-DTffBT** and **PP$_{EH}$-DTffBT**.

Polymers synthesised within this chapter, **PP$_{HD}$-DTBT** and **PP$_{EH}$-DTBT**, exhibited lower PCE when compared with the carbazole-BT based polymer **PCDTBT** prepared by Al-Faifi *et al.*,[13] which uses a carbazole unit as the electron donor, instead of pyrene, and which has an efficiency of 4.30 %. It is hypothesised that the higher efficiency of **PCDTBT**, relative to **PP$_{HD}$-DTBT** and **PP$_{EH}$-DTBT**, is a result of a higher *FF* (61.8 %) and J_{sc} (8.91 mA cm^{-2}) values. It could also be due to the improved stacking of **PCDTBT**:$PC_{70}BM$ in the active layer which in turns should result in improved charge mobility and extraction of photogenerated charge carriers in photovoltaic devices.

Table 2.2. Device Performance of the four polymers **PP$_{HD}$-DTBT**, **PP$_{EH}$-DTBT**, **PP$_{HD}$-DTffBT** and **PP$_{EH}$-DTffBT**.

Polymer	J_{sc} (mA cm^{-2})	V_{oc} (V)	FF (%)	PCE (%)
PP$_{EH}$-DTBT	4.14	0.74	60.58	1.86
PP$_{EH}$-DTffBT	2.28	0.79	46.06	0.83
PP$_{HD}$-DTBT	2.38	0.90	45.81	0.98
PP$_{HD}$-DTffBT	1.36	0.93	52.22	0.66

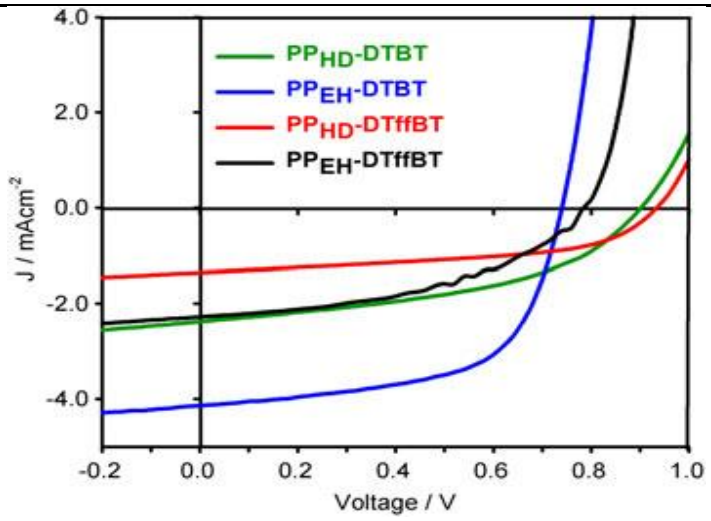

Figure 2.9. The J-V characteristic curves of **PP$_{HD}$-DTBT**, **PP$_{EH}$-DTBT**, **PP$_{HD}$-DTffBT** and **PP$_{EH}$-DTffBT**.

2.3. Conclusions

Four novel pyrene-BT alternating copolymers were synthesised via Stille coupling. 2-Hexyldecyl or 2-ethylhexyl chains were attached to the pyrene moiety to assess the impact this had on the properties of the resulting polymers. All of the polymers displayed good solubility in common organic solvents. GPC analysis showed that incorporation of 2-hexyldecyl chains allowed polymers to be obtained with higher molecular weights and enabled the additional intermolecular interactions brought about by fluorination of the BT moieties along polymer chains to be overcome. Thus, **PP_{HD}-DTBT** and **PP_{HD}-DTffBT** displayed similar number average molecular weights. **PP_{EH}-DTBT** and **PP_{EH}-DTffBT** displayed narrower optical band gaps relative to their analogous polymers, **PP_{HD}-DTBT** and **PP_{HD}-DTffBT**. Additionally, **PP_{EH}-DTBT** and **PP_{EH}-DTffBT** displayed shallower HOMO levels relative to their analogous polymers. Both of these phenomena can be attributed to shorter alkyl chains being attached to the pyrene donor. The shorter alkyl chains are less disrupting to intermolecular interactions when compared with the larger alkyl chains. Thus, polymers bearing shorter alkyl chains adopt a more planar structure in the solid state. This hypothesis was confirmed with PXRD studies, which showed polymers bearing 2-ethylhexyl chains possessed smaller lamellar and π-π stacking distances relative to polymers bearing 2-hexyldecyl chains. BHJ solar cells were fabricated from all polymers. $PC_{70}BM$ was used as the electron acceptor and blends of polymer:$PC_{70}BM$ ratios of 1:3 were investigated. All of the polymers displayed modest efficiencies. **PP_{EH}-DTBT** displayed the highest efficiency with a PCE of 1.86 %. Further studies into the optimization of the photovoltaic properties of these promising materials are underway.

2.4. References

1 M. Willander, S. C. Jain and K. Vikram, *Elsevier*, 2007, **81**.

2 B. Fu, J. Baltazar, Z. Hu, A.-T. Chien, S. Kumar, C. L. Henderson, D. M. Collard and E. Reichmanis, *Chem. Mater.*, 2012, **24**, 4123–4133.

3 Z. B. Henson, K. Müllen and G. C. Bazan, *Nat. Chem.*, 2012, **4**, 699–704.

4 T. Xu and L. Yu, *Mater. Today*, 2014, **17**, 11–15.

5 P. P. Khlyabich, B. Burkhart, A. E. Rudenko and B. C. Thompson, *Polym.*, 2013, **54**, 5267–5298.

6 L. Lu, T. Zheng, Q. Wu, A. M. Schneider, D. Zhao and L. Yu, *Chem. Rev.*, 2015, **115**, 12666–12731.

7 I. H. Jung, D. Zhao, J. Jang, W. Chen, E. S. Landry, L. Lu, D. V Talapin and L. Yu, *Chem. Mater.*, 2015, **27**, 5941–5948.

8 H. Zhou, L. Yang, S. Stoneking and W. You, *ACS Appl. Mater. Interfaces*, 2010, **2**, 1377–1383.

9 H. Zhou, L. Yang and W. You, *Macromolecules*, 2012, **45**, 607–632.

10 A. Facchetti, *Mater. Today*, 2013, **16**, 123–132.

11 Y. Liu, J. Zhao, Z. Li, C. Mu, W. Ma, H. Hu, K. Jiang, H. Lin, H. Ade and H. Yan, *Nat. Commun.*, 2014, **5**.

12 N. Wang, Z. Chen, W. Wei and Z. Jiang, *J. Am. Chem. Soc.*, 2013, **135**, 17060–17068.

13 H. Yi, S. Al-Faifi, A. Iraqi, D. C. Watters, J. Kingsley and D. G. Lidzey, *J. Mater. Chem.*, 2011, **21**, 13649–13656.

14 Y. Wang, X. Xin, Y. Lu, T. Xiao, X. Xu, N. Zhao, X. Hu, B. S. Ong and S. C. Ng, *Macromolecules*, 2013, **46**, 9587–9592.

15 T. M. Figueira-Duarte and K. Müllen, *Chem. Rev.*, 2011, **111**, 7260–7314.

16 E. L. Williams, T. S. Ang, Z. Ooi, P. Sonar, T. T. Lin, W. T. Neo, J. Song and J. Hobley,

Polymers, 2014, **7**, 69–90.

17 P. Sonar, S. P. Singh, E. L. Williams, Y. Li, M. S. Soh and A. Dodabalapur, *J. Mater. Chem.*, 2012, **22**, 4425–4435.

18 M. S. Almeataq, H. Yi, S. Al-Faifi, A. A. Alghamdi, A. Iraqi, N. W. Scarratt, T. Wang and D. G. Lidzey, *Chem. Commun.*, 2013, **49**, 2252–2254.

19 J. M. Casas-Solvas, J. D. Howgego and A. P. Davis, *Org. Biomol. Chem.*, 2014, **12**, 212–232.

20 N. Wang, X. Bao, Y. Yan, D. Ouyang, M. Sun, V. A. L. Roy, C. S. Lee and R. Yang, *J. Polym. Sci. Part A Polym. Chem.*, 2014, **52**, 3198–3204.

21 D. S. Yang, K. H. Kim, M. J. Cho, J. Jin and D. H. Choi, *J. Polym. Sci. Part A Polym. Chem.*, 2013, **51**, 1457–1467.

22 J.-H. Kim, H. U. Kim, I.-N. Kang, S. K. Lee, S.-J. Moon, W. S. Shin and D.-H. Hwang, *Macromolecules*, 2012, **45**, 8628–8638.

23 L. Cartwright, H. Yi and A. Iraqi, *New J. Chem.*, 2016, **40**, 1655-1662.

24 L. Cartwright, A. Iraqi, Y. Zhang, T. Wang and D. G. Lidzey, *RSC Adv.*, 2015, **5**, 46386–46394.

25 L. Cartwright, L. J. Taylor, H. Yi, A. Iraqi, Y. Zhang, N. W. Scarratt, T. Wang and D. G. Lidzey, *RSC Adv.*, 2015, **5**, 101607–101615.

26 P. Patel, T. R. Hull, R. E. Lyon, S. I. Stoliarov, R. N. Walters, S. Crowley and N. Safronava, *Polym. Degrad. Stab.*, 2011, **96**, 12–22.

27 T. Umeyama, Y. Watanabe, E. Douvogianni and H. Imahori, *J. Phys. Chem. C*, 2013, **117**, 21148–21157.

28 Z. Li, J. Lu, S.-C. Tse, J. Zhou, X. Du, Y. Tao and J. Ding, *J. Mater. Chem.*, 2011, **21**, 3226–3233.

29 A. Misra, P. Kumar, R. Srivastava, S. K. Dhawan, M. N. Kamalasanan and S. Chandra, *Indian J. Pure Appl. Phys.*, 2005, **44**, 921–925.

Chapter III:

Preparation and Photovoltaic Properties of Pyrene-Thieno[3,4-c]pyrrole-4,6-dione-Based Donor-Acceptor Polymers

Preparation and Photovoltaic Properties of Pyrene-Thieno[3,4-c]pyrrole-4,6-dione-Based Donor-Acceptor Polymers

Abstract

Four new donor-acceptor conjugated copolymers, containing pyrene moieties flanked by thienyl or bithienyl groups as a donor units and thieno[3,4-c]pyrrole-4,6-dione (TPD) as acceptor units, were prepared successfully via a direct arylation polymerisation method. While all of the polymers prepared had 2-ethylhexyloxy-substituents on the pyrene repeat units, two different alkyl-substituents (octyl or 4-hexylphenyl groups) were attached to their TPD moieties. The influence of these different substituents as well as the number of thienyl units linking the pyrene and TPD units along polymer chains on the photophysical, electronic and photovoltaic properties of these materials was investigated. All polymers displayed good thermal stability up to 315 °C. The optical band gap of the four polymers, **PP$_{EH}$DT-TPD$_{O}$**, **PP$_{EH}$DT-TPD$_{HP}$**, **PP$_{EH}$DT2-TPD$_{O}$** and **PP$_{EH}$DT2-TPD$_{HP}$**, were estimated to be 2.00, 2.06, 1.94 and 1.91 eV, respectively. Polymers that possessed a single thiophene unit attached to the pyrene unit, **PP$_{EH}$DT-TPD$_{O}$** and **PP$_{EH}$DT-TPD$_{HP}$**, displayed deeper HOMO levels compared to those with bithiophene units, **PP$_{EH}$DT2-TPD$_{O}$ and PP$_{EH}$DT2-TPD$_{HP}$**. Photovoltaic devices were fabricated from all polymers. **PP$_{EH}$DT2-TPD$_{O}$** boasted the highest efficiency with a PCE (2.06 %), a *FF* of 53.07 %, a J_{sc} of 4.66 mA/cm^2 and a V_{oc} of 0.83 V.

3.1. Introduction

Solar energy has proven to be a promising alternate energy source to the finite, environmentally harmful fossil fuels that are currently used as the world's main source of energy.[1] Inorganic solar cells, based on crystalline silicon, have demonstrated efficiencies in excess of 25 %.[2] However, their manufacturing costs, high embodied energy and temperature dependant performance have restricted the widespread use of this technology.[2,3] Consequently, research into alternative photovoltaic devices has been initiated. Organic photovoltaic devices, which utilise conjugated polymers and fullerene derivatives in the active layer, have shown promise as an alternative to traditional inorganic solar cells.[2,4] Organic solar cells possess several advantages over their inorganic counterparts including: abundant materials for fabrication, can be manufactured using low-cost solution based manufacturing on flexible substrates, are lightweight and can be recycled.[2,4] However, organic solar devices have three major disadvantages: stability, lifetime and efficiency.[5] Organic solar cells exhibit efficiencies lower than traditional devices, however, power conversion efficiencies exceeding 10 % have been recorded with these cells.[6] Work continues in order to improve the stability and efficiency of organic solar cells in order to make organic photovoltaics a sustainable technology.[6]

Traditional palladium-catalysed cross-coupling reactions (Suzuki or Stille) are used commonly in the preparation of conjugated polymers used in the active layer of organic photovoltaic devices.[7] These cross-coupling reactions involve the use of organo-boron or tin reagents which are expensive to prepare and toxic in the case of tin compounds.[8,9] These drawbacks have accelerated the development of alternative cross-coupling reactions. Amongst these methods, direct arylation polymerisation (DArP) has shown great promise as an alternative to traditional routes.[7,9] DArP activates the C-H bond of heteroarenes facilitating coupling to an aryl halide. This occurs without the need for organometallic reagents which minimises the number of synthetic steps.[7,9]

The thieno[3,4-c]pyrrole-4,6-dione (TPD) moiety has been extensively investigated for use in organic solar cells.[10,11] The TPD moiety possesses a high degree of structural symmetry and planarity, which can aid electronic delocalisation along the polymer backbone resulting in a low band gap and more efficient harvesting of sunlight. The electron deficient imide group renders the TPD moiety electron-deficient.[10,12] Thus, when polymerised with an electron-rich monomer, the TPD unit can form a highly advantageous donor-acceptor arrangement which can improve charge

transfer along the polymer backbone. Furthermore, the TPD moiety can be functionalised by attaching different solubilising groups to the nitrogen of the imide group.[13] Leclerc *et al.* initiated research into the TPD moiety by copolymerising TPD with benzodithiophene (BDT). The resulting copolymer exhibited an efficiency of 5.5 %.[14] Chu and co-workers synthesised the high molecular weight **PDTSTPD-C8** copolymer which demonstrated an efficiency of 7.5 % when fabricated into BHJ photovoltaic devices.[15] Recently, Clément *et al.* investigated the impact side chains have in **PBDTTPD** polymers and the influence they have on the efficiency of BHJ devices. The research group discovered that TPD moieties substituted with n-heptyl substituents exhibited devices with a power conversion efficiency up to 8.5 % and a V_{oc} of 0.97 V.[16]

Pyrene as a class of polycyclic aromatic hydrocarbons (PAHs) have been used in OLED, FET and recently OPV devices.[17,18] Pyrene-based conjugated polymers have gained little interest from researchers relative to others PAH compounds such as anthracene and naphthalene.[19,20] The main reason for the limited numbers of reports is the restricted methodology for the functionalization of the pyrene moiety. The majority of synthesis reported in the literature has investigated the substitution of pyrene at the "1,3,6,8", "2,7" and "4,5,9,10" positions.[17,21] Pyrene is an electron rich, planar and symmetrical unit that should display a strong π-π stacking.[22] Liu *et al.* reported the synthesis of series of pyrene-diketopyrrolopyrrole based oligomers for use in organic solar cells.[18] **$Py_2Ph_2Th_4(DPP)_3$** exhibited a low band gap of 1.60 eV. When fabricated into photovoltaic devices **$Py_2Ph_2Th_4(DPP)_3$** exhibited an efficiency of 3.71 %.[18] Recently, Wang *et al.* synthesised **PDTPy-alt-DPP** which demonstrated an efficiency of 4.43 % when fabricated into BHJ solar cells using $PC_{70}BM$ as an acceptor.[22]

In this chapter, we report the synthesis and characterisation of four novel D–A polymers comprising alternate pyrene and TPD units, which were used as the electron donor and electron acceptor, respectively. Poly((2,7-di(thien-2-yl)-4,5,9,10-tetrakis(2-ethylhexyloxy)-pyrene-*alt*-(5-octyl-thieno[3,4,c]pyrrole-4,6-dione)) (**$PP_{EH}DT\text{-}TPD_O$**), poly((2,7-di(thien-2-yl)-4,5,9,10-tetrakis(2-ethylhexyloxy)-pyrene-*alt*-(5-(4-hexylphenyl)-thieno[3,4-c]pyrrole-4,6-dione)) (**$PP_{EH}DT\text{-}TPD_{HP}$**), poly((2,7-di(2,2'-bithiophen-5-yl)-4,5,9,10-tetrakis(2-ethylhexyloxy)-pyrene-*alt*-(5-octyl-thieno[3,4,c]pyrrole-4,6-dione)) (**$PP_{EH}DT2\text{-}TPD_O$**) and poly((2,7-di(2,2'-bithiophen-5-yl)-4,5,9,10-tetrakis(2-ethylhexyloxy)-pyrene-*alt*-(5-(4-hexylphenyl)-thieno[3,4-c]pyrrole-4,6-dione)) (**$PP_{EH}DT2\text{-}TPD_{HP}$**) were synthesised via a direct arylation polymerisation

method (figure 3.1). Studies on the photophysical, electronic and photovoltaic properties of the four polymers are presented and discussed.

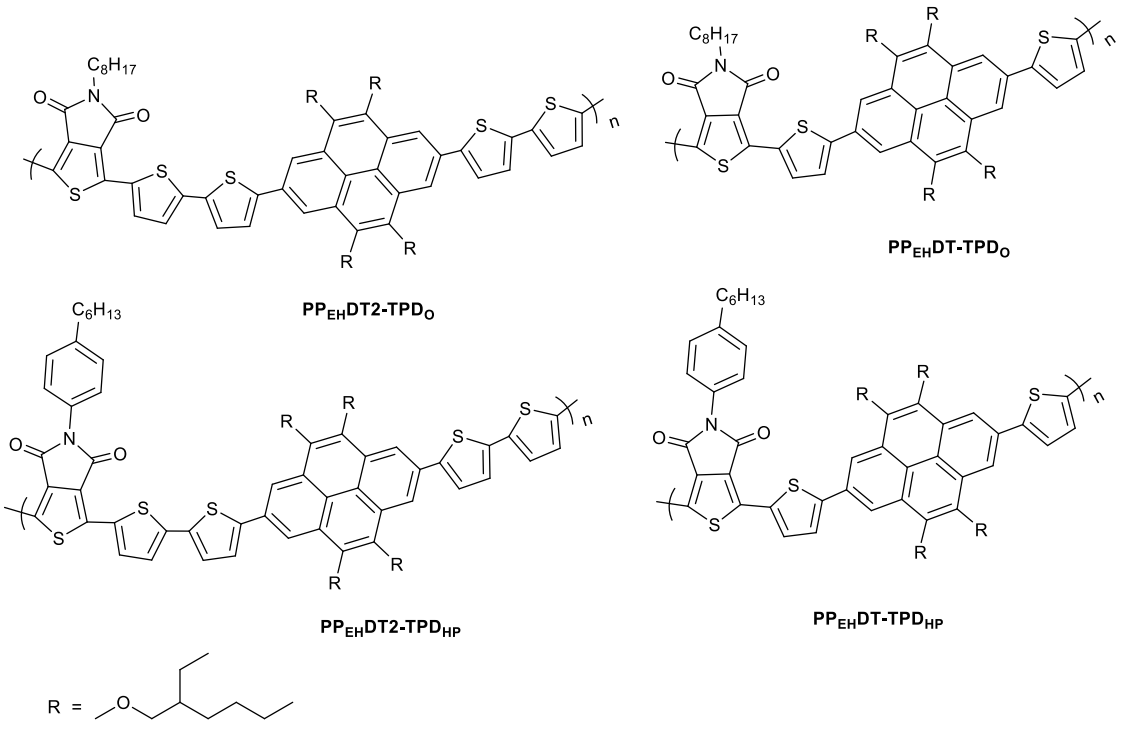

Figure 3.1. Structures of **PP$_{EH}$DT-TPD$_O$**, **PP$_{EH}$DT-TPD$_{HP}$**, **PP$_{EH}$DT2-TPD$_O$** and **PP$_{EH}$DT2-TPD$_{HP}$**.

3.2. Results and Discussions

3.2.1. Monomer synthesis

The synthetic steps of 2,7-bis(5-bromo-thien-2-yl)-4,5,9,10-tetrakis(2-ethylhexyloxy)-pyrene (**M4**) and 2,7-bis-(5'-bromo-[2,2']bithiophenyl-5-yl)-4,5,9,10-tetrakis(2-ethylhexyloxy)-pyrene (**M5**) are depicted in Scheme 3.1. The synthesis of 2,7-dibromo-4,5,9,10-tetrakis((2-ethylhexyl)oxy)pyrene (**M2**) was already described in Chapter II. Stille coupling of (**M2**) with 2-tributylstannylthiophene and with 2,2'-bithiophen-5-yl-trimethylstannane produced 2,7-di(thien-2-yl)-4,5,9,10-tetrakis(2-ethylhexyloxy)-pyrene (**7**) and 2,7-di(2,2'-bithiophen-5-yl)-4,5,9,10-tetrakis(2-ethylhexyloxy)-pyrene (**8**), respectively. Bromination of compound **7** and **8** using *N*-bromosuccinimide (NBS) yielded the target monomers, **M4** and **M5**, in yields of 84 and 95 %, respectively.

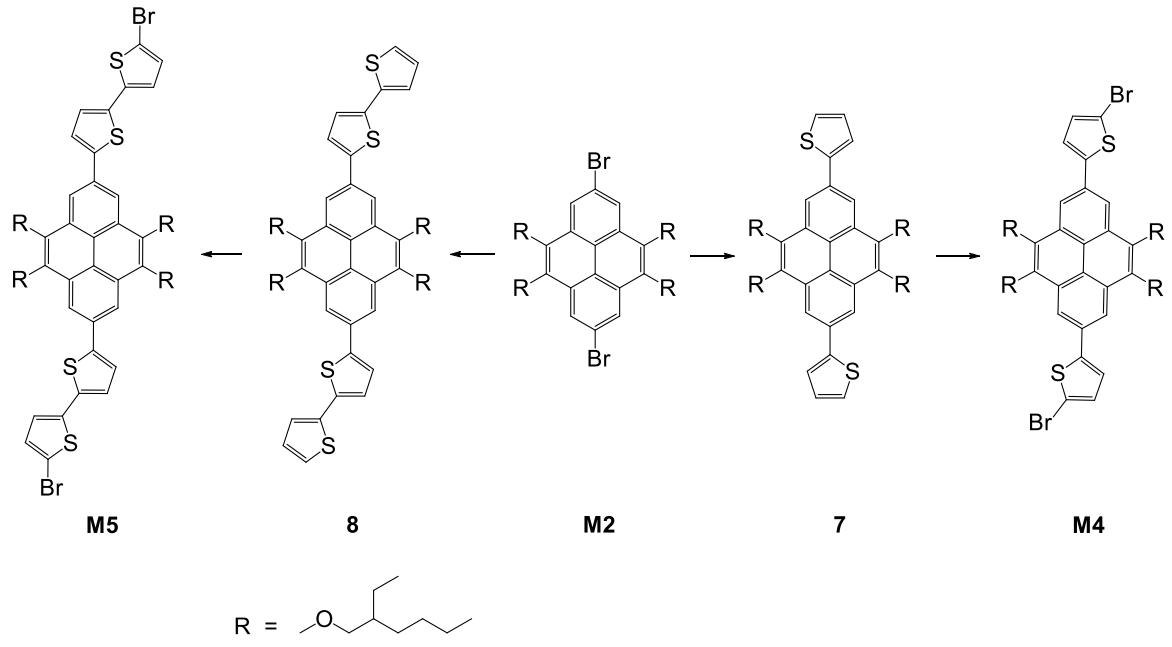

Scheme 3.1. Synthetic routes towards monomers **M4** and **M5**.

^{1}H NMR spectroscopy was employed to confirm the structures of the pyrene units. The ^{1}H NMR spectra of **M4** and **M5** are depicted in figure 3.2 and figure 3.3, respectively. The aromatic region of **M4** showed three resonances at 8.60, 7.37 and 7.17 ppm. The singlet resonance at 8.60 ppm was assigned to the protons on the pyrene unit, whereas the two doublets resonances at 7.37 and 7.17 ppm correlated to the protons located on the thiophene rings. The ^{1}H NMR spectra of **M5** exhibited the expected signals in the aromatic area to be singlet, doublet, doublet and doublets of doublet at 8.68, 7.54, 7.22 and 7.04 ppm, respectively. The resonances positioned below 4.40 ppm correspond to the protons located on the alkyl chains.

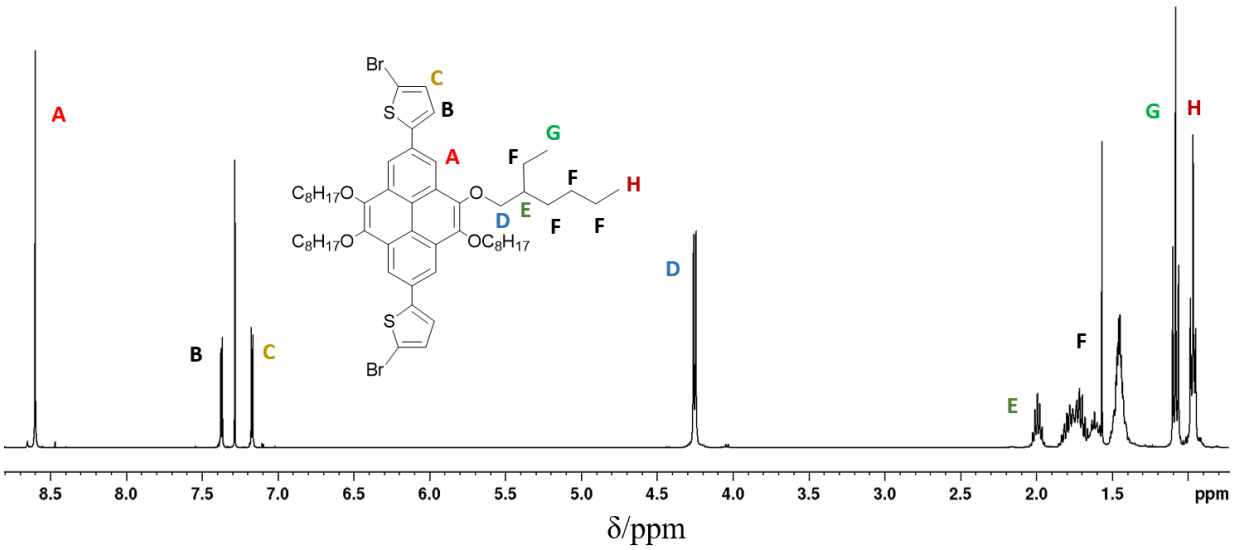

Figure 3.2. ^{1}H NMR spectrum of **M4** in $CDCl_3$.

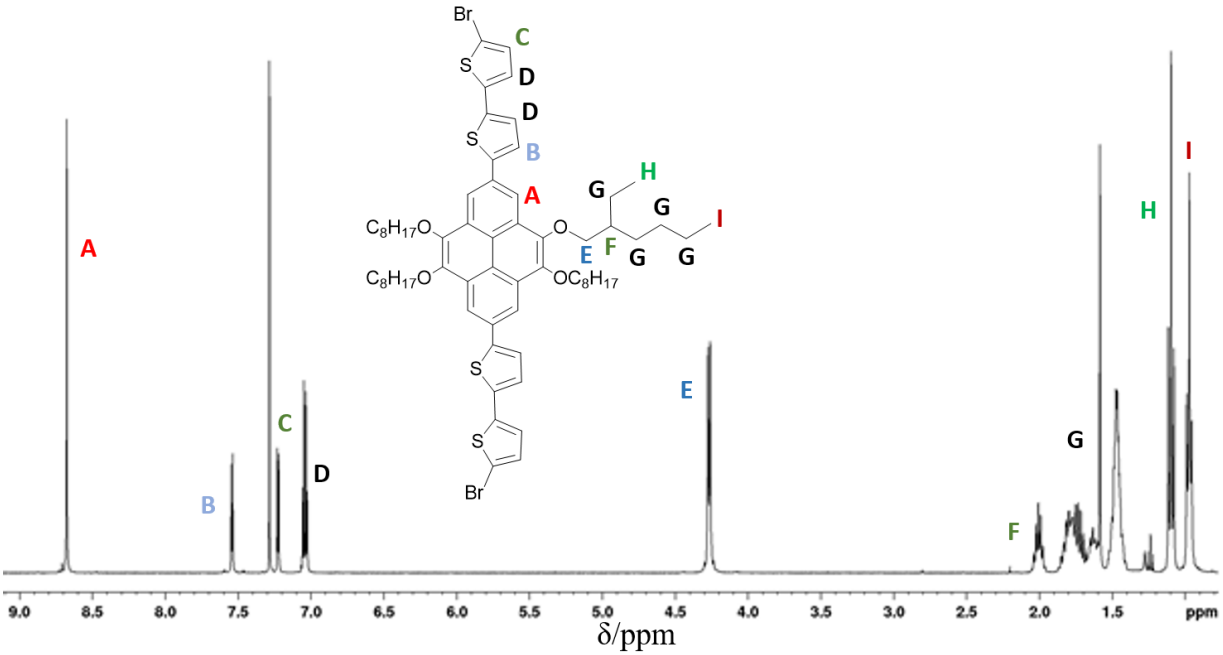

Figure 3.3. ^{1}H NMR spectrum of **M5** in $CDCl_3$.

The synthetic steps of 5-octyl-4H-thieno[3,4-c]pyrrole-4,6(5H)-dione[23] (**M6**) and 5-(4-hexylphenyl)-4H-thieno[3,4-c]pyrrole-4,6(5H)-dione (**M7**) are depicted in Scheme 3.2. Synthetic procedures are described in the experimental part.

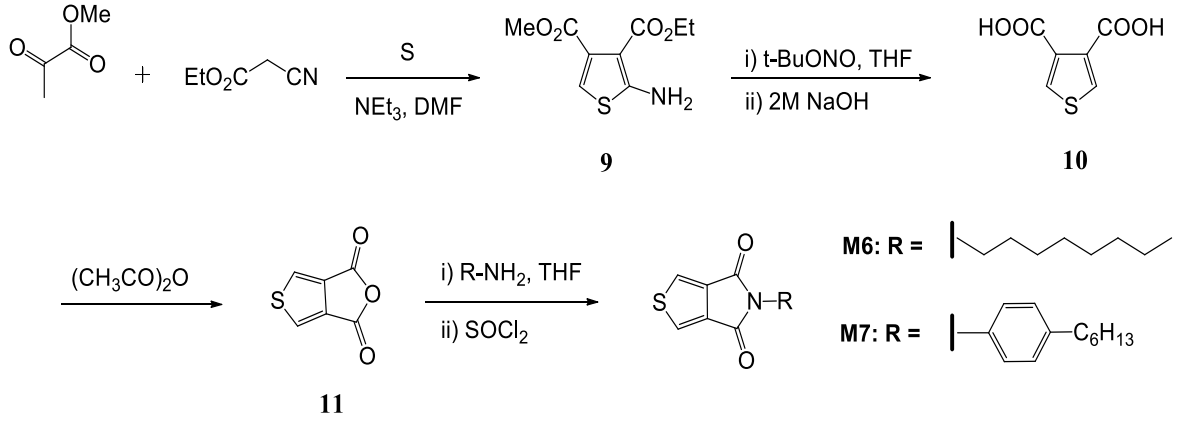

Scheme 3.2. Synthetic routes used to afford monomers **M6** and **M7**.

The first step in the synthesis of **M6** and **M7** is the preparation of 3-ethyl-4-methyl-2-aminothiophene-3,4-dicarboxylate (**9**). The synthesis of compound **9** was performed according to the Gewald reaction.[11] The reaction mechanism is shown in Scheme 3.3. The reaction process follows the condensation of methyl 2-oxopropanoate (the ketone) with ethyl cyanoactetate (α-active methylene nitrile) in the presence of sulfur and trimethylamine. The step of condensation of the ketone group with the activated nitrile under basic conditions resulted in the removal of water to produce the intermediate **a**. The reaction mechanism for the next steps of the reaction is not fully well-known. Though, it is expected that the addition of elemental sulfur in the presence of a base would thiolate the methylene group to produce ylidene-sulfur adduct (**b**) as an intermediate. Ring closing of the intermediate **b** followed by tautomerisation produced the target product.

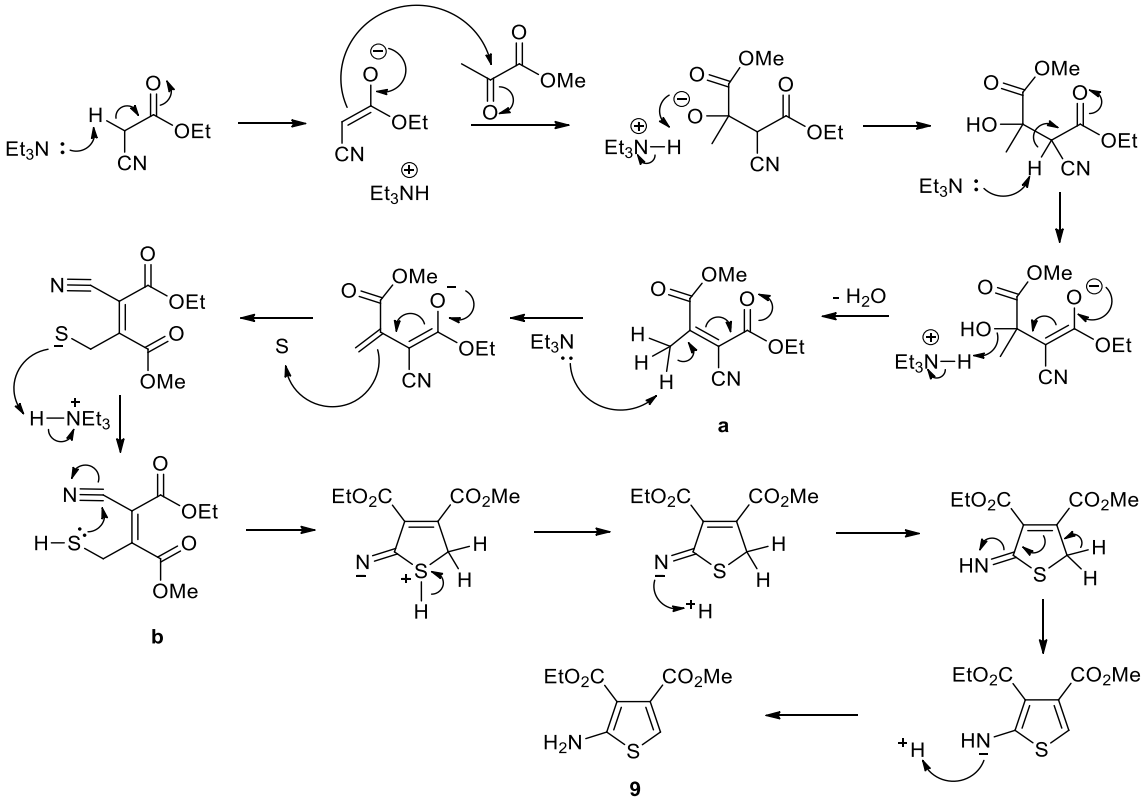

Scheme 3.3. Reaction mechanism of the production of compound **9**.

The second step in the synthesis of **M6** and **M7** was the preparation of thiophene-3,4-dicarboxylic acid (**10**) which first involves a modified Sandmeyer reaction using *t*-butyl nitrite in order to eliminate the tertiary amine group, which result in the formation of 3-ethyl 4-methyl thiophene-3,4-dicarboxylate (**c**) as an intermediate. The reaction mechanism is shown in Scheme 3.4. A simple ester hydrolysis of the intermediate, **c**, resulted in the formation of the target product (**10**).

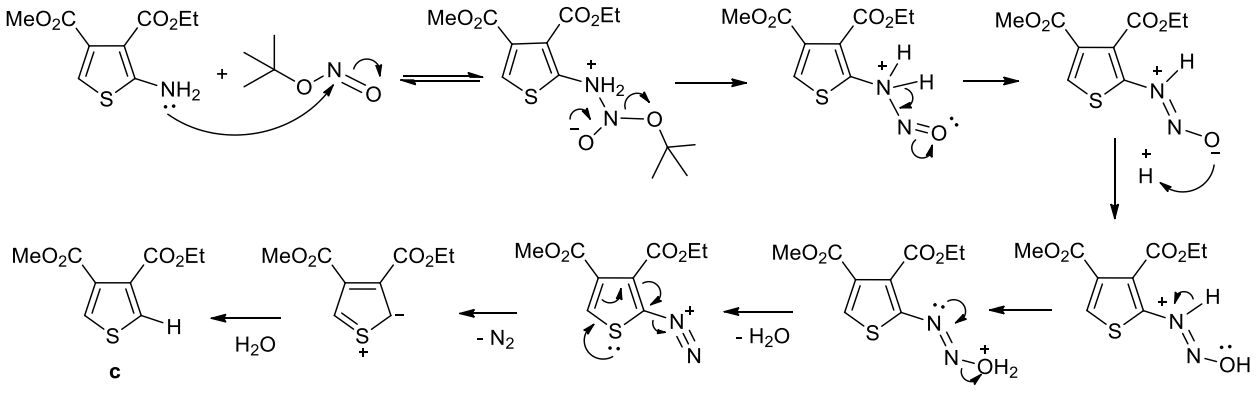

Scheme 3.4. Reaction mechanism of the formation of intermediate **c**.

Thieno[3,4-c]furan-1,3-dione (**11**) was prepared by heating compound **10** in acetic anhydride which is employed as a dehydrating agent leading to the formation of the cyclic anhydride (**11**) via loss of water.

The last step in the preparation of the TPD monomers included the reaction of the cyclic anhydride material (**11**) with a primary amine, *n*-octylamine or 4-hexylaniline, followed by reaction with thionyl chloride to yield the target monomers, **M6** and **M7**, respectively. The reaction mechanism is shown in Scheme 3.5. The introduction of solubilising groups into the molecular would enhance the solubility of the resultant monomer and also would create an electron accepting imide group which is an important aspect for the monomer electron accepting characteristics.

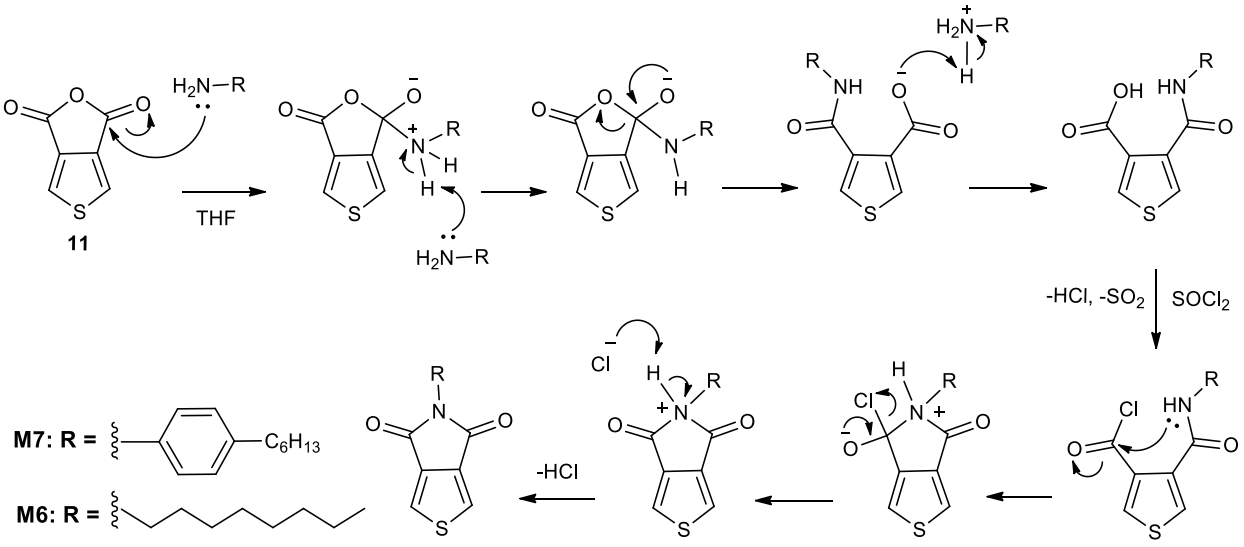

Scheme 3.5. Reaction mechanism of **M6** and **M7**.

The structures of the two monomers were confirmed by ^{1}H NMR spectroscopy. The ^{1}H NMR spectra of **M6** and **M7** are depicted in figure 3.4 and figure 3.5, respectively. The aromatic region of both monomers showed a singlet resonance at 7.82 ppm which assign to the protons on the thiophene unit. The spectrum of **M7** displayed a splitting pattern with a quartet resonance positioned at 7.31 ppm. The resonances positioned below 3.80 ppm corresponded to the protons located on the alkyl chains.

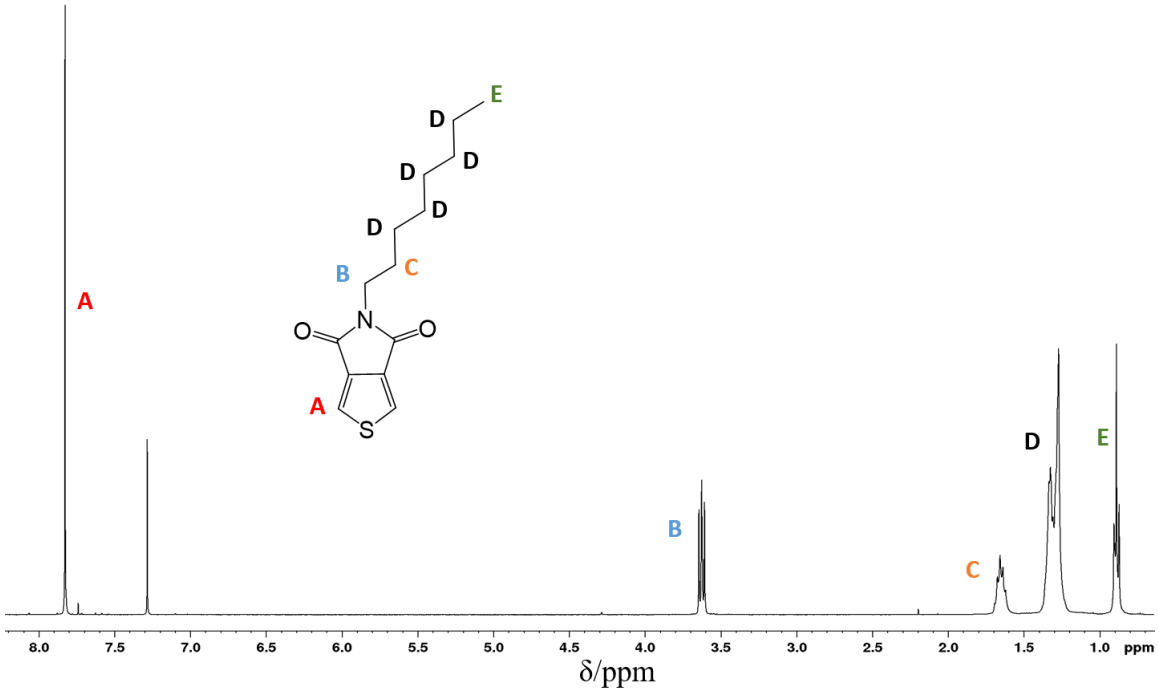

Figure 3.4. ^{1}H NMR spectrum of **M6** in $CDCl_3$.

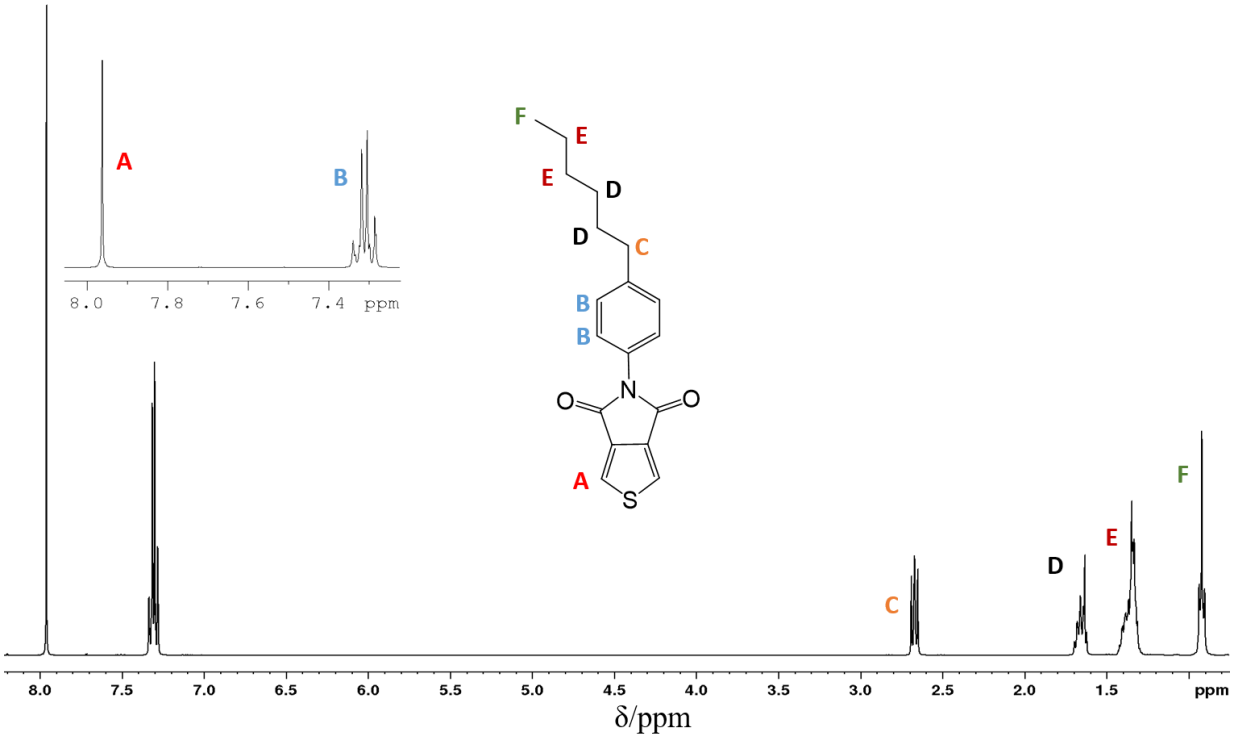

Figure 3.5. ^{1}H NMR spectrum of **M7** in $CDCl_3$.

3.2.2. Polymer synthesis

The four polymers were prepared *via* direct arylation polymerization. $PdCl_2(MeCN)_2$ and $P(C_6H_4$-o-$OMe)_3$ were used as the catalyst and caesium carbonate (Cs_2CO_3) as the base. Pivalic acid (PivOH) was used as the carboxylate source and THF as the solvent. Previous literature has shown that a carboxylate source is essential for direct arylation.[24] The carboxylate source generates a palladium carboxylate, which breaks the C-H bond of heteroarenes facilitating the cross-coupling reaction. A suggested mechanism is shown in scheme 3.6.

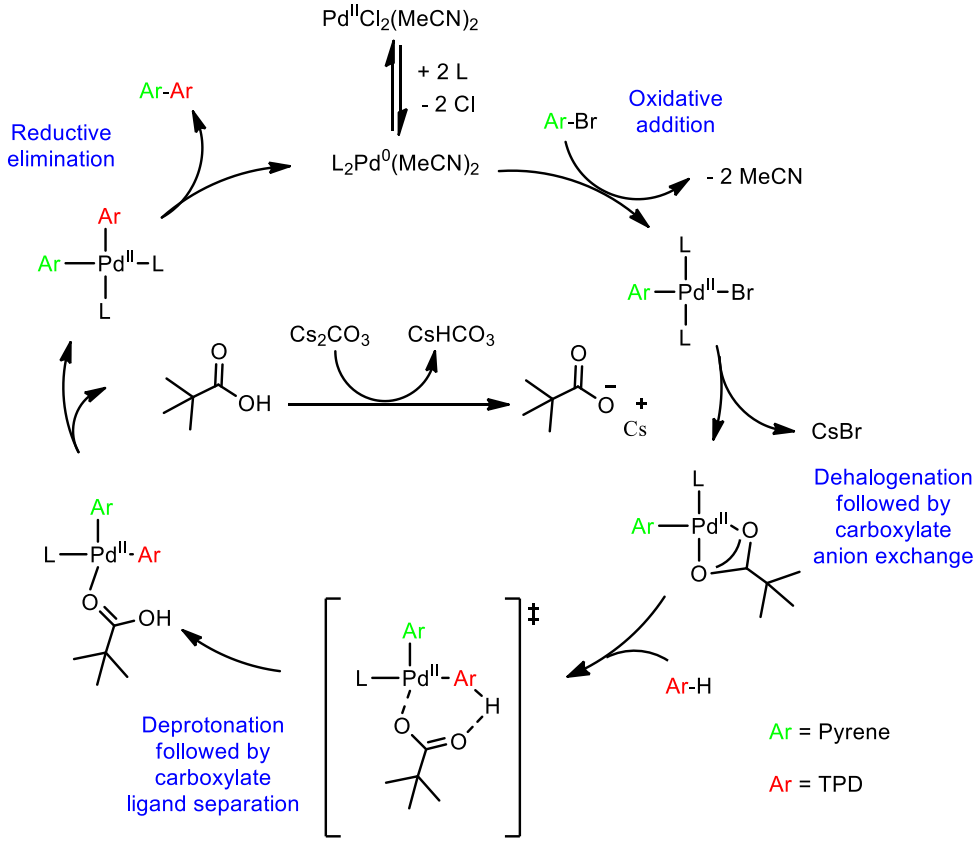

Scheme 3.6. Suggested mechanism for the direct arylation reaction.

The polymerisations of **PP$_{EH}$DT-TPD$_O$** and **PP$_{EH}$DT-TPD$_{HP}$** were left for 48 hours. In contrast, the polymerisation of **PP$_{EH}$DT2-TPD$_O$** and **PP$_{EH}$DT2-TPD$_{HP}$** were left for 2 and 5 hours respectively, as in the preparation of the latter two polymers, large quantities of precipitate formed at the early stages of the reactions. The crude polymers were purified *via* Soxhlet extraction using methanol, acetone and hexane to remove catalytic residues and oligomers. Toluene and chloroform were then used in succession to extract the polymers. **PP$_{EH}$DT-TPD$_{HP}$** provided most of its high

molecular weight fraction from the toluene fraction while for **PP$_{EH}$DT-TPD$_O$**, **PP$_{EH}$DT2-TPD$_O$** and **PP$_{EH}$DT2-TPD$_{HP}$**, the chloroform fractions extracted the desired fractions of the polymers.

The chemical structures of **PP$_{EH}$DT-TPD$_O$**, **PP$_{EH}$DT-TPD$_{HP}$**, **PP$_{EH}$DT2-TPD$_O$** and **PP$_{EH}$DT2-TPD$_{HP}$** were confirmed by ^{1}H NMR spectroscopy and elemental analysis. The number average molecular weight (M_n) and weight average molecular weight (M_w) of all polymers were estimated from high temperature (140 °C) gel permission chromatography (GPC) analysis using a series of polystyrene standards, and 1,2,4-trichlorobenzene (TCB) as the eluent. The data is summarized in Table 3.1. Polymers that are substituted with the aromatic 4-hexylphenyl groups displayed lower molecular weights relative to their counterparts with octyl substituents. It is speculated that the planar aromatic ring attached to the TPD moieties in these polymers promotes planarity and aggregation of polymer backbones, which impedes the extent of their degree of polymerisation. Polymers that incorporate bithiophene units between the pyrene and TPD units (**PP$_{EH}$DT2-TPD$_O$** and **PP$_{EH}$DT2-TPD$_{HP}$**) exhibited lower molecular weights relative to their counterparts which possess a single thiophene unit. When compared to thiophene, the bithiophene unit possesses extended π-conjugation, which promotes aggregation of polymer chains and a reduced molecular weight.

Table 3.1. GPC, optical and electrochemical data for **PP$_{EH}$DT-TPD$_O$**, **PP$_{EH}$DT-TPD$_{HP}$**, **PP$_{EH}$DT2-TPD$_O$** and **PP$_{EH}$DT2-TPD$_{HP}$**

Polymers	M_n (Da)[c]	M_w (Da)[c]	PDI	λ_{max} (nm)		$E_{g\ opt}$ (eV)[d]	HOMO (eV)[e]	LUMO (eV)[f]	E_g^{ele} (eV)[g]
				Solution	Film				
PP$_{EH}$DT-TPD$_O$[a]	19700	38400	1.95	474	529	2.00	-5.57	-3.59	1.98
PP$_{EH}$DT-TPD$_{HP}$[b]	5700	8700	1.53	469	489	2.06	-5.55	-3.54	2.01
PP$_{EH}$DT2-TPD$_O$[a]	9100	12700	1.40	517	564	1.94	-5.50	-3.52	1.98
PP$_{EH}$DT2-TPD$_{HP}$[a]	5500	9200	1.67	499	532	1.91	-5.46	-3.51	1.95

[a]Measurements conducted on the chloroform fraction of the polymers. [b]Measurements conducted on the toluene fraction of the polymers. [c]Determined by GPC in 1,2,4-trichlorobenzene at 140 °C. [d]Optical band gap. [e]HOMO level determined from the onset of oxidation. [f]LUMO level determined from the onset of reduction. [g]Electrochemical band gap.

3.2.3. UV-vis absorption spectroscopy

The UV-vis absorption spectra of **$PP_{EH}DT\text{-}TPD_O$, $PP_{EH}DT\text{-}TPD_{HP}$**, **$PP_{EH}DT2\text{-}TPD_O$** and **$PP_{EH}DT2\text{-}TPD_{HP}$** were recorded in chloroform solution (Figure 3.6.a) and thin film (Figure 3.6.b). The results are summarized in Table 3.1. All polymers displayed absorption bands in the range of 300-450 nm and 450-750 nm. The bands located at short wavelengths can be attributed to the π–π* transitions of the conjugated backbone, while those located at long wavelengths correspond to intramolecular charge transfer (ICT) bands along the conjugated polymer backbone from the electron rich unit (the pyrene moieties flanked by thienyl or dithienyl units) to the electron deficient unit (the TPD moiety). In dilute chloroform solutions, the ICT band of **$PP_{EH}DT\text{-}TPD_O$, $PP_{EH}DT\text{-}TPD_{HP}$**, **$PP_{EH}DT2\text{-}TPD_O$** and **$PP_{EH}DT2\text{-}TPD_{HP}$** are positioned at 474, 469, 517 and 499 nm, respectively. In thin film this was red-shifted to 529, 489, 564 and 532 nm for **$PP_{EH}DT\text{-}TPD_O$**, **$PP_{EH}DT\text{-}TPD_{HP}$**, **$PP_{EH}DT2\text{-}TPD_O$** and **$PP_{EH}DT2\text{-}TPD_{HP}$**, respectively. The red-shifts indicate that the polymers adopt more ordered, planar structures in the solid state.

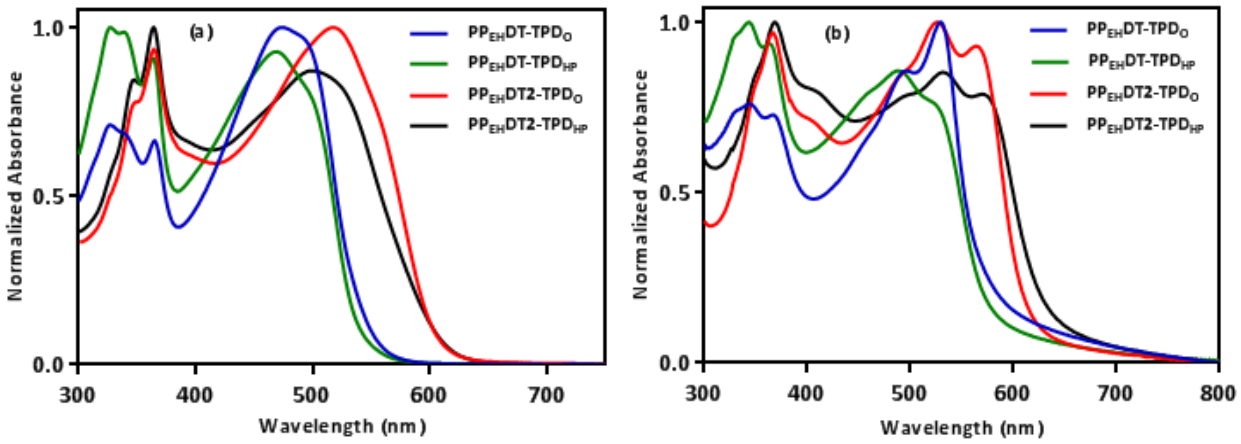

Figure 3.6. Normalised UV-vis absorption spectra of **$PP_{EH}DT\text{-}TPD_O$**, **$PP_{EH}DT\text{-}TPD_{HP}$**, **$PP_{EH}DT2\text{-}TPD_O$** and **$PP_{EH}DT2\text{-}TPD_{HP}$** in: (a) chloroform solutions; and (b) thin films.

Shoulder peaks appeared in the solid state, at longer wavelengths for all polymers. Interestingly, these shoulder peaks are not very prominent in solution. This phenomenon can be attributed to more ordered structures of polymer backbones in the solid state and is believed to arise from a pronounced stacking and aggregation of polymer chains in films. **$PP_{EH}DT2\text{-}TPD_O$** and **$PP_{EH}DT2\text{-}TPD_{HP}$**, which possess bithiophene spacer units, display red shifted absorption maxima, relative to their analogous polymers that contain single thiophene units. This can be attributed to the

extended conjugation length of the bithiophene unit, which yields a more planar conformation. Furthermore, the electron donating properties of the bithiophene units are higher than those of a single thiophene unit leading to more pronounced intramolecular charge transfer between the donor and acceptor units. The optical band gaps of **PP$_{EH}$DT-TPD$_{O}$, PP$_{EH}$DT-TPD$_{HP}$**, **PP$_{EH}$DT2-TPD$_{O}$** and **PP$_{EH}$DT2-TPD$_{HP}$** were estimated to be 2.00, 2.06, 1.94 and 1.91 eV, respectively. **PP$_{EH}$DT2-TPD$_{O}$** and **PP$_{EH}$DT2-TPD$_{HP}$** exhibited narrower optical band gaps relative to **PP$_{EH}$DT-TPD$_{O}$** and **PP$_{EH}$DT-TPD$_{HP}$**. The bithiophene unit enhances intramolecular charge transfer along the polymer backbone, increasing the electron delocalization leading to a lower optical band gap.

PP$_{EH}$DT-TPD$_{O}$, **PP$_{EH}$DT-TPD$_{HP}$**, **PP$_{EH}$DT2-TPD$_{O}$** and **PP$_{EH}$DT2-TPD$_{HP}$** are similar polymers to anthracene-TPD based polymers prepared by Cartwright *et al*.[25] TIPS-functionalized anthracene was used as an electron donor instead of pyrene moiety.[25] **PTATPD(O)**, **PTATPD(DMO)**, and **PTATPD(BP)** were synthesised with optical band gaps of 2.16, 2.14, and 2.12 eV, respectively. The pyrene-TPD based copolymers synthesised in this contribution exhibited lower optical band gaps relative to those prepared by Cartwright *et al.*[25] This can be ascribed to the additional benzene ring in the pyrene moiety which increases the conjugation length, producing higher coplanar polymer structures that increases π-π stacking in the thin films. However, it should be noted that the anthracene-TPD based copolymers did not possess any thiophene spacer units.[25] The authors speculated that the lack of a spacer unit yield large amounts of intramolecular steric repulsion between solubilising groups along polymer chains which reduces the planarity and decreased the electronic conjugation.[25] Work conducted within this chapter suggests that the incorporation of spacer units, thiophene or bithiophene, minimises these intramolecular steric repulsions facilitating the formation of more planar polymer backbones with lower optical band gaps.

3.2.4. Thermal properties

The thermal characteristics of all polymers were investigated via thermogravimetric analysis (TGA). The analysis was conducted in an inert nitrogen atmosphere using a heating rate of 10°C min^{-1}. All polymers showed good thermal stabilities with degradation temperatures (5 % weight loss) in excess of 300 °C (Figure 3.7). **PP$_{EH}$DT-TPD$_{O}$, PP$_{EH}$DT-TPD$_{HP}$, PP$_{EH}$DT2-TPD$_{O}$** and **PP$_{EH}$DT2-TPD$_{HP}$** showed two decomposition temperatures occurring at 321/516, 320/472, 330/513 and 316/500 °C, respectively. The initial weight-loss corresponds to the loss of the alkyl

chains from the pyrene unit. The second decomposition phase can be attributed to degradation of the residual polymer backbone.

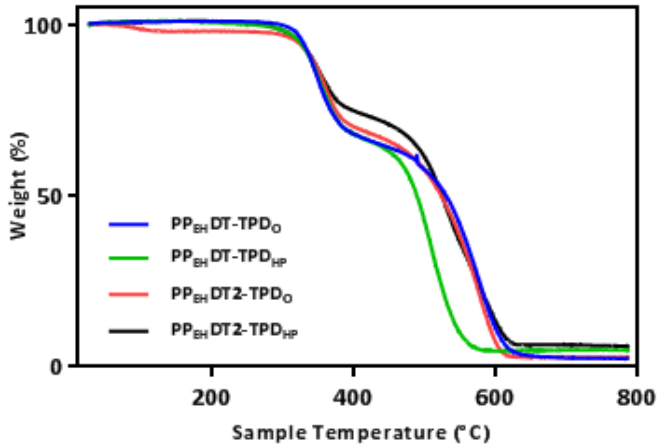

Figure 3.7. TGA curves of **$PP_{EH}DT\text{-}TPD_O$**, **$PP_{EH}DT\text{-}TPD_{HP}$**, **$PP_{EH}DT2\text{-}TPD_O$** and **$PP_{EH}DT2\text{-}TPD_{HP}$**.

3.2.5. Cyclic Voltammetry

The electrochemical properties of **$PP_{EH}DT\text{-}TPD_O$**, **$PP_{EH}DT\text{-}TPD_{HP}$**, **$PP_{EH}DT2\text{-}TPD_O$** and **$PP_{EH}DT2\text{-}TPD_{HP}$** were analysed using cyclic voltammetry (CV) (Figure 3.8). The CV measurements were performed under an inert atmosphere of argon on drop-cast polymer thin films with a scan rate of 100 mV s^{-1}. The analysis was conducted in a tetrabutylammonium perchlorate electrolyte solution. The HOMO and LUMO energy levels were calculated from the onset of the oxidation and reduction, respectively. The data is summarised in Table 3.1. The HOMO/LUMO energy levels of **$PP_{EH}DT\text{-}TPD_O$**, **$PP_{EH}DT\text{-}TPD_{HP}$**, **$PP_{EH}DT2\text{-}TPD_O$** and **$PP_{EH}DT2\text{-}TPD_{HP}$** were estimated to be -5.57/-3.59, -5.55/-3.54, -5.50/-3.52 and -5.46/-3.51 eV, respectively. Polymers that possess a single thiophene spacer unit, **$PP_{EH}DT\text{-}TPD_O$** and **$PP_{EH}DT\text{-}TPD_{HP}$**, displayed deeper HOMO levels relative to those with bithiophene units, **$PP_{EH}DT2\text{-}TPD_O$** and **$PP_{EH}DT2\text{-}TPD_{HP}$**. The shallower HOMO levels of polymers incorporating bithiophene units is a consequence of increased intramolecular charge transfer along the polymer backbone; a finding consistent with the lower optical band gaps of **$PP_{EH}DT2\text{-}TPD_O$** and **$PP_{EH}DT2\text{-}TPD_{HP}$** relative to **$PP_{EH}DT\text{-}TPD_O$** and **$PP_{EH}DT\text{-}TPD_{HP}$**.

Both of **$PP_{EH}DT\text{-}TPD_{HP}$** and **$PP_{EH}DT2\text{-}TPD_{HP}$** which have 4-hexylphenyl substituents on their TPD units have exhibited slightly shallower HOMO levels relative to their analogous polymers **$PP_{EH}DT\text{-}TPD_{O}$** and **$PP_{EH}DT2\text{-}TPD_{O}$** which have octyl substituents on their TPD units. This can be attributed to the higher electron donating properties of the 4-hexylphenyl substituents when compared to those of octyl chains. This as a result reduces the electron accepting properties of the TPD units which in turns reduces the intramolecular charge transfer between donor and acceptor units along polymer chains and provides slightly shallower HOMO levels as well as LUMO levels that are slightly closer to the vacuum level. The LUMO values of all polymers are higher than the LUMO level of $PC_{70}BM$ (-3.90 eV).[26] Previous literature has shown that a minimum energy offset of 0.3 eV between the LUMO of the p-type material (conjugated polymer) and the n-type material (fullerene derivative) is enough to facilitate efficient exciton dissociation.[10] All polymers synthesised in this contribution display an energy offset in excess of this 0.3 eV minimum. Therefore, all polymers should display efficient exciton dissociation when fabricated into BHJ photovoltaic devices. The electrochemical band gaps (E_g^{elc}) of **$PP_{EH}DT\text{-}TPD_{O}$, $PP_{EH}DT\text{-}TPD_{HP}$, $PP_{EH}DT2\text{-}TPD_{O}$** and **$PP_{EH}DT2\text{-}TPD_{HP}$** were estimated to be 1.98, 2.01, 1.98 and 1.95 eV, respectively. The E_g^{elc} of the four polymers are comparable to their optical band gaps.

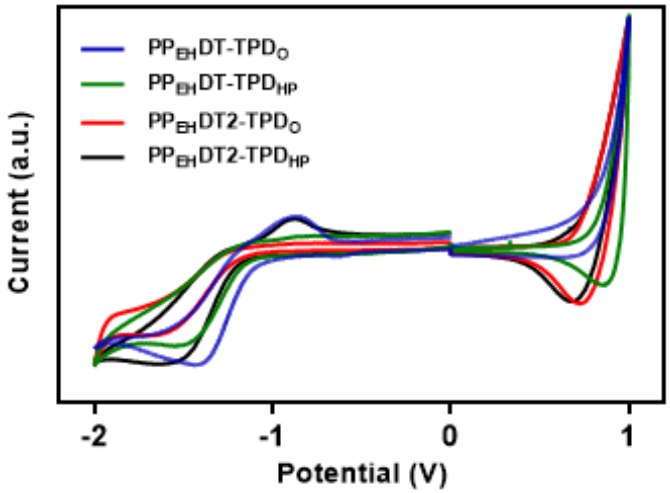

Figure 3.8. Cyclic voltammograms of **$PP_{EH}DT\text{-}TPD_{O}$**, **$PP_{EH}DT\text{-}TPD_{HP}$**, **$PP_{EH}DT2\text{-}TPD_{O}$** and **$PP_{EH}DT2\text{-}TPD_{HP}$**.

3.2.6. Powder X-ray diffraction (PXRD)

The molecular organization and crystallinity of **PP$_{EH}$DT-TPD$_O$**, **PP$_{EH}$DT-TPD$_{HP}$**, **PP$_{EH}$DT2-TPD$_O$** and **PP$_{EH}$DT2-TPD$_{HP}$** in solid state were investigated by powder X-ray diffraction (PXRD) (Figure 3.9). For efficient charge transport and high performance BHJ devices, polymer chains need to display well-ordered structures in the solid-state.[27] **PP$_{EH}$DT-TPD$_O$** and **PP$_{EH}$DT-TPD$_{HP}$** both demonstrated small peaks in the small angle region at 2θ values of 3.85 and 3.62°, respectively, which correspond to lamellar stacking distances of 22.9 and 24.4 Å, respectively. **PP$_{EH}$DT-TPD$_O$** and **PP$_{EH}$DT-TPD$_{HP}$** also display a broad diffuse peak in the wide angle at a 2θ value of 21.0°, which corresponds to a π – π stacking distance of 4.22 Å. **PP$_{EH}$DT-TPD$_{HP}$** exhibited a larger lamellar stacking distance relative to **PP$_{EH}$DT-TPD$_O$**, which can be attributed to the sterically bulky 4-hexylphenyl group attached to the TPD moiety. The same phenomenon is observed when comparing **PP$_{EH}$DT2-TPD$_O$** and **PP$_{EH}$DT2-TPD$_{HP}$**. They also revealed a similar lamellar distance to **PP$_{EH}$DT-TPD$_O$** and **PP$_{EH}$DT-TPD$_{HP}$** with lamellar stacking distances of 22.9 and 24.4 Å, respectively. Both **PP$_{EH}$DT2-TPD$_O$** and **PP$_{EH}$DT2-TPD$_{HP}$** displayed a reduced π – π stacking distance of 3.61 Å relative to **PP$_{EH}$DT-TPD$_O$** and **PP$_{EH}$DT-TPD$_{HP}$**. The results suggest that polymers containing bithiophene spacer units adopt a more defined arrangement in solid state because of the extended electronic conjugation brought about by the incorporation of bithiophene spacer units.

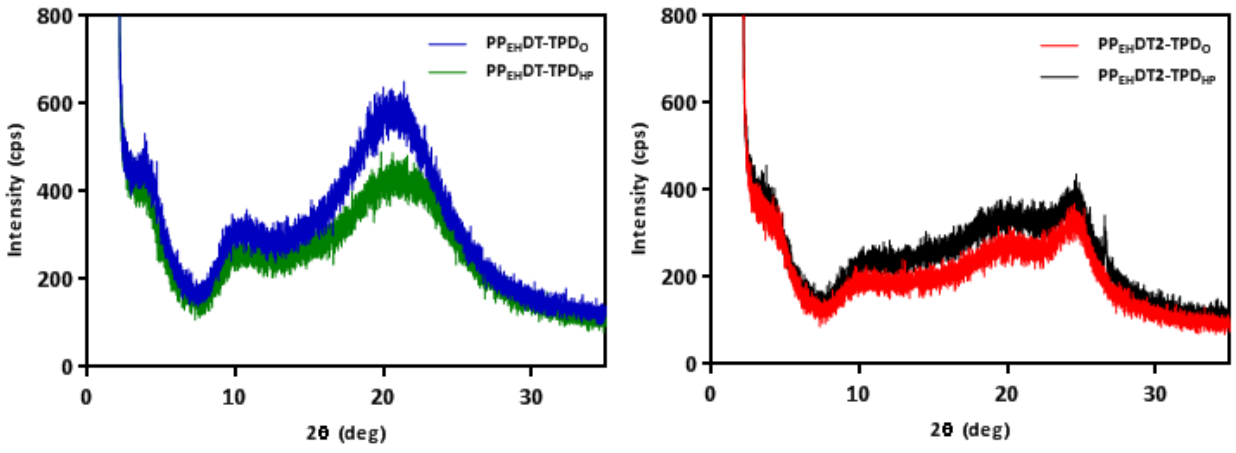

Figure 3.9. PXRD patterns of **PP$_{EH}$DT-TPD$_O$**, **PP$_{EH}$DT-TPD$_{HP}$**, **PP$_{EH}$DT2-TPD$_O$** and **PP$_{EH}$DT2-TPD$_{HP}$**.

3.2.7. Photovoltaic Properties

Preliminary photovoltaic measurements of **PP$_{EH}$DT-TPD$_{O}$**, **PP$_{EH}$DT-TPD$_{HP}$**, **PP$_{EH}$DT2-TPD$_{O}$** and **PP$_{EH}$DT2-TPD$_{HP}$** were conducted on a series of Glass/ITO/PEDOT:PSS/Polymer:$PC_{70}BM$/Ca/Al devices using blends of polymer:$PC_{70}BM$ in weight ratios 1:3. Chlorobenzene was used as the processing solvent. The *J-V* characteristic curves of the highest performance devices are shown in Figure 3.10. The results are summarised in Table 3.2. **PP$_{EH}$DT-TPD$_{O}$** exhibited the highest open circuit voltage in this series of polymers with a V_{oc} value of 0.92 V. This finding is in agreement with the deep HOMO level of the polymer in comparison to the other polymers. However, the power conversion efficiency (PCE) of devices made with **PP$_{EH}$DT-TPD$_{O}$** are only 0.33 % as a result of the poor short-circuit currents observed (J_{sc} = 0.84 mA/cm^2). A similar PCE of 0.33 % was observed from **PP$_{EH}$DT-TPD$_{HP}$** which was also chiefly as a result of a low Jsc value (1.09 mA/cm^2).

The photovoltaic results suggest that polymers which incorporate a bithiophene spacer unit display higher efficiencies when compared to those which incorporate single thiophene spacers. Photovoltaic devices fabricated from **PP$_{EH}$DT2-TPD$_{O}$** displayed the highest PCE with a value of 2.06 %. The device demonstrated a *FF* of 53.07 %, a J_{sc} 4.66 mA/cm^2 and a V_{oc} of 0.83 V. In contrast, **PP$_{EH}$DT2-TPD$_{HP}$** displayed a lower PCE (1.46 %) with a *FF* of 46.74 %, J_{sc} 3.69 mA/cm^2 and a V_{oc} of 0.85 V. It is hypothesised that the higher efficiency of **PP$_{EH}$DT2-TPD$_{O}$**, relative to **PP$_{EH}$DT2-TPD$_{HP}$**, as well as to **PPEHDT-TPD$_{HP}$** and **PP$_{EH}$DT-TPD$_{O}$**, is a result of improved packing of polymer chains in polymer : $PC_{70}BM$ blends. This yields improved charge mobility and extraction of photo-generated charge carriers. However, atomic force microscopy images and external quantum efficiency measurements are required to confirm this hypothesis.

The four polymers prepared within this chapter exhibited relatively low power conversion efficiencies when compared with the reported TPD-based copolymers in the literature. For example, Leclerc *et al.* copolymerised TPD moiety with benzodithiophene (BDT) as the electron donor.[14] The resulting polymer, **PBDTTPD**, showed an efficiency of 5.5 %, which is higher than **PP$_{EH}$DT-TPD$_{O}$**, **PP$_{EH}$DT-TPD$_{HP}$**, **PP$_{EH}$DT2-TPD$_{O}$** and **PP$_{EH}$DT2-TPD$_{HP}$**. It is believed that the higher efficiency of **PBDTTPD** is due to its smaller optical band gap (1.8 eV) as well as to its higher J_{sc} (9.81 mA cm^{-2}) and *FF* (66 %) values.

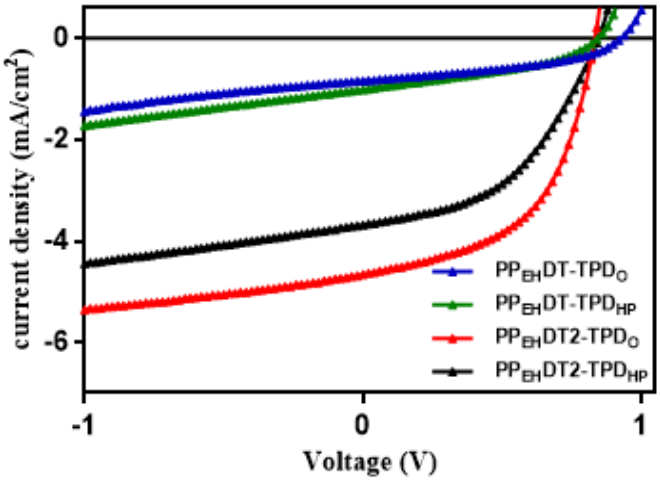

Figure 3.10. The J-V characteristic curves of **$PP_{EH}DT\text{-}TPD_O$**, **$PP_{EH}DT\text{-}TPD_{HP}$**, **$PP_{EH}DT2\text{-}TPD_O$** and **$PP_{EH}DT2\text{-}TPD_{HP}$**.

Table 3.2. Device Performance of **$PP_{EH}DT\text{-}TPD_O$**, **$PP_{EH}DT\text{-}TPD_{HP}$**, **$PP_{EH}DT2\text{-}TPD_O$** and **$PP_{EH}DT2\text{-}TPD_{HP}$**.

Polymer	J_{sc} (mA/cm^2)	V_{oc} (V)	*FF* (%)	PCE (%)
$PP_{EH}DT\text{-}TPD_O$	0.84	0.92	42.20	0.33
$PP_{EH}DT\text{-}TPD_{HP}$	1.09	0.84	38.47	0.33
$PP_{EH}DT2\text{-}TPD_O$	4.66	0.83	53.07	2.06
$PP_{EH}DT2\text{-}TPD_{HP}$	3.69	0.85	46.74	1.46

3.3. Conclusion

Four novel pyrene-*alt*-thieno[3,4-c]pyrrole-4,6-dione copolymers were prepared via direct arylation polymerisation. Either octyl or 4-hexylphenyl substituents were attached to the TPD moieties along polymer chains in order to evaluate the influence of these substituents on the photophysical, electronic and photovoltaic properties of the resulting polymers. Polymers that possessed 4-hexylphenyl substituents, **PP$_{EH}$DT-TPD$_{HP}$** and **PP$_{EH}$DT2-TPD$_{HP}$**, exhibited lower molecular weights relative to their octyl analogues, **PP$_{EH}$DT-TPD$_{O}$** and **PP$_{EH}$DT2-TPD$_{O}$**. It is speculated that the planar phenyl ring on the 4-hexylphenyl substituents promote backbone planarity resulting in aggregation of polymer chains. This phenomenon prevents the formation of high molecular weight materials. **PP$_{EH}$DT2-TPD$_{O}$ and PP$_{EH}$DT2-TPD$_{HP}$** displayed lower optical band gaps when compared to **PP$_{EH}$DT-TPD$_{O}$** and **PP$_{EH}$DT-TPD$_{HP}$**, a consequence of incorporating bithiophene spacers along the polymer backbone which promote improved intramolecular charge transfer. PXRD suggested that polymers with bithiophene units, **PP$_{EH}$DT2-TPD$_{O}$** and **PP$_{EH}$DT2-TPD$_{HP}$**, possessed smaller π-π stacking distances relative to polymers with a single thiophene unit, **PP$_{EH}$DT-TPD$_{O}$** and **PP$_{EH}$DT-TPD$_{HP}$**. BHJ photovoltaic devices fabricated from **PP$_{EH}$DT2-TPD$_{O}$** and **PP$_{EH}$DT2-TPD$_{EH}$** displayed modest efficiencies of 2.06 and 1.46 %, respectively. The higher PCE value of **PP$_{EH}$DT2-TPD$_{O}$** was a result of a higher *FF* and J_{sc} values. Both **PP$_{EH}$DT-TPD$_{HP}$** and **PP$_{EH}$DT-TPD$_{O}$** displayed poor efficiencies with values not exceeding 0.33 %. These preliminary results have shown that the use of pyrene-TPD copolymers display promise as p-type materials in BHJ photovoltaic cells. Further work is being conducted into the use of these novel polymers in BHJ photovoltaic devices.

3.4. References

1 Q. Ye and C. Chi, *Solar Cells—New Aspects and Solutions, Kosyachenko LA (ed.). InTech: Rijeka*, 2011, 453-476.

2 L. Cartwright, A. Iraqi, Y. Zhang, T. Wang and D. G. Lidzey, *RSC Adv.*, 2015, **5**, 46386–46394.

3 G. Li, R. Zhu and Y. Yang, *Nat. Photonics*, 2012, **6**, 153–161.

4 T. M. Clarke and J. R. Durrant, *Chem. Rev.*, 2010, **110**, 6736–6767.

5 S. A. Gevorgyan, M. V. Madsen, B. Roth, M. Corazza, M. Hösel, R. R. Søndergaard, M. Jørgensen and F. C. Krebs, *Adv. Energy Mater.*, 2015, 1–17.

6 T. Ameri, P. Khoram, J. Min and C. J. Brabec, *Adv. Mater.*, 2013, **25**, 4245–4266.

7 K. Wang and M. Wang, *Curr. Org. Chem.*, 2013, **17**, 999–1012.

8 P.-O. Morin, T. Bura, B. Sun, S. I. Gorelsky, Y. Li and M. Leclerc, *ACS Macro Lett.*, 2014, **4**, 21–24.

9 E. Iizuka, M. Wakioka and F. Ozawa, *Macromolecules*, 2015, **48**, 2989–2993.

10 H. Zhou, L. Yang and W. You, *Macromolecules*, 2012, **45**, 607–632.

11 P. Berrouard, S. Dufresne, A. Pron, J. Veilleux and M. Leclerc, *J. Org. Chem.*, 2012, **77**, 8167–8173.

12 J. W. Rumer, C. K. L. Hor, I. Meager, C. P. Yau, Z. Huang, C. B. Nielsen, S. E. Watkins, H. Bronstein and I. McCulloch, *J. Org. Semicond.*, 2013, **1**, 30.

13 L. Lu, T. Zheng, Q. Wu, A. M. Schneider, D. Zhao and L. Yu, *Chem. Rev.*, 2015, **115**, 12666–12731.

14 Y. Zou, A. Najari, P. Berrouard, S. Beaupré, B. Réda Aïch, Y. Tao and M. Leclerc, *J. Am. Chem. Soc.*, 2010, **132**, 5330-5331.

15 T. Chu, J. Lu, S. Beaupré, Y. Zhang, J. Pouliot, J. Zhou, A. Najari, M. Leclerc and Y. Tao, *Adv. Funct. Mater.*, 2012, **22**, 2345–2351.

16 C. Cabanetos, A. El Labban, J. A. Bartelt, J. D. Douglas, W. R. Mateker, J. M. J. Fréchet, M. D. McGehee and P. M. Beaujuge, *J. Am. Chem. Soc.*, 2013, **135**, 4656–4659.

17 L. Zöphel, D. Beckmann, V. Enkelmann, D. Chercka, R. Rieger and K. Müllen, *Chem. Commun.*, 2011, **47**, 6960–6962.

18 S.-Y. Liu, W.-Q. Liu, J.-Q. Xu, C.-C. Fan, W.-F. Fu, J. Ling, J.-Y. Wu, M.-M. Shi, A. K.-Y. Jen and H.-Z. Chen, *ACS Appl. Mater. Interfaces*, 2014, **6**, 6765–6775.

19 M. S. Almeataq, H. Yi, S. Al-Faifi, A. a B. Alghamdi, A. Iraqi, N. W. Scarratt, T. Wang and D. G. Lidzey, *Chem. Commun.*, 2013, **49**, 2252–4.

20 M. Zhao, K. Hashimoto and K. Tajima, *Synth. Met.*, 2013, **175**, 9–14.

21 T. M. Figueira-Duarte and K. Müllen, *Chem. Rev.*, 2011, **111**, 7260–7314.

22 N. Wang, X. Bao, Y. Yan, D. Ouyang, M. Sun, V. A. L. Roy, C. S. Lee and R. Yang, *J. Polym. Sci. Part A Polym. Chem.*, 2014, **52**, 3198–3204.

23 J. Warnan, C. Cabanetos, A. El Labban, M. R. Hansen, C. Tassone, M. F. Toney and P. M. Beaujuge, *Adv. Mater.*, 2014, **26**, 4357–4362.

24 M. Wakioka, N. Ichihara, Y. Kitano and F. Ozawa, *Macromolecules*, 2014, **47**, 626−631.

25 L. Cartwright, T. J. Neal, N. J. Rutland and A. Iraqi, *Polym. Adv. Technol.*, 2015, **27**, 525-531.

26 Y. He, J. You, L. Dou, C.-C. Chen, E. Richard, K. C. Cha, Y. Wu, G. Li and Y. Yang, *Chem. Commun.*, 2012, **48**, 7616.

27 C. Du, W. W. Li, Y. Duan, C. H. Li, H. L. Dong, J. Zhu, W. P. Hu and Z. S. Bo, *Polym. Chem.*, 2013, **4**, 2773–2782.

Chapter IV:

Pyrene- Benzo[1,2,5]thiadiazole Based Conjugated polymers for Application in BHJ solar cells

Pyrene- Benzo[1,2,5]thiadiazole Based Conjugated polymers for Application in BHJ solar cells

Abstract

Ethylhexyloxy-functionalised pyrene (**P_{EH}**) was prepared and copolymerised with both dithienyl-benzo[*c*]-[1,2,5]thiadiazole and dibithiophenyl-benzo[*c*]-[1,2,5]thiadiazole via a Stille coupling polymerisation method to yield **PP_{EH}-DTBT-8** and **PP_{EH}-DT2BT-8**, respectively. A comparative study was conducted to assess the impact of substituting thiophene for bithiophene repeat units upon the resulting properties of the conjugated polymers. **PP_{EH}-DT2BT-8** which has bithiophene spacers between pyrene and benzothiadiazole repeat units, exhibited a narrower optical and electrochemical band gap relative to **PP_{EH}-DTBT-8**; a consequence of the incorporating bithiophene spacer units which promotes intramolecular charge transfer between the electron donating and electron accepting moieties. Both **PP_{EH}-DTBT-8** and **PP_{EH}-DT2BT-8** showed deep HOMO levels of -5.54 and -5.50 eV, respectively. The polymers possess good thermal stabilities with degradation temperatures in excess of 310 °C. The photovoltaic performance of the two polymers was studied by fabricating bulk heterojunction (BHJ) photovoltaic devices using $PC_{70}BM$ as the acceptor. **PP_{EH}-DTBT-8** and **PP_{EH}-DT2BT-8** demonstrated efficiencies of 0.33 and 1.83 %, respectively. The higher efficiency of **PP_{EH}-DT2BT-8** can be attributed to vastly improved *FF* and J_{sc} values.

4.1. Introduction

Organic solar cells based on conjugated polymers have attracted a vast interest from the academic community owing to their attractive advantages such as flexibility, low cost, ease of processing and tunable electronic properties.[1,2] The highest efficiencies in organic solar cells have been achieved when a bulk heterojunction (BHJ) architecture is employed.[2] This architecture possesses a light harvesting active layer that comprises an interdigitated blend of electron-donating and electron-accepting materials. Conjugated polymers are employed as the electron-donor whilst fullerene and its derivatives have found widespread use as the electron-accepting material.[2,3,4]

The light harvesting properties of the active layer are largely dictated by the conjugated polymer.[3,4] Conjugated polymers that possess high molecular weights, broad absorption in the UV-vis-NIR region, high charge carrier mobilities and narrow band gaps will often display high efficiencies when fabricated into organic solar cells.[5] Polymers based on the donor-acceptor principle often display the desirable aforementioned characteristics. The intramolecular charge transfer between the alternating electron-rich donor moieties and the electron-deficient acceptor units along polymer chains, enables the band gap of the conjugated polymer to be finely tuned.[6-9]

Recent advancements have shown that the length, position and structure of the solubilising chains have a measureable impact on the active layer morphology when placed into organic solar cells.[10] Liu *et al.* synthesised a high performance polymer, **PffBT4T-2OD**, that possessed efficiencies ranging from 9.6 – 10.8 % when made into bulk heterojunction solar cells.[10] The temperature dependant aggregation behaviour of the **PffDT4T-2OD** originates from the 2-octyldodecyl chains attached to its tetrathiophene units. Cartwright *et al.* synthesised two benzothiadiazole-fluorene copolymers that possessed different length alkyl chains on the fluorene moiety.[5] Despite **PFDo-DffBT** possessing a higher molecular weight, relative to **PFO-DffBT**, this did not correspond to significantly lower optical band gap or a higher power conversion efficiency. In actuality, **PFO-DffBT** possessed a higher power conversion efficiency when fabricated into photovoltaic devices. The authors concluded that the smaller alkyl chains attached to the fluorene moiety in **PFO-DffBT** facilitated the formation of advantageous fine-length scale features in polymer-fullerene blends.[5]

2,1,3-Benzothiadiazole (BT) is one of the most extensively studied electron-accepting units.[6,11,12] It has found widespread use in highly efficient bulk heterojunction photovoltaic devices. Polymers that contain BT moieties often exhibit narrow optical band gaps, good thermal stabilities and deep

HOMO levels.[6,11,12] BT has been copolymerised with various electron-rich donor units. Amongst these, cyclopentadithiophene (**CPDT**) have displayed excellent promise owing to their planar structure and extended conjugation length.[13] The 4,7-positions of benzothiadiazole have been functionalised with various heterocyclic spacers.[14,15,16] Previous literature has shown that the incorporation of thienyl groups at the 4,7-positions of BT decrease steric hindrance between the donor and acceptor units yielding more planar polymers with narrower optical band gap.[6,12] Both the electronic properties and solubility can be finely tuned by modifying the thienyl units attached to the 4,7-positions of benzothiadiazole. Substituents can be attached to the 5,6-positions of the benzothiadiazole units and can greatly impact the optical, electrochemical, physical and morphological properties of the resulting polymer. Commonly used substituents included cyano, alkoxy and fluorine groups.[6] Recently, Gong *et al*. synthesised a series benzodithiophene-benzothiadiazole based copolymers for use in BHJ solar cells. Devices fabricated from these polymers exhibited efficiencies as high as 7.7%.[17]

In this study, we report the preparation of two pyrene-*alt*-benzothiadiazole D-A copolymers, poly{4,5,9,10-tetrakis[(2-ethylhexyl)oxy]pyren-*alt*-5,6-bis(octyloxy)-4,7-di(thiophen-2-yl)benzo [c][1,2,5]thiadiazole} **(PP_{EH}-DTBT-8)** and poly{4,5,9,10-tetrakis[(2-ethylhexyl)oxy]pyren-*alt*-4,7-di([2,2'-bithiophen]-5-yl)-5,6-bis(octyloxy)benzo[c][1,2,5]thiadiazole} **(PP_{EH}-DT2BT-8)**. The addition of octyloxy chains at the 5,6-positions of the BT units was designed to enhance the solubility of the resulting polymers. Previous literature work has also shown that these solubilising substituents increase the planarity of polymer backbones owing to supramolecular S–O interactions.[18] The physical properties of the two polymers were investigated by GPC, TGA, UV−vis absorption, cyclic voltammetry and XRD. The photovoltaic performance of both polymers in BHJ solar cells was evaluated. **PP_{EH}-DTBT-8** and **PP_{EH}-DT2BT-8** exhibited power conversion efficiencies of 0.33 and 1.83 %, respectively.

4.2. Results and Discussions

4.2.1. Monomer Synthesis

The synthetic routes of 5,6-bis(octyloxy)-4,7-bis(5-(trimethylstannyl)thiophen-2-yl)benzo[c] [1,2,5]thiadiazole (**M8**) are depicted in Scheme 4.1. The benzothiadiazole monomer, **M8**, was prepared from the commercially available 1,2-dihydroxybenzene (catechol) (**13**). The catechol was first deprotonated using a base (K_2CO_3) and then was alkylated using 1-bromooctane following nucleophilic substitution (S_N2) to produce 1,2 bis(octyloxy)benzene (**14**).

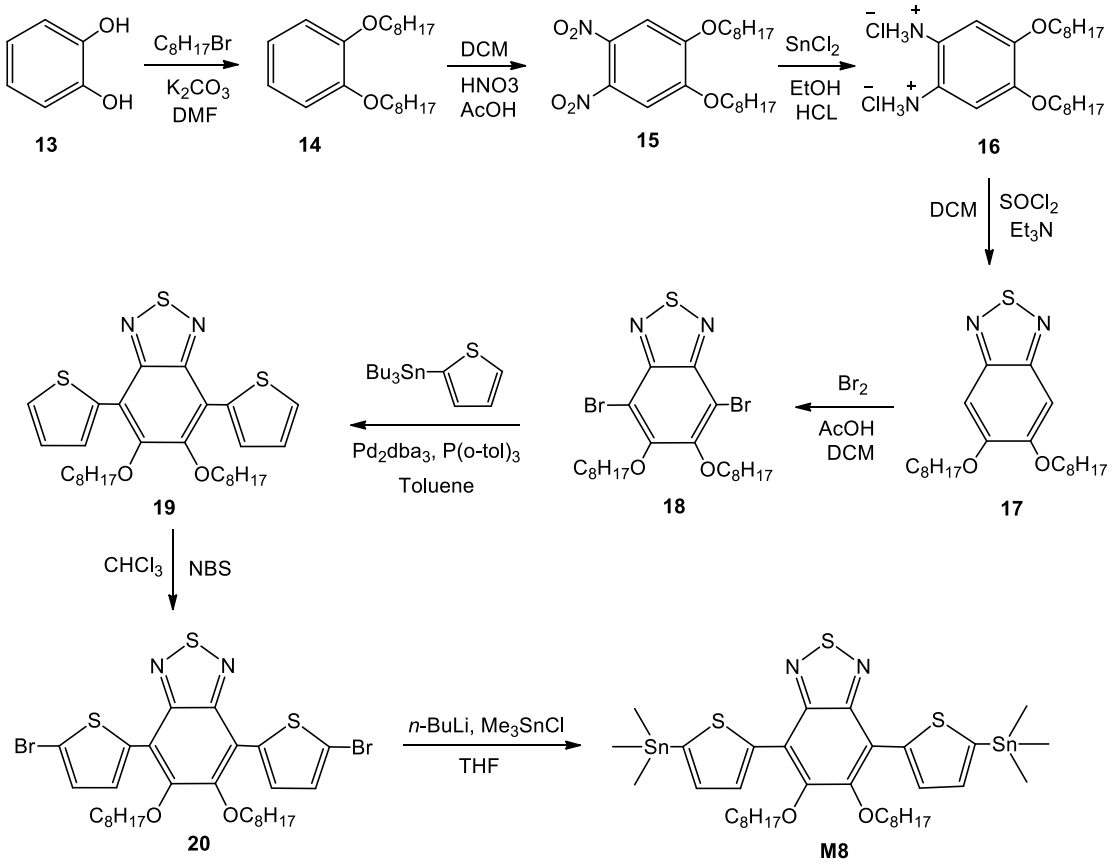

Scheme 4.1. Synthetic routes towards **M8**.

The second step involved the nitration of compound **14** at 4,5-positions via electrophilic aromatic substitution using nitric acid 65 % and fuming nitric acid to yield 1,2-dinitro-4,5-bis(octyloxy)benzene (**15**).

The third step involved the reduction of the two nitro groups, **15**, with tin (II) chloride to afford 4,5-bis(octyloxy)benzene-1,2-diaminium chloride (**16**) as its hydrochloride salt. The resultant product was used directly without any purification due to its instability.

Compound **16** was then reacted with thionyl chloride and trimethylamine to produce 5,6-bis(octyloxy)benzo[c][1,2,5]thiadiazole (**17**). The reaction was heated up to reduce the reaction time as well as to increase the yield. The mechanism of the reaction is shown in Scheme 4.2.

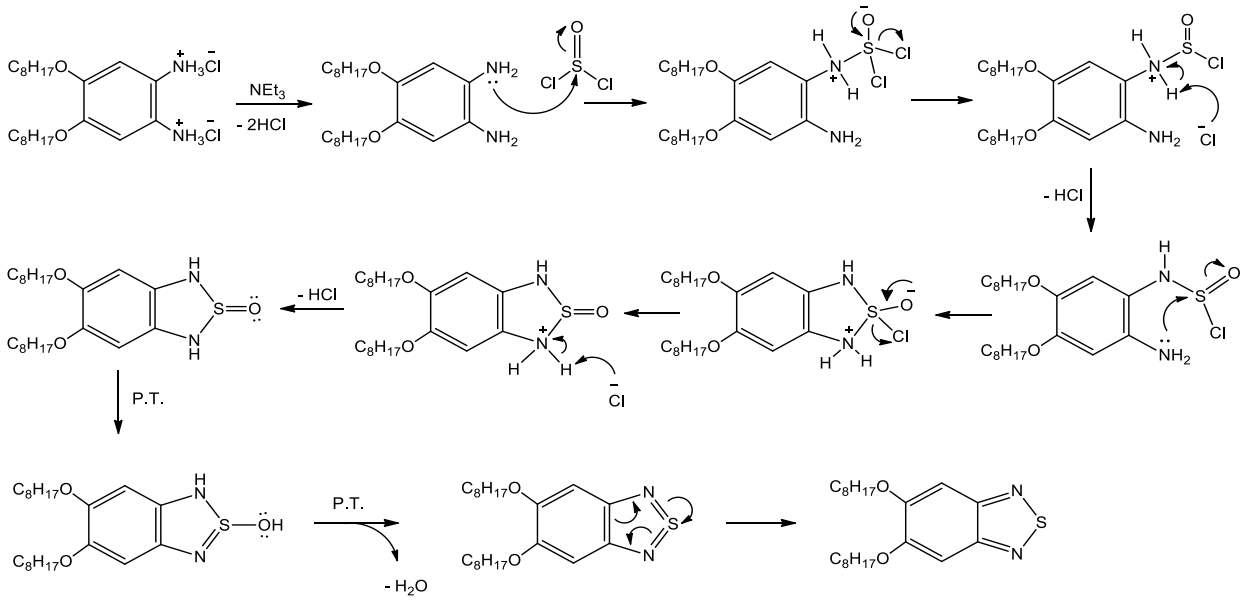

Scheme 4.2. Reaction mechanism of compound **17**.

Bromination of compound **17** at the 4,7-positions using Br_2 in acetic acid and DCM gave 4,7-dibromo-5,6-bis(octyloxy)benzo[c][1,2,5]thiadiazole (**18**). The addition of bromine happened at the 4,7-positions owing to the activating nature of the two nitrogens at the 5-membered ring.

Stille coupling of compound **18** with 2-(tributylstannyl)thiophene using tri-*o*-tolylphosphine and Pd_2dba_3 in dry toluene produced 5,6-bis(octyloxy)-4,7-di(thiophen-2-yl)benzo[c][1,2,5] thiadiazole (**19**).

Reaction of compound **19** with *N*-bromosuccinimide (NBS) in acetic acid and $CHCl_3$ via electrophilic aromatic substitution afforded 4,7-bis(5-bromothiophen-2-yl)-5,6-bis(octyloxy) benzo[c][1,2,5] thiadiazole (**20**).

The final step involved the lithiation of compound **20** with *n*-butyllithium, followed by the addition of trimethyltin chloride enabled the formation of 5,6-bis(octyloxy)-4,7-bis(5-(trimethylstannyl) thiophen-2-yl)benzo[c][1,2,5]thiadiazole (**M8**). The product was prepared via a nucleophilic aromatic substitution (S_N2). The structure of the monomer was confirmed by ^{1}H NMR spectroscopy (figure 4.1). The ^{1}H NMR spectrum showed two doublet resonances at 8.53 and 7.34 ppm corresponding to the two protons on the thiophene ring. The resonances located below 4.20 ppm correspond to the protons on the alkyl chains.

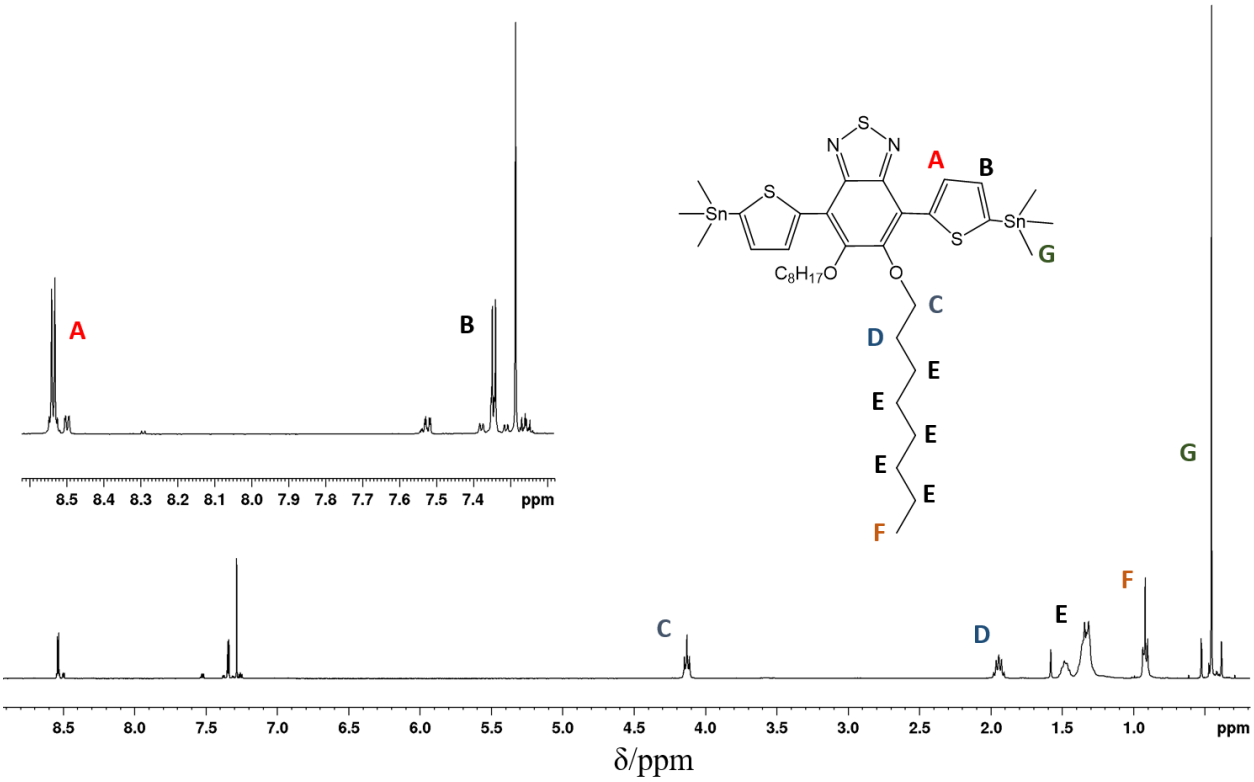

Figure 4.1. ^{1}H NMR spectrum of **M8** in $CDCl_3$.

The synthetic routes of 5,6-bis(octyloxy)-4,7-bis(5'-(trimethylstannyl)-[2,2'-bithiophen]-5-yl)benzo[c][1,2,5]thiadiazole (**M9**) are depicted in Scheme 4.3. Synthetic procedures are described in the experimental part.

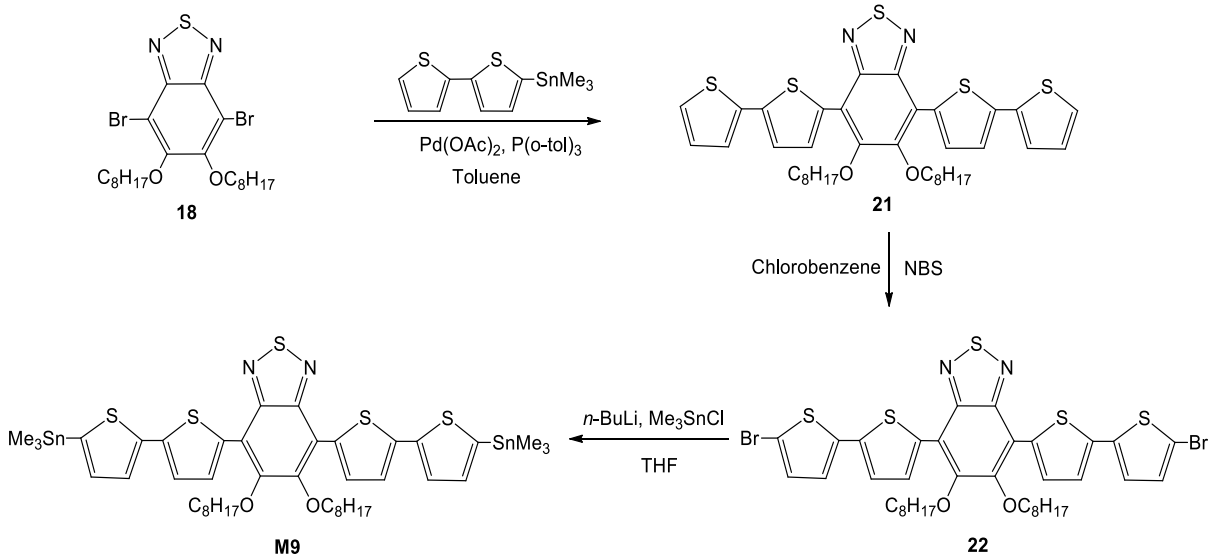

Scheme 4.3. Synthetic routes towards **M9**.

The synthesis of 4,7-dibromo-5,6-bis(octyloxy)benzo[c][1,2,5]thiadiazole (**18**) has already been described in the preparation of **M8** in this chapter. Stille coupling of compound **18** with [2,2]bithiophenyl-5-yl-trimethyl-stannane using $Pd(OAc)_2$ and tri-*o*-tolylphosphine in dry toluene produced 4,7-di([2,2'-bithiophen]-5-yl)-5,6-bis(octyloxy)benzo[c][1,2,5]thiadiazole (**21**).

Reaction of compound **21** with N-bromosuccinimide (NBS) via electrophilic aromatic substitution afforded 4,7-bis(5'-bromo-[2,2'-bithiophen]-5-yl)-5,6-bis(octyloxy)benzo[c] [1,2,5]thiadiazole (**22**).

Finally, metal-halogen exchange on compound **22** with *n*-butyllithium, followed by trans-metalation using trimethyltin chloride produced the target monomer, 5,6-bis(octyloxy)-4,7-bis(5'-(trimethylstannyl)-[2,2'-bithiophen]-5-yl)benzo[c][1,2,5]thiadiazole (**M9**). The product was prepared *via* a nucleophilic aromatic substitution (S_N2). The structure of the monomer was confirmed by ^{1}H NMR spectroscopy (figure 4.2). The ^{1}H NMR spectrum showed four doublet resonances at 8.52, 7.42, 7.31 and 7.16 ppm corresponding to the four protons on the thiophene ring. The resonances located below 4.20 ppm correspond to the protons on the alkyl chains.

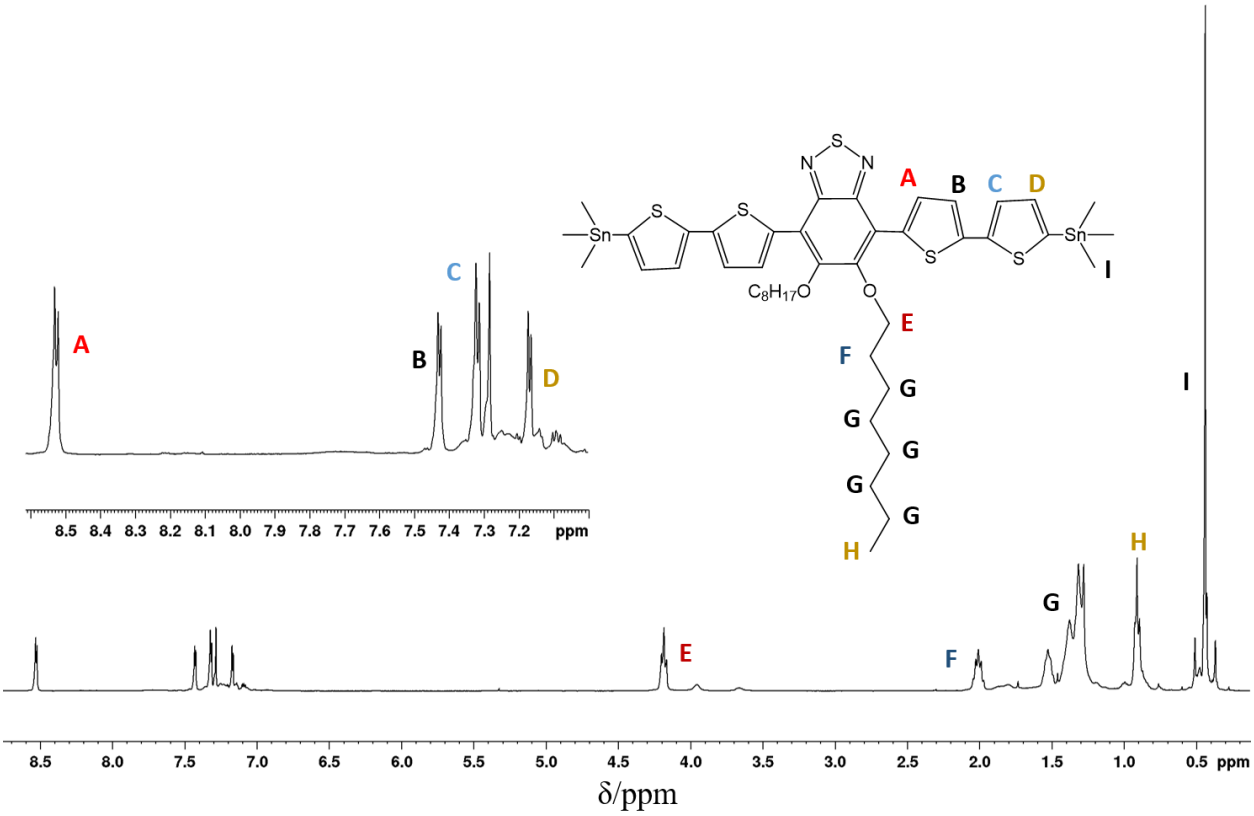

Figure 4.2. ^{1}H NMR spectrum of **M9** in $CDCl_3$.

4.2.2. Polymer Synthesis

In Chapter II, the preparation of pyrene-*alt*-benzothiadiazole D-A copolymers has been reported. When blended with $PC_{70}BM$ and fabricated into BHJ solar cells the resulting devices displayed modest power conversion efficiencies. In order to explore the potential of pyrene-*alt*-benzothiadiazole copolymers the impact of replacing hydrogen atoms at the 5,6-positions of benzothiadiazole with octyloxy substituents was investigated. Additionally, the effect of replacing thiophene spacers between pyrene and benzothiadiazole alternating units with bithiophene spacers to probe the impact of this substitution on the properties of the resulting polymer was also investigated.

Stille coupling of 2,7-dibromo-4,5,9,10-tetrakis(2-ethylhexyloxy)-pyrene **(M2)** with **M8**, and with **M9** afforded **PP$_{EH}$-DTBT-8** and **PP$_{EH}$-DT2BT-8**, in yields of 25 and 68%, respectively (Scheme 4.4). The structures of the two polymers were verified by ^{1}H NMR spectroscopy and elemental analysis. Both polymerisations were deemed complete after 72 hours. **PP$_{EH}$-DTBT-8** and **PP$_{EH}$-**

DT2BT-8 were purified via Soxhlet extraction using in succession methanol, acetone, hexane and toluene. The majority of **PP$_{EH}$-DTBT-8** was collected in the hexane fraction. In contrast, the bulk of **PP$_{EH}$-DT2BT-8** was collected in the toluene fraction. It is speculated that the low degree of polymerisation of **PP$_{EH}$-DTBT-8** is a consequence of steric hindrance during the coupling reaction upon repulsion between octyloxy substituents on **M8** and monomer **M2**. It is probable that these interactions also reduce the planarity of the polymer backbone increasing its solubility in hexane. Gel permeation chromatography (GPC) was used to estimate the number-average molecular weights (M_n) and weight-average molecular weights (M_w) of the two polymers against polystyrene standards. The results are outlined in Table 4.1. **PP$_{EH}$-DTBT-8** was estimated to have a weight average molecular weight of 7,000 Da, which is lower than its analogous polymer, **PP$_{EH}$-DT2BT-8**, which has a molecular weight of 20,900 Da. The higher degree of polymerisation of **PP$_{EH}$-DT2BT-8**, is explained by lesser steric hindrance between the octyloxy substituents on **M9** and **M2** during the coupling reaction.

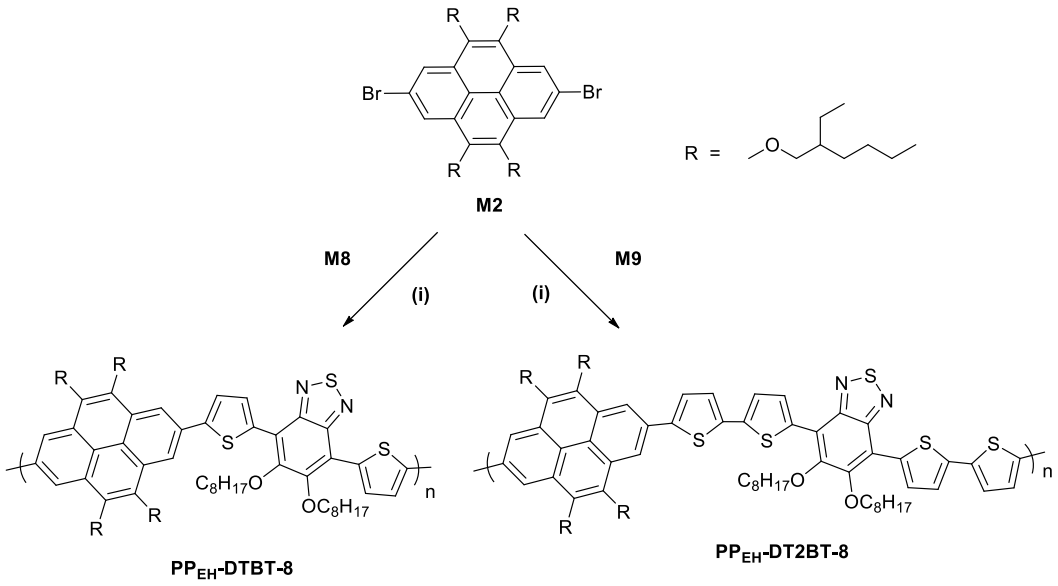

Scheme 4.4. Synthetic route and chemical structures of **PP$_{EH}$-DTBT-8** and **PP$_{EH}$-DT2BT-8**: (i) $Pd(OAc)_2$, tri(*o*-tolyl)phosphine and toluene.

Table 4.1. GPC, UV-vis absorption and electrochemical data for **PP_{EH}-DTBT-8** and **PP_{EH}-DT2BT-8**.

Polymers	M_n(Da)[c]	M_w(Da)[c]	PDI	λ_{max} (nm)		ε (M^{-1} cm^{-1})[d]	$E_{g\ opt}$ (eV)[d]	HOMO (eV)[e]	LUMO (eV)[f]	$E_{g\ ele}$ (eV)[g]
				Solution	Film					
PP_{EH}-DTBT-8[a]	4700	7000	1.49	494	510	39585	2.06	-5.54	-3.27	2.27
PP_{EH}-DT2BT-8[b]	11200	20900	1.87	521	551	73100	1.87	-5.50	-3.46	2.04

[a]Measurements conducted on the hexane fraction of the polymer. [b]Measurements conducted on the toluene fraction of the polymers. [c]Determined by GPC using 1,2,4-trichlorobenzene as the eluent at 140 °C. [d]Extinction coefficient measured at λ_{max} in $CHCl_3$. [e]Optical band gap. [f]HOMO level determined from the onset of oxidation. [g]LUMO level determined from the onset of reduction. [h]Electrochemical band gap.

4.2.3. UV-vis absorption spectroscopy

UV-vis spectroscopy was used to study the optical properties of the two polymers in both solution and film states (Figure 4.3). The results are outlined in Table 4.1. Both polymers demonstrated two sets of absorption bands. The absorption bands positioned at shorter wavelengths correspond to π-π* transitions from the monomer repeat units, while the absorption bands located at longer wavelengths are attributed to intramolecular charge transfer (ICT) between the pyrene units flanked by thiophene or bithiophene groups as the electron donor moieties and benzothiadiazole as the electron-deficient units. In solution, the ICT band of **PP_{EH}-DTBT-8** and **PP_{EH}-DT2BT-8** are positioned at 493 and 521 nm, respectively. The ICT band of **PP_{EH}-DTBT-8** and **PP_{EH}-DT2BT-8** are red-shifted to 510 and 551 nm, respectively, when cast into films. The bathochromic shift can be ascribed to improved ordering and a more planar polymer backbone in solid state. It is perhaps worth noting that the ICT band of **PP_{EH}-DT2BT-8** displays a larger bathochromic shift from solution to films (30 nm), in comparison to that observed for **PP_{EH}-DTBT-8** (16 nm). The larger shift of **PP_{EH}-DT2BT-8** can be attributed to its extended conjugation. Furthermore, the large red-shift also suggests that **PP_{EH}-DT2BT-8** possess superior intramolecular order in two dimensional-stacking in films relative to **PP_{EH}-DTBT-8**. The UV-vis spectra of **PP_{EH}-DT2BT-8** exhibited an additional broad band at 412 nm in solution and at 427 nm in the solid state. This band is totally absent in **PP_{EH}-DTBT-8**. This phenomenon is a consequence of substituting thiophene for bithiophene spacer units. The extended conjugation of bithiophene, and its higher electronic density, may result in more pronounced ICT. The absorption of **PP_{EH}-DT2BT-8** covers a greater part of the visible spectrum; a prerequisite for good photovoltaic performance in devices.

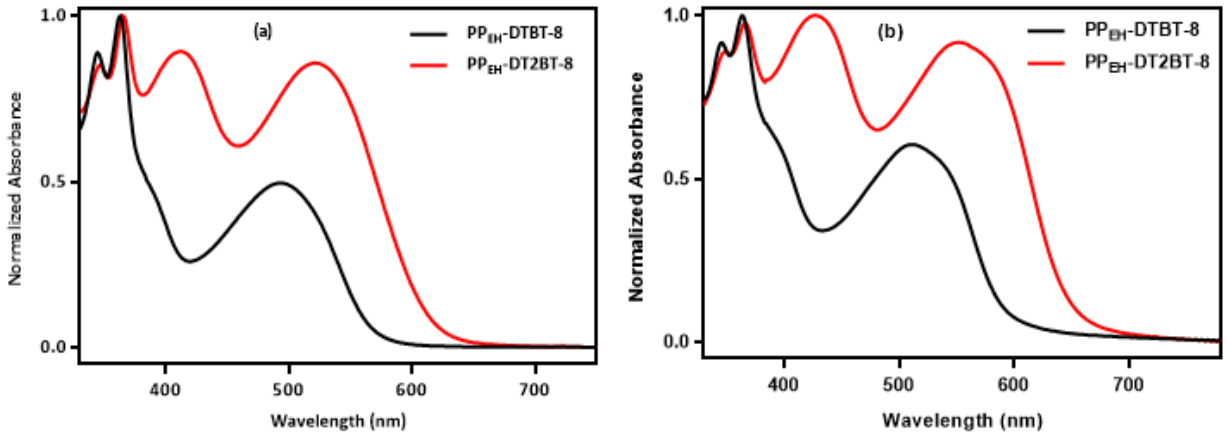

Figure 4.3. Normalised absorption spectra of **PP$_{EH}$-DTBT-8** and **PP$_{EH}$-DT2BT-8** in: (*a*) chloroform solution; and (*b*) thin film.

The optical band gaps ($E_{g\ opt}$) of **PP$_{EH}$-DTBT-8** and **PP$_{EH}$-DT2BT-8** were calculated from their onsets of absorption in film states and were estimated to be 2.06 and 1.87 eV, respectively. The lower optical band gap of **PP$_{EH}$-DT2BT-8** is a consequence of its extended conjugation in the solid state and also the higher electron donating ability of bithiophene spacers *vs.* thiophene spacers which improves ICT between donor and acceptor units along polymer chains.

The extinction coefficients of **PP$_{EH}$-DTBT-8** and **PP$_{EH}$-DT2BT-8** in solution were measured and the results are presented in table 1. **PP$_{EH}$-DT2BT-8** yielded an extinction coefficient of 73100 M^{-1} cm^{-1} which is almost twice as high as **PP$_{EH}$-DTBT-8** (39585 M^{-1} cm^{-1}). The improvement in absorption for **PP$_{EH}$-DT2BT-8** is probably due to its more extended electronic conjugation.

The two polymers prepared within this chapter possess wider optical band gaps relative to the fluorinated and non-fluorinated benzothiadiazole-pyrene based polymers, **PP$_{EH}$-DTffBT** and **PP$_{EH}$-DTBT**, prepared in Chapter II. **PP$_{EH}$-DTffBT** and **PP$_{EH}$-DTBT** possess optical band gaps of 1.81 and 1.76 eV, respectively. The wider optical band gaps of **PP$_{EH}$-DTBT-8** and **PP$_{EH}$-DT2BT-8**, relative to **PP$_{EH}$-DTffBT** and **PP$_{EH}$-DTBT**, can be attributed to the use of octyloxy substituents on BT units. Not only are these solubilising chains more sterically demanding but they are also electron donating. Consequently, incorporation of these chains 'pushes' electronic density onto the benzothiadiazole moiety resulting in wider band gap polymers.

4.2.4. Thermal Properties

Thermogravimetric analysis (TGA) was carried out to investigate the thermal properties of **PP_{EH}-DTBT-8** and **PP_{EH}-DT2BT-8**. Both polymers exhibited good thermal stabilities with degradation temperatures (5% weight loss) higher than 310 °C (Figure 2). **PP_{EH}-DTBT-8** and **PP_{EH}-DT2BT-8** displayed two onsets of degradation. Both polymers exhibit an initial onset at 315 °C which corresponds to the elimination of thermally labile alkyl chains from the polymer backbone. The second onset occurred at 494 and 500 °C for **PP_{EH}-DTBT-8** and **PP_{EH}-DT2BT-8**, respectively. This was attributed to the degradation of the polymer backbone.

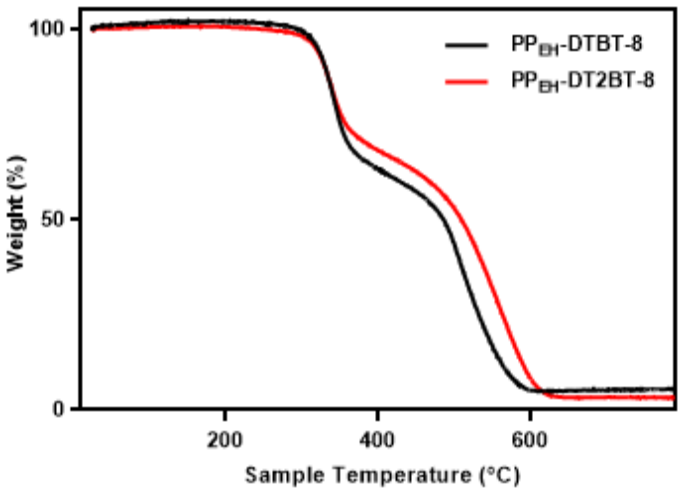

Figure 4.4. TGA curves of **PP_{EH}-DTBT-8** and **PP_{EH}-DT2BT-8**.

4.2.5. Cyclic Voltammetry

The electrochemical properties of **PP_{EH}-DTBT-8** and **PP_{EH}-DT2BT-8** were investigated by cyclic voltammetry (CV). Measurements were performed on drop-cast polymer films in acetonitrile and tetrabutylammonium perchlorate as electrolyte with a scan rate of 100 mV s^{-1}. The HOMO and LUMO energy levels of the two polymers were measured from the onset of their oxidation and reduction curves, respectively. The HOMO and LUMO levels of the two polymers are summarised in Table 4.1. The redox curves of the two polymers are depicted in Figure 4.5. Previous literature has shown that introducing electron-withdrawing substituents such as fluorine decreases the HOMO level of the polymer. In contrast, the introduction of electron donating species has the opposite effect.[8]

The HOMO level of **PP$_{EH}$-DTBT-8** (-5.54 eV) was slightly deeper than that of **PP$_{EH}$-DT2BT-8** (-5.50 eV); a result that could be due to the higher electron donating ability of bithiophene spacer units in **PP$_{EH}$-DT2BT-8** *vs.* thiophene units for **PP$_{EH}$-DTBT-8**. The LUMO level of **PP$_{EH}$-DT2BT-8** (-3.46 eV) is deeper than that of its analogous polymer **PP$_{EH}$-DTBT-8** (-3.27 eV). It is speculated that the lower molecular weight of **PP$_{EH}$-DTBT-8**, relative to **PP$_{EH}$-DT2BT-8**, and the higher electronic conjugation of the latter polymer is responsible of this observation. Work conducted previously has shown that increasing the molecular weight of the polymer yields a rapid decrease in the LUMO level relative to the HOMO level; a consequence of the LUMO level becoming localised on the acceptor moiety. It is speculated that the low molecular weight of **PP$_{EH}$-DTBT-8** will decrease the polymer packing density resulting in poor charge transportation.

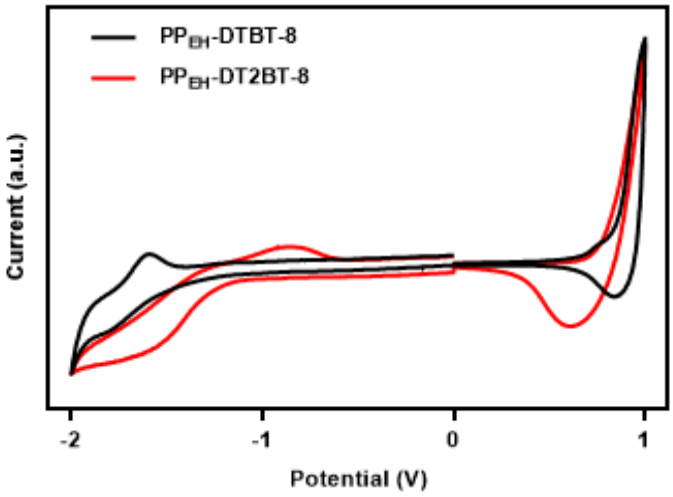

Figure 4.5. Cyclic voltammograms of thin films of **PP$_{EH}$-DTBT-8** and **PP$_{EH}$-DT2BT-8** on platinum disc electrodes (area 0.031 cm^2).

The two polymers prepared within this work, **PP$_{EH}$-DTBT-8** and **PP$_{EH}$-DT2BT-8**, exhibited deeper HOMO levels relative to analogous anthracene-benzothiadiazole based polymers **PPATBT-8** and **PPAT2BT-8** prepared by Almeataq *et al*.[19] **PPATBT-8** and **PPAT2BT-8** possess HOMO levels of -5.44 and -5.48 eV, respectively. The deeper HOMO levels of **PP$_{EH}$-DTBT-8** and **PP$_{EH}$-DT2BT-8** are attributed to a weaker electron donating ability of pyrene units relative to the 4-dodecyloxybenzene 9,10-functionalised anthracene units. The electrochemical band gaps of **PP$_{EH}$-DTBT-8** and **PP$_{EH}$-DT2BT-8** were estimated to be 2.27 and 2.04 eV, respectively. These are relatively close to the optical band gaps of the polymers.

4.2.6. Powder X-ray diffraction

Powder X-ray diffraction (PXRD) was used to investigate the molecular order of **PP$_{EH}$-DTBT-8** and **PP$_{EH}$-DT2BT-8** in the solid state (Figure 4.6). Both **PP$_{EH}$-DTBT-8** and **PP$_{EH}$-DT2BT-8** exhibited broad, poorly resolved peaks in the small angle region at 2θ values of 3.78 and 4.22°, respectively, which correspond to stacking distances of 23.34 and 20.91 Å, respectively which correspond to side-chain distances between lamella-packed polymer backbones. Both **PP$_{EH}$-DTBT-8** and **PP$_{EH}$-DT2BT-8** display a broad diffuse peak in the wide angle region at 2θ values of 20.5 and 21.6°, respectively, which correspond to π – π stacking distances of 4.32 and 4.11 Å, respectively. Unsurprisingly, **PP$_{EH}$-DTBT-8** displayed larger stacking distances relative to **PP$_{EH}$-DT2BT-8**, a consequence of more planar backbone in the latter polymer.

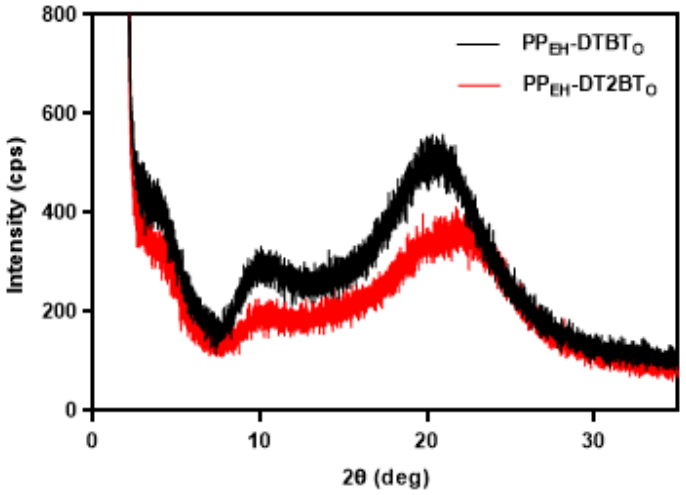

Figure 4.6. PXRD patterns of **PP$_{EH}$-DTBT-8** and **PP$_{EH}$-DT2BT-8**.

4.2.7. Photovoltaic Properties

Preliminary photovoltaic studies of **PP$_{EH}$-DTBT-8** and **PP$_{EH}$-DT2BT-8** were conducted on bulk heterojunction solar cells using blends of polymer:PC$_{70}$BM (1:3 w/w ratios) and chlorobenzene as the processing solvent. The general device structure was glass/ITO/PEDOT:PSS/Polymer: PC$_{70}$BM/Ca/Al. The experimental section provides in-depth information regarding device fabrication. Figure 4.7 displays the *J-V* curves of the most efficient devices. The results are outlined in Table 4.2. Devices fabricated from **PP$_{EH}$-DTBT-8** displayed a low PCE (0.33 %) with a V_{oc} of 0.72 V, a J_{sc} 1.88 mA/cm^2 and a poor *FF* of 24.53 %. **PP$_{EH}$-DT2BT-8** demonstrated better results with a PCE of 1.83 %, a V_{oc} of 0.78 V, a J_{sc} 6.11 mA/cm^2 and *FF* of 38.25 %. The higher PCE of

PP$_{EH}$-DT2BT-8 compared to **PP$_{EH}$-DTBT-8** is due to the significantly higher J_{sc} and *FF* values. It is hypothesised that the low J_{sc} values of devices made from **PP$_{EH}$-DTBT-8** are a consequence of its lower molecular weight and its lower extinction coefficient relative to **PP$_{EH}$-DT2BT-8**, and poor packing of polymer chains in polymer:$PC_{70}BM$ blends.

BHJ solar cells fabricated from **PP$_{EH}$-DTBT-8** and **PP$_{EH}$-DT2BT-8** presented poorer efficiencies when compared with those, **PPATBT-8** (3.92 %) and **PPAT2BT-8** (4.17 %), reported by Almeataq *et al.*,[19] which uses an anthracene functionalised with 4-dodecyloxybenzene as the electron donor unit instead of pyrene moiety. It is suggested that the higher efficiency of **PPATBT-8** and **PPAT2BT-8** relative to **PP$_{EH}$-DTBT-8** and **PP$_{EH}$-DT2BT-8** is a consequence of a higher *FF* (48.20 and 55.88 %, respectively) and J_{sc} (9.70 and 10.49 mA cm^{-2}, respectively) values. The high PCE might also be owing to the improved stacking of **PPATBT-8** and **PPAT2BT-8** in the photoactive layer and to the enhanced charge mobility.

Table 4.2. Device Performance of the two polymers: **PP$_{EH}$-DTBT-8** and **PP$_{EH}$-DT2BT-8**.

Polymer	J_{sc} (mA/cm^2)	V_{oc} (V)	*FF* (%)	PCE (%)
PP$_{EH}$-DTBT-8	1.88	0.72	24.53	0.33
PP$_{EH}$-DT2BT-8	6.11	0.78	38.25	1.83

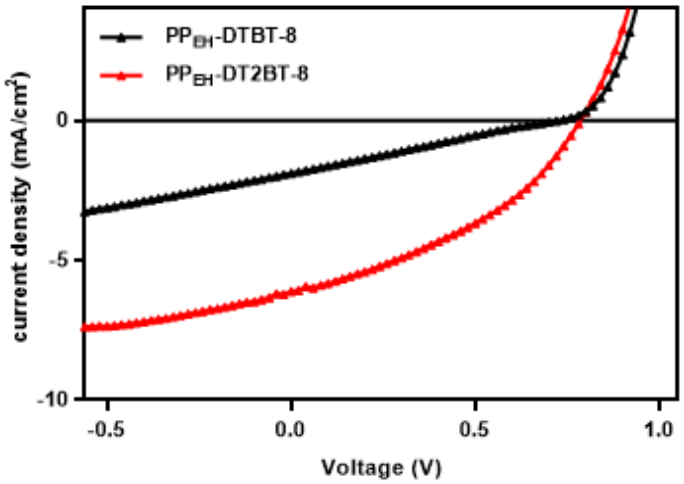

Figure 4.7. The J-V characteristic curves of **PP$_{EH}$-DTBT-8** and **PP$_{EH}$-DT2BT-8**.

4.3. Conclusions

In this chapter, 2-ethylhexyloxy-functionalised pyrene based donor-acceptor alternating copolymers were prepared through Stille coupling polymerisation. Reactions of 2,7-dibromo-4,5,9,10-tetrakis(2-ethylhexyloxy)-pyrene and 5,6-bis(octyloxy)-4,7-bis(5-(trimethylstannyl) thiophen-2yl) benzo[c][1,2,5]thiadiazole or 5,6-bis(octyloxy)-4,7-bis(5'-(trimethylstannyl)-[2,2'-bithiophen]-5-yl)benzo[c][1,2,5]thiadiazole afforded **PP_{EH}-DTBT-8** and **PP_{EH}-DT2BT-8**, respectively. A comparative study was carried out in order to evaluate the effects of substituting thiophene for bithiophene upon the properties of the resulting conjugated polymers. The chemical structures of the two polymers were confirmed with ^{1}H NMR spectroscopy and elemental analysis. The properties of the polymers were investigated by GPC, TGA, UV−vis absorption, cyclic voltammetry and XRD. GPC data revealed that **PP_{EH}-DTBT-8** possessed a lower molecular weight relative to its bithiophene analogue, **PP_{EH}-DT2BT-8**; a consequence of the steric hindrance between the octyloxy-solubilising groups on benzothiadiazole monomer **M8** and pyrene-based monomer **M2** during the coupling reaction. **PP_{EH}-DT2BT-8** exhibited a lower optical and electrochemical band gap relative to **PP_{EH}-DTBT-8**. It is believed the incorporation of bithiophene spacer units are responsible for this. These promote a more planar backbone, extending the conjugation length and yielding increased charge transfer along the polymer backbone in view the enhanced electron donating ability of bithiophene units *vs*. thiophene units. BHJ solar cells were fabricated from the two polymers. $PC_{70}BM$ was used as the electron acceptor. BHJ solar cells fabricated from **PP_{EH}-DTBT-8** possessed a PCE of 0.33 % which is lower than that of **PP_{EH}-DT2BT-8** which has a PCE of 1.83%. The higher efficiency of **PP_{EH}-DT2BT-8** compared to that of **PP_{EH}-DTBT-8** is due to the significantly higher J_{sc} and *FF* values. It is hypothesised that this is a consequence of the higher molecular weight of **PP_{EH}-DT2BT-8**, relative to **PPEH-DTBT-8**, a higher extinction coefficient and improved packing of polymer chains in polymer:$PC_{70}BM$ blends.

4.4. References

1 P. Ding, C. Chu, B. Liu, B. Peng, Y. Zou, Y. He, K. Zhou and C. Hsu, *Macromol. Chem. Phys.*, 2010, **211**, 2555–2561.

2 Y. Li, Y. Chen, X. Liu, Z. Wang, X. Yang, Y. Tu and X. Zhu, *Macromolecules*, 2011, **44**, 6370–6381.

3 C.-H. Cho, H. J. Kim, H. Kang, T. J. Shin and B. J. Kim, *J. Mater. Chem.*, 2012, **22**, 14236-14245.

4 P. P. Maharjan, Q. Chen, L. Zhang, O. Adebanjo, N. Adhikari, S. Venkatesan, P. Adhikary and B. Vaagensmith, *Phys. Chem. Chem. Phys.*, 2013, **15**, 6856–6863.

5 L. Cartwright, A. Iraqi, Y. Zhang, T. Wang and D. G. Lidzey, *RSC Adv.*, 2015, **5**, 46386–46394.

6 H. Zhou, L. Yang and W. You, *Macromolecules*, 2012, **45**, 607–632.

7 M. L. Keshtov, S. A. Kuklin, D. Y. Godovsky, A. R. Khokhlov, R. Kurchania, F. C. Chen, E. N. Koukaras and G. D. Sharma, *J. Polym. Sci. Pt. A Polym. Chem.*, 2015, **54**, 155–168.

8 N. Wang, Z. Chen, W. Wei and Z. Jiang, *J. Am. Chem. Soc.*, 2013, **135**, 17060–17068.

9 H. Zhou, L. Yang, S. Xiao, S. Liu and W. You, *Macromolecules*, 2010, **43**, 811–820.

10 Y. Liu, J. Zhao, Z. Li, C. Mu, W. Ma, H. Hu, K. Jiang, H. Lin, H. Ade and H. Yan, *Nat. Commun.*, 2014, **5**.

11 M. Wang, X. Hu, P. Liu, W. Li, X. Gong, F. Huang and Y. Cao, *J. Am. Chem. Soc.*, 2011, **133**, 9638–9641.

12 M. Zhou, M. Wang, L. Zhu, Z. Yang, C. Jiang, D. Cao and Q. Li, *Macromol. Rapid Commun.*, 2015, **36**, 2156–2161.

13 L. Lu, T. Zheng, Q. Wu, A. M. Schneider, D. Zhao and L. Yu, *Chem. Rev.*, 2015, **115**, 12666–12731.

14 B. Liu, X. Chen, Y. Zou, L. Xiao, X. Xu, Y. He, L. Li and Y. Li, *Macromolecules*, 2012, **45**, 6898-6905.

15 A. A. Alghamdi, D. C. Watters, H. Yi, S. Al-Faifi, M. S. Almeataq, D. Coles, J. Kingsley, D. G. Lidzey and A. Iraqi, *J. Mater. Chem. A*, 2013, **1**, 5165-5171.

16 C. Duan, A. Furlan, J. J. Van Franeker, R. E. M. Willems, M. M. Wienk and R. A. Janssen, *Adv. Mater.*, 2015, **27**, 4461–4468.

17 Z. Bo, X. Gong, G. Li, C. Li and J. Zhang, *J. Mater. Chem. A*, 2015, **3**, 20195–20200.

18 C. Du, W. W. Li, Y. Duan, C. H. Li, H. L. Dong, J. Zhu, W. P. Hu and Z. S. Bo, *Polym. Chem.*, 2013, **4**, 2773–2782.

19 M. S. Almeataq, H. Yi, S. Al-Faifi, A. B. Alghamdi, A. Iraqi, N. W. Scarratt, T. Wang and D. G. Lidzey, *Chem. Commun.*, 2013, **49**, 2252-2254.

Chapter V:

Conclusion and Future Work

5. Conclusion and Future Work

The object of this project was to prepare new types of donor-acceptor conjugated polymers for application in organic photovoltaic devices. Few literature sources reported the use of the pyrene moiety as an electron donor in donor-acceptor approach. Therefore, this project mainly focused on the incorporation of the pyrene unit in all donor-acceptor copolymers to cover some of the deficiencies found in the literature. Two different alkyl chains were substituted at the 4,5,9,10-positions of the pyrene unit to evaluate their impact on the properties of the resultant conjugated polymers. Benzothiadiazole and thieno[3,4-c]pyrrole-4,6-dione were linked to the pyrene moiety at the 2,7-positions. There has been significant interest in the properties of naphthalene and anthracene based polymers for applications in optoelectronic devices. However, pyrene, which has an analogous molecular framework, has received little attention in the literature. The key results from all polymers were summarised and they were compared with each other, where appropriate.

Chapter II reported the synthesis of four pyrene-*alt*-benzothiadiazole polymers, **PP$_{HD}$-DTBT**, **PP$_{EH}$-DTBT**, **PP$_{HD}$-DTffBT** and **PP$_{EH}$-DTffBT**. The four polymers were prepared via Stille coupling. Their thermal, optical and electrochemical properties in the solid state were investigated. Also, their molecular organisation and photovoltaic properties in thin film were characterised. GPC revealed that polymers substituted with the larger 2-hexyldecyl chains, **PP$_{HD}$-DTBT** and **PP$_{HD}$-DTffBT**, exhibited higher molecular weights (20,500 Da and 20,700 Da, respectively) when compared with polymers substituted with the shorter 2-ethylhexyl chains **PP$_{EH}$-DTBT** and **PP$_{EH}$-DTffBT** (12,800 Da and 5,300 Da, respectively). It is believed that attaching the larger 2-hexyldecyl chains onto the pyrene moiety hindered intermolecular interactions along the polymer chains aiding the formation of higher molecular weight polymers. However, polymers substituted with shorter alkyl chains, **PP$_{EH}$-DTBT** and **PP$_{EH}$-DTffBT**, showed lower optical band gaps and shallower HOMO levels compared with their counterpart polymers (**PP$_{HD}$-DTBT** and **PP$_{HD}$-DTffBT**). It is hypothesized that the shorter alkyl chains adopt a higher planar conformation, relative to the larger alkyl chains, which enhances the ICT between the electron donor and electron acceptor units. PXRD studies confirmed this hypothesis and showed that polymers bearing shorter alkyl chains displayed decreased lamellar and π-π stacking distances relative to those with larger alkyl chains. The two fluorinated polymers showed higher optical band gaps and deeper HOMO energy levels compared to their non-fluorinated counterparts, as a result of incorporating electron withdrawing substituents to the benzothiadiazole moiety. BHJ devices fabricated from **PP$_{HD}$-**

DTBT, **PP$_{EH}$-DTBT**, **PP$_{HD}$-DTffBT** and **PP$_{EH}$-DTffBT** revealed that **PP$_{EH}$-DTBT** displayed the highest power conversion efficiency of 1.86 %; as a result of higher J_{sc} and fill factor values.

Chapter III investigated the preparation of a series of four polymers comprising the pyrene unit, linked with thienyl or bithienyl units, and thieno[3,4-c]pyrrole-4,6-dione (TPD) moiety, substituted with octyl or 4-hexylphenyl groups, by using direct arylation reactions and yielded **PP$_{EH}$DT-TPD$_{O}$**, **PP$_{EH}$DT-TPD$_{HP}$**, **PP$_{EH}$DT2-TPD$_{O}$** and **PP$_{EH}$DT2-TPD$_{HP}$**. GPC analysis showed that the molecular weight of **PP$_{EH}$DT-TPD$_{HP}$** and **PP$_{EH}$DT2-TPD$_{HP}$** were significantly lower than their analogues, **PP$_{EH}$DT-TPD$_{O}$** and **PP$_{EH}$DT2-TPD$_{O}$**. This was as a result of attaching highly planar phenyl rings, which resulted in an increase in polymer aggregation. Polymers that are flanked by bithiophene units, **PP$_{EH}$DT2-TPD$_{O}$ and PP$_{EH}$DT2-TPD$_{HP}$**, showed lower optical band gaps and shallower HOMO levels compared to those flanked with one thienyl unit, **PP$_{EH}$DT-TPD$_{O}$** and **PP$_{EH}$DT-TPD$_{HP}$**. This is a consequence of attaching bithiophene units which increases the intramolecular charge transfer along the polymer backbone. PXRD results showed that polymers flanked by bithiophene groups, **PP$_{EH}$DT2-TPD$_{O}$** and **PP$_{EH}$DT2-TPD$_{HP}$**, exhibited decreased π-π stacking distances relative to those flanked by single thiophene units, **PP$_{EH}$DT-TPD$_{O}$** and **PP$_{EH}$DT-TPD$_{HP}$**; as a result of adopting a well ordered arrangement in solid state. BHJ devices fabricated from the four polymers revealed that **PP$_{EH}$DT2-TPD$_{O}$** displayed the highest *FF* (53.07 %), J_{sc} (4.66 mA/cm^2) and V_{oc} (0.83 V) values and hence exhibited the highest PCE (2.06 %) value. Clearly, changing the acceptor unit from benzothiadiazole to TPD has a noticeable impact on the optical and electrochemical properties of the resulting polymers. **PP$_{EH}$-DTBT** and **PP$_{EH}$-DTffBT** showed lower optical band gaps when compared with **PP$_{EH}$DT-TPD$_{O}$** and **PP$_{EH}$DT-TPD$_{HP}$**. This is probably owing to the enhanced intramolecular charge transfer between the pyrene unit and the benzothiadiazole moiety. The HOMO levels of the TPD-pyrene based copolymers (**PP$_{EH}$DT-TPD$_{O}$** and **PP$_{EH}$DT-TPD$_{HP}$**) are slightly deeper relative to the HOMO levels of the benzothiadiazole-pyrene based copolymers (**PP$_{EH}$-DTBT** and **PP$_{EH}$-DTffBT**); suggesting that TPD moiety is a stronger acceptor than benzothiadiazole unit.

In chapter IV, two pyrene-alt-benzothiadiazole polymers, **PP$_{EH}$-DTBT-8** and **PP$_{EH}$-DT2BT-8**, were successfully synthesised by using Stille coupling polymerization. A comprehensive study has been made to evaluate the influence of replacing a thienyl unit with bithiophene groups on the properties of the resultant polymers. GPC revealed that the polymer flanked by one thienyl unit,

PP$_{EH}$-DTBT-8, exhibited lower molecular weights (7,000 Da) compared to that flanked by bithiophene groups, **PP$_{EH}$-DT2BT-8**, (20,900 Da). This can be attributed to the presence of steric hindrance that introduced by the solubilising groups on both donor and acceptor units, which resulted in impeding the polymerization. TGA analysis displayed that both polymers showed relatively high thermal stabilities with decomposition temperatures up to 310°C. UV−vis absorption studies revealed that **PP$_{EH}$-DT2BT-8** showed a lower optical band gap (1.87 eV) compared to **PP$_{EH}$-DTBT-8** (2.06 eV) as a result of the attaching bithiophene groups, which enhanced the ICT between the electron donating and electron accepting units. The LUMO level of **PP$_{EH}$-DT2BT-8** (-3.46 eV) was significantly deeper compared to its counterpart copolymer **PP$_{EH}$-DTBT-8** (-3.27 eV). This phenomenon can be assigned to the higher molecular weight of **PP$_{EH}$-DT2BT-8**, compared to **PP$_{EH}$-DTBT-8**. PXRD results showed that both polymers exhibited broad diffuse peaks in the small and wide angle regions. BHJ devices fabricated from **PP$_{EH}$-DTBT-8** and **PP$_{EH}$-DT2BT-8**, using $PC_{70}BM$ as the acceptor, revealed that **PP$_{EH}$DT2-TPD$_O$** displayed higher *FF* (38.25 %), J_{sc} (6.11 mA/cm^2) and V_{oc} (0.78 V) values compared to **PP$_{EH}$-DTBT-8**, which resulted in a higher efficiency with PCE of 1.83 %. It is worth mentioning that **PP$_{EH}$-DTBT-8** and **PP$_{EH}$-DT2BT-8** are similar polymers to **PP$_{EH}$-DTBT** and **PP$_{EH}$-DTffBT** which has hydrogen or fluorine atoms, respectively, at the 5,6-positions of benzothiadiazole. **PP$_{EH}$-DTBT-8** and **PP$_{EH}$-DT2BT-8** showed wider optical band gaps when compared with **PP$_{EH}$-DTBT** and **PP$_{EH}$-DTffBT**. This can be attributed to the use of octyloxy chains on benzothiadiazole moieties. Not only are these solubilising chains more sterically demanding but they are also electron donating. Accordingly, incorporation of these octyloxy substituents would push the electronic density onto the benzothiadiazole unit leading to wider band gap polymers.

We have shown that photovoltaic devices fabricated from all polymers were conducted on BHJ devices using a mixture of polymer:$PC_{70}BM$ in a weight ratio of 1:3. All polymers displayed modest efficiencies ranging between 0.33% and 2.06%. Future work will include optimizing the device conditions such as using 1,8-diiodooctane (DIO) as an additive, and varying the weight ratios of polymer:$PC_{70}BM$ (e.g. 1:1, 1:2 and 1:4) in order to improve the devices performance. Atomic force microscopy (AFM) will be employed to analyse the surface morphology of the blend films (polymer:$PC_{70}BM$) of all polymers using tapping mode. Chapter II reported the synthesis of four pyrene-*alt*-benzothiadiazole polymers. **PP$_{EH}$-DTffBT** exhibited poor solubility and hence low molecular weight. To address this issue, an alkyl chain will be introduced to the thiophene

ring in order to enhance solubility and also to synthesize a polymer with a higher molecular weight. Different types of alkyl chains will be inserted to the pyrene unit to examine the impact of these substituents on the optical, electrochemical and photovoltaic properties. Chapter III reported the preparation of four pyrene-*alt*-TPD copolymers. In order to explore more the potential of pyrene-*alt*- TPD copolymers several alkyl chains will be attached to the imide functionality to study the influence of these alkyl chains on the properties of the resulting polymers.

Chapter VI: Experimental

6.1. Materials

All materials were purchased from commercial suppliers and used as received, unless otherwise stated. Toluene was dried and distilled over sodium under an inert argon atmosphere. Acetonitrile was dried and distilled over phosphorous pentoxide under an inert argon atmosphere, then stored over molecular sieves (3 Å). 5,6-Difluoro-4,7-bis(5-(trimethylstannyl)thiophene-2-yl)benzo[c][1,2,5]thiadiazole was prepared by Luke Cartwright of the Iraqi group.

6.2. Measurements

^{1}H and ^{13}C nuclear magnetic resonance (NMR) spectra were recorded on a Bruker AV 250 (250 MHz) or a Bruker AV 400 (400 MHz) using chloroform-d ($CDCl_3$), deuterated dimethyl sulfoxide (DMSO-d_6) or deuterated acetone (acetone-d_6) as the solvent at room temperature. ^{1}H NMR of the polymers were recorded on a Bruker Avance III HD 500 (500 MHz) spectrometer at 100 $^{\circ}C$ using 1,2-dideutrotetrachloroethane ($C_2D_2Cl_4$) as the solvent. Coupling constants are given in Hertz (Hz). Carbon, hydrogen, nitrogen and sulfur elemental analysis was performed on a Perkin Elmer 2400 series 11 CHNS/O analyser. Analysis of halides was undertaken using the Schöniger flask combustion method. GPC analysis was conducted on polymer solutions using 1,2,4-trichlorobenzene at 140 ^{o}C as the eluent. Polymer samples were spiked with toluene as a reference. GPC curves were obtained using a Viscotek GPCmax VE2001 GPC solvent/sample module and a Waters 410 Differential Refractometer, which was calibrated using a series of narrow polystyrene standards (Polymer Laboratories). TGA's were obtained using a Perkin Elmer TGA-1 Thermogravimetric Analyser at a scan rate of 10 $^{o}C\ min^{-1}$ under an inert nitrogen atmosphere. Powder X-ray diffraction samples were recorded on a Bruker D8 advance diffractometer with a CuKα radiation source (1.5418 Å, rated as 1.6 kW). The scanning angle was conducted over the range 2-40^{o}. UV-visible absorption spectra were recorded using a Hitachi U-2010 Double Beam UV/Visible spectrophotometer. Polymer solutions were made using chloroform and measured using quartz cuvettes (path length = $1x10^{-2}$ m). Thin films, used for absorption spectra were prepared by drop-casting solutions onto quartz plates using 1 mg cm^{-3} polymer solutions that were prepared with chloroform. Cyclic voltammograms were recorded using a Princeton Applied Research Model 263A Potentiostat/Galvanostat. A three electrode system was employed comprising a Pt disc, platinum wire and Ag/AgCl as the working electrode, counter electrode and reference electrode, respectively. Measurements were conducted in a tetrabutylammonium

perchlorate acetonitrile solution (0.1 mol dm^{-3}) on polymer films that were prepared by drop casting polymer solution. Ferrocene was employed as the reference redox system; in accordance with IUPAC's recommendations. The energy level of Fc/Fc^+ was assumed at –4.8 eV to vacuum. The half-wave potential of Fc/Fc^+ redox couple was found to be 0.08 V *vs.* Ag/Ag^+ reference electrode. The HOMO energy levels of polymers were estimated by the equation: $E_{HOMO} = -(4.8 - E_{1/2,\ Fc,Fc+} + E_{ox,\ onset})$. $E_{ox,\ onset}$ is the onset oxidation potential relative to the Ag/Ag^+ reference electrode. The LUMO energy levels of polymers were calculated using the equation: $E_{LUMO} = -(4.8 - E_{1/2,\ Fc,Fc+} + E_{red,\ onset})$. $E_{red,onset}$ is the onset reduction potential relative to the Ag/Ag^+ reference electrode.

6.3. Fabrication and testing of BHJ polymer solar cells

The polymers and $PC_{70}BM$ were dissolved in chlorobenzene, and were then put on a hot plate held at 70 °C overnight with stirring to allow dissolution. The polymer : fullerene blend ratios were 1:3. Photovoltaic devices were fabricated onto pre-patterned ITO glass substrates (20 ohms per square) that were supplied by Ossila Limited. The ITO/glass substrates were first cleaned by sonication in dilute NaOH followed by IPA. A 30 nm thick PEDOT:PSS layer was spin-coated onto the ITO/glass substrates. These were then transferred to a hot-plate held at 120 °C for 10 minutes before being transferred to a nitrogen glove-box. All active layers were spin cast onto the glass/ITO/PEDOT:PSS substrate. The devices were then transferred into a thermal evaporator for deposition of a cathode (5 nm of calcium followed by a 100 nm of aluminium evaporated at a base pressure of $\sim 10^{-7}$ mbar). The cathode was deposited through a shadow-mask producing a series of independent pixels. Devices were encapsulated using a glass slide and epoxy glue before testing. PCEs were determined by using a Newport 92251A-1000 AM 1.5 solar simulator. An National Renewable Energy Laboratory calibrated silicon cell was used to calibrate the power output to 100 mW cm^{-2} at 25 °C. An aperture mask having an area of 2.06 mm^2 was placed over devices to define the test area.

6.4. Preparation of monomers

Pyrene-4,5,9,10-tetraone (2)

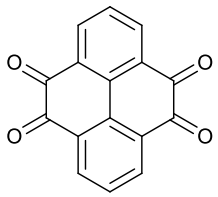

Pyrene (15.0 g, 74.22 mmol) was dissolved in ethyl acetate (180 mL). Raney nickel (7.5 g) was added and the reaction was left to stir for 48 hours. Upon completion, the Raney nickel was filtered off and the solvent was removed *in vacuo* to yield pure pyrene (13.0 g, 64.33 mmol, 87 %).[1] Pyrene (6.06 g, 30 mmol) was dissolved in CH_2Cl_2 (120 mL) and CH_3CN (120 mL). $NaIO_4$ (52.5 g, 81.8 mmol), $RuCl_3$. xH_2O (0.25 g, 1.2 mmol) and H_2O (150 mL) were added to the reaction mixture. The dark green suspension was heated up to 40 °C and left to stir for 18 hours. The reaction mixture was poured into water (500 mL). The organic phase was separated, and the aqueous phase was extracted with a large amount of CH_2Cl_2. The organic extracts were combined and washed with water multiple times to yield a dark orange solution. The organic solvent was evaporated to give a dark orange solid.[2] The product was purified *via* hot recrystallisation with *m*-Xylene at 150 °C to yield pyrene-4,5,9,10-tetraone (1.40 g, 5.3 mmol, 18 %).[3] M.p. = 358 - 360 °C. ^{1}H NMR (400 MHz, DMSO-d_6): δ (ppm) 8.33 (d, J = 7.92 Hz, 4H), 7.75 (t, J = 7.92 Hz, 2H) EI-MS (*m/z*): $[M]^+$ calculated for $C_{16}H_6O_4$ 262.02, found 262.00. Elem. Anal. Calcd for $C_{16}H_6O_4$: C 73.28, H 2.30; found C 72.34, H 2.24.

2,7-Dibromopyrene-4,5,9,10-tetraone (3)

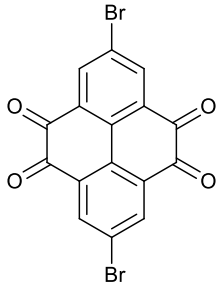

Pyrene-4,5,9,10-tetraone (2.45 g, 9.35 mmol) was dissolved in H_2SO_4 (98 %, 65 mL) and the reaction was held at room temperature. *N*-bromosuccinimide (NBS) (3.66 g, 20.57 mmol, 2.2 equiv.) was added portion-wise to the reaction mixture. Upon complete addition, the reaction mixture was stirred for three hours. Once the reaction was complete, the reaction was poured onto ice water. The precipitate was filtered off and washed with water. The crude material was stirred in methanol, filtered and dried to yield 2,7-dibromopyrene-4,5,9,10-tetraone (2.4 g, 5.8 mmol, 62 %).[4] M.p. = 379 - 381 °C. ^{1}H NMR (400 MHz, $C_2D_2Cl_4$, 100 °C): δ (ppm) 8.43 (s, 4H). EI-MS (*m/z*): $[M]^+$ calculated for $C_{16}H_4Br_2O_4$ 420, found 420. Elem. Anal. calcd. for $C_{16}H_4Br_2O_4$: C 45.75, H 0.96, Br 38.05; found C 46.60, H 1.1, Br 37.18.

2,7-Dibromo-4,5,9,10-tetrakis((2-hexyldecyl)oxy)pyrene (M1)

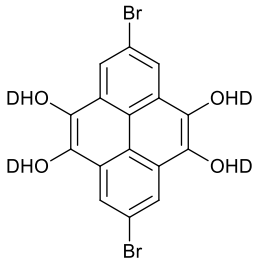

2,7-Dibromopyrene-4,5,9,10-tetraone (0.25 g, 0.6 mmol), $Na_2S_2O_4$ (1.21 g, 0.7 mmol), *n*-BuNBr (0.24 g, 0.75 mmol), H_2O (3 mL) and THF (4 mL) were placed in a round bottom flask and stirred for 10 minutes at 25 °C. After 30 minutes, 1-bromo-2-hexyldecane (1.2 g, 3.95 mmol) and aq. KOH (4 mL, 36 mmol) were added to the mixture. The mixture was stirred for 5 hours at 70 °C. Upon completion, the reaction was quenched with brine. The crude material was extracted with THF. The organic layer was washed with brine (3 x 100 mL). The organic layer was separated, dried ($MgSO_4$), filtered and the solvent removed *in vacuo*. The crude material was purified via silica gel column chromatography using petroleum ether as the eluent to yield 2,7-dibromo-4,5,9,10-tetrakis((2-hexyldecyl)oxy)pyrene as colourless oil (0.400 g, 0.30mmol, 51 %).[5] ^{1}H NMR (400 MHz, $CDCl_3$): δ (ppm) 8.54 (s, 4H), 4.18 (d, J = 6.06 Hz, 8H), 2.02-1.93 (m, 4H), 1.72-1.61 (m, 8H); 1.60-1.22 (br, 88H), 0.91 (t, J = 6.65 Hz, 24H). ^{13}C NMR (250 MHz, $CDCl_3$): δ (ppm) 144. 00, 130. 2, 121. 9, 121. 1, 118. 9, 39. 3, 31. 9, 31. 5, 30. 2, 29. 9, 29. 7, 29. 4, 27.00, 26. 95, 22. 7, 22. 7, 14. 1. EI-MS (*m/z*): $[M]^+$ calculated for $C_{80}H_{136}Br_2O_4$ 1321, found 1321. 2. Elem. Anal. Calcd. for $C_{80}H_{136}Br_2O$: C 72.70, H 10.37, Br 12.09; found C 73.22, H 10.47, Br 11.98.

2,7-Dibromo-4,5,9,10-tetrakis((2-ethylhexyl)oxy)pyrene (M2)

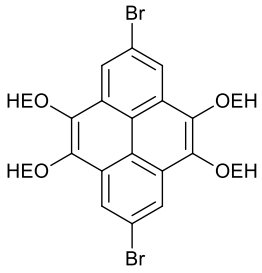

2,7-Dibromopyrene-4,5,9,10-tetraone (1.5 g, 3.57 mmol), $Na_2S_2O_4$ (7.25 g, 41.66 mmol), *n*-BuNBr (1.44 g, 4.46 mmol), H_2O (12 mL) and THF (24 mL) were placed in a round bottom flask and stirred for 10 minutes at 25 °C. Once the time had elapsed, 1-bromo-2-ethylhexyl (4.20 ml, 23.5 mmol) and aq. KOH (6.01g, 12 mL) were added to the mixture. The mixture was stirred for 5 hours at 70 °C. Upon completion, the reaction was quenched with brine. The crude material was extracted with THF. The organic layer was washed with brine (3 x 100 mL). The organic layer was separated, dried ($MgSO_4$), filtered and the solvent removed *in vacuo*. The crude material was purified *via* silica gel column chromatography using petroleum ether as the eluent to yield 2,7-dibromo-4,5,9,10-tetrakis((2-ethylhexyl)oxy)pyrene as yellow oil (1.8 g, 2.06 mmol, 46 %).[5] ^{1}H NMR (400 MHz, $CDCl_3$): δ (ppm) 8.54 (s, 4H), 4.19 (d, J = 6.0 Hz, 8H), 2.00-1.89 (m, 4H), 1.80-1.37 (m, 32H), 1.06 (t, J = 7.31 Hz, 12H), 0.98 (t, J = 6.95 Hz, 12H). ^{13}C NMR (250 MHz, $CDCl_3$): δ (ppm) 144. 1, 130. 2, 121. 9, 121. 1, 119. 00, 40.

8, 30. 6, 29. 2, 23. 9, 23. 2, 14. 1, 11. 2. EI-MS (*m/z*): $[M]^+$ calculated for $C_{48}H_{72}Br_2O_4$ 872.37, found 872.5. Elem. Anal. Calcd. for $C_{80}H_{136}Br_2O$: C 66.05, H 8.31, Br 18.31; found C 66.23, H 8.22, Br 18.42.

2,7-Di(thien-2-yl)-4,5,9,10-tetrakis(2-ethylhexyloxy)-pyrene (7)

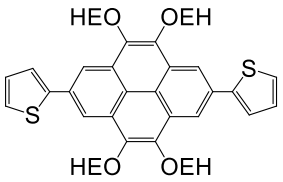

2,7-Dibromo-4,5,9,10-tetrakis(2-ethylhexyloxy)-pyrene (**M2**) (600 mg, 0.687 mmol), tri-*o*-tolylphosphine (67 mg, 0.02 mmol) and Pd_2dba_3 (25 mg, 0.03 mmol) were placed in a one neck round bottom flask and placed under an inert argon atmosphere. Anhydrous toluene (15 mL) and 2-tributylstannylthiophene (0.57 ml, 1.78 mmol) were added to the reaction mixture. The reaction mixture was maintained under reflux for 16 hours. The solvent was removed and the crude product was purified by silica gel column chromatography using petroleum:$CHCl_3$ (5:1) as the eluent. The title product was collected as a yellow oil (0.54 g, 0.61 mmol, 89 %).[6] ^{1}H NMR (400 MHz, $CDCl_3$) δ (ppm): 8.71 (s, 4H), 7.65 (dd, *J* = 3.60 and 1.09 Hz, 2H), 7.42 (dd, *J* = 5.09 and 1.03 Hz, 2H), 7.22 (dd, *J* = 5.03 and 3.61 Hz, 2H), 4.27 (d, *J* = 5.08 Hz, 8H), 2.06-1.95 (m, 4H), 1.88-1.37 (m, 32H), 1.09 (t, *J* = 7.48 Hz, 12H), 0.95 (t, *J* = 7.08 Hz, 12H). ^{13}C NMR (400 MHz, $CDCl_3$) δ (ppm): 145. 6, 144. 7, 132. 1, 129. 2, 128. 3, 125. 4, 123. 6, 120. 2, 116. 3, 40. 9, 30. 8, 29. 4, 24. 00, 23. 3, 14. 2, 11. 4. EI-MS (*m/z*): $[M]^+$ calculated for $C_{56}H_{78}O_4S_2$ 878.53; Found 878.4. Elem. Anal. Calcd. for $C_{56}H_{78}O_4S_2$: C, 76.49; H, 8.94; S, 7.01. Found: C, 76.42; H, 8.83; S, 7.01.

2,7-Bis(5-bromo-thien-2-yl)-4,5,9,10-tetrakis(2-ethylhexyloxy)-pyrene (M4)

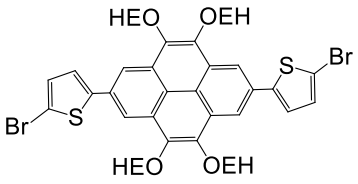

2,7-Di(thien-2-yl)-4,5,9,10-tetrakis(2-ethylhexyloxy)-pyrene (**7**) (513 mg, 0.584 mmol) was dissolved in glacial acetic acid (15 ml) and $CHCl_3$ (15 ml). *N*-Bromosuccinimide (NBS) (208 mg, 1.17 mmol) was added and the reaction mixture was left to stir in the dark, at room temperature, for 20 hours. Upon completion of the reaction, the solvent was removed *in vacuo* and the crude material was purified *via* silica gel column chromatography using petroleum ether:$CHCl_3$ (10:3) as the eluent. The title product (**M4**) was obtained as a yellow solid (511 mg, 0.50 mmol, 84 %).[7] M.p. = 69 - 73 °C. ^{1}H NMR (400 MHz, $CDCl_3$) δ (ppm): 8.60 (s, 4H), 7.37 (d, *J* = 3.08 Hz, 2H), 7.17 (d, *J* = 3.79 Hz, 2H), 4.25 (d, *J* = 5.92 Hz, 8H), 2.04-1.93 (m, 4H), 1.85-1.37 (m, 32H), 1.08 (t, *J* = 7.56 Hz, 12H), 0.96 (t, *J* = 7.07 Hz, 12H). ^{13}C NMR (400 MHz, $CDCl_3$) δ (ppm): 147. 00, 144. 7, 131. 4, 131. 2, 129. 34, 123. 7, 120. 2, 115. 9, 112. 0, 40.

90, 30. 9, 29. 4, 24. 00, 23. 3, 14. 2, 11. 3. EI-MS (*m/z*): $[M]^+$ calculated for $C_{56}H_{76}Br_2O_4S$ 1036.35; Found 1036.20. Elem. Anal. Calcd. for $C_{56}H_{76}Br_2O_4S_2$: C, 64.85; H, 7.39; Br, 15.41; S, 5.92. Found: C, 64.40; H, 7.24; Br, 15.79; S, 5.92.

2,7-Di(2,2'-bithiophen-5-yl)-4,5,9,10-tetrakis(2-ethylhexyloxy)-pyrene (8)

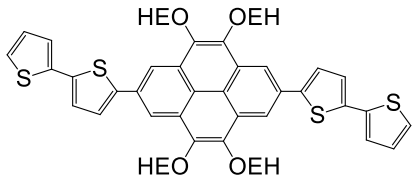

2,7-Dibromo-4,5,9,10-tetrakis(2-ethylhexyloxy)-pyrene (**M2**) (454 mg, 0.52 mmol), tri-*o*-tolylphosphine (67 mg, 0.02 mmol) and Pd_2dba_3 (25 mg, 0.03 mmol) were placed in a one neck round bottom flask and placed under an inert argon atmosphere. The mixture was dissolved in anhydrous toluene (15 mL) and 2,2'-bithiophen-5-yltrimethylstannane (444 mg, 1.35 mmol) was added. The reaction mixture was maintained under reflux overnight. Upon completion, the solvent was removed *in vacuo* and the crude product was purified by silica gel column chromatography using petroleum ether:$CHCl_3$ (5:1) as the eluent. The title product was obtained as a yellow oil (382 mg, 0.36 mmol, 71 %).[8] ^{1}H NMR (400 MHz, $CDCl_3$) δ (ppm): 8.70 (s, 4H), 7.56 (d, *J* = 3.82 Hz, 2H), 7.30 (dd, *J* = 4.56 and 3.29 Hz, 6H), 7.10 (dd, *J* = 5.11 and 3.62 Hz, 2H), 4.27 (d, *J* = 5.08 Hz, 8H), 2.06-1.95 (m, 4H), 1.88-1.37 (m, 32H), 1.09 (t, *J* = 7.48 Hz, 12H), 0.95 (t, *J* = 7.08 Hz, 12H). ^{13}C NMR (400 MHz, $CDCl_3$) δ (ppm): 144. 7, 144. 3, 137. 6, 137. 3, 131. 8, 129. 3, 127. 9, 124. 9, 124. 5, 124. 2, 123. 7, 120. 2, 116. 00, 41. 00, 30. 9, 29. 5, 24. 00, 23. 3, 14. 2, 11. 4. EI-MS (*m/z*): $[M]^+$ calculated for $C_{64}H_{82}O_4S_4$ 1042.5; Found 1042.6. Elem. Anal. Calcd. for $C_{64}H_{82}O_4S_4$: C, 73.66; H, 7.92; S, 12.29. Found: C, 73.57; H, 7.82; S, 10.25.

2,7-Bis-(5'-bromo-[2,2']bithiophenyl-5-yl)-4,5,9,10-tetrakis(2-ethylhexyloxy)-pyrene (M5)

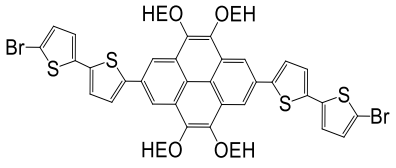

2,7-Di(2,2'-bithiophen-5-yl)-4,5,9,10-tetrakis(2-ethylhexyloxy)-pyrene (**8**) (170 mg, 0.14 mmol) was dissolved in anhydrous chlorobenzene (10 mL). NBS (58.04 mg, 3.26 mmol) was added and the reaction mixture was left to stir in the dark, overnight at 50 °C. Once this time had elapsed, the temperature was raised to 100 °C and the reaction was stirred for a further 15 minutes. The solvent was removed *in vacuo* and the crude product was dissolved in diethyl ether (5 mL) and precipitated in methanol (25 mL) and separated by filtration to produce the title product, **M5**, as a yellow solid (185 mg, 0.13 mmol, 95 %).[8] M.p. = 109 - 112 °C. ^{1}H NMR (400 MHz, $CDCl_3$) δ (ppm): 8.67 (s, 4H), 7.54 (d, *J* = 3.78 Hz, 2H), 7.22 (d, *J* =

3.73 Hz, 2H), 7.04 (dd, *J* = 9.12 and 3.87 Hz, 4H), 4.27 (d, *J* = 5.08 Hz, 8H), 2.06-1.95 (m, 4H), 1.88-1.37 (m, 32H), 1.09 (t, *J* = 7.48 Hz, 12H), 0.95 (t, *J* = 7.08 Hz, 12H). ^{13}C NMR (400 MHz, $CDCl_3$) δ (ppm): 144. 8, 144. 7, 139. 1, 136. 2, 131. 6, 130. 7, 129. 3, 125. 2, 124. 3, 123. 7, 120. 2, 116. 00, 111. 1, 40. 9, 30. 90, 29. 5, 24. 00, 23. 4, 14. 2, 11. 4. EI-MS (*m/z*): $[M]^+$ calculated for $C_{64}H_{80}Br_2O_4S_4$ 1200.3; Found 1200.4. Elem. Anal. Calcd. for $C_{64}H_{80}Br_2O_4S_4$: C, 63.98; H, 6.71; Br, 13.30; S, 10.68. Found: C, 62.16; H, 6.60; Br, 13.41; S, 9.85.

1-Bromo-2-hexyldecane (6)

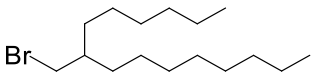

To a solution of 2-hexyldecan-1-ol (9.69 g, 40 mmol) in DCM (400 mL) were added NBS (8.543 g, 48 mmol) and triphenylphosphine (TPP) (12.59 g, 48 mmol). The solution was stirred for 15 minutes at room temperature. Upon completion, the reaction mixture was washed with saturated $NaHCO_3$ (2 x 200ml), dried ($MgSO_4$), filtered and the solvent removed *in vacuo*. The resultant material was purified by silica gel column chromatography using petroleum ether as the eluent. Pure product was obtained as a colourless oil (10.07 g, 32.13 mmol, 83 %).[9] ^{1}H NMR (250 MHz, $CDCl_3$): δ (ppm) 3.45 (d, J = 4.76 Hz, 2H), 1.57 (bm, 1H), 1.43-1.18 (m, 24H), 0.95-0.81(m, 6H). ^{13}C NMR (250 MHz, $CDCl_3$): δ (ppm) 41. 4, 39. 6, 39. 6, 32. 6, 31. 9, 29. 8, 29. 50, 29. 4, 29. 3, 29. 1, 26. 6, 22. 6, 20. 4, 14. 3, 14. 1, 11. 4. EI-MS (*m/z*): $[M]^+$ calculated for $C_{16}H_{33}Br$ 305, found 305. Elem. Anal. Calcd. for $C_{16}H_{33}Br$: C 62.94, H 10.89, Br 26.17; found C 63.28, H 10.89, Br 25.14.

[2,2'-Bithiophen]-5-yltrimethylstannane (12)

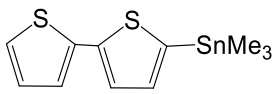

Under an inert argon atmosphere, 2,2'-bithiophene (1 g, 6.02 mmol) was dissolved in anhydrous THF (15 mL). The reaction was then cooled to -78 °C and *n*-BuLi (2.5 M in hexane, 2.40 ml, 6.02 mmol) was added dropwise. The mixture was stirred for 90 minutes at -78 °C. Upon completion, the temperature was raised up to room temperature and the solution was left to stir for 30 minutes. The reaction was then cooled to -78 °C and trimethyltin chloride (1.43 g, 7.20 mmol) in anhydrous THF (9 mL) was added dropwise. The reaction was left to stir overnight. The reaction mixture was quenched with a saturated solution of NH_4Cl. The crude material was extracted with DCM (3 x 100mL). The solvent was removed *in vacuo* to yield the title product as green oil (1.8 g, 5.47 mmol, 91 %).[10] The product was used in the next reaction without any purification due to its instability.

4,7-Di(thiophen-2-yl)benzo[c][1,2,5]thiadiazole (5)

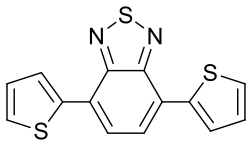

4,7-Dibromo-2,1,3-benzothiadiazole (**4**) (2.5 g, 8.57 mmol) and $Pd(PPh_3)_2Cl_2$ (0.15 g, 0.21 mmol) were placed in a one neck round bottom flask and placed under an argon atmosphere. Anhydrous toluene (25 mL) and 2-tributylstannylthiophene (6.81 ml, 21.44 mmol) was added to the reaction mixture. The reaction was degassed, placed under an inert argon atmosphere and maintained under reflux for 16 hours. Upon completion, the reaction was cooled to room temperature and the solvent was removed *in vacuo*. The crude material was purified via silica gel column chromatography using CH_2Cl_2:petroleum ether (1:1 v/v) as the eluent. The still crude material was purified with ethanol to produce 4,7-di(thiophen-2-yl)benzo[c][1,2,5]thiadiazole as an orange solid (2.20 g, 7.37 mmol, 86 %).[11] M.p. = 122 – 124 °C. ^{1}H NMR (400 MHz, $CDCl_3$): δ (ppm) 8.14 (dd, J = 3.74, 1.2 Hz, 2H), 7.9 (s, 2H), 7.48 (dd, J = 5.13, 1.22 Hz, 2H), 7.24 (dd, J = 5.17, 3.87 Hz, 2H). ^{13}C NMR (400 MHz, $CDCl_3$): δ (ppm) 152. 6, 139. 4, 128. 00, 127. 5, 126. 8, 126. 00, 125. 7. EI-MS (*m/z*): $[M]^+$ calculated for $C_{14}H_8N_2S_3$ 299.985, found 300.1. Elem. Anal. Calcd. for $C_{14}H_8N_2S_3$: C 55.97; H 2.68; N 9.32; S 32.02 Found: C 56.08; H 2.9; N 9.19; S 31.76.

4,7-Bis(5-(trimethylstannyl)thiophen-2-yl)benzo[c][1,2,5]thiadiazole (M3)

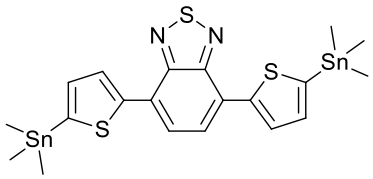

2,2,6,6-Tetramethylpiperdine (1.46 mL, 8.66 mmol) and anhydrous THF (20 mL) were placed in a two neck round bottom flask and placed under an inert argon atmosphere. The reaction was cooled to -78 °C and *n*-BuLi (2.5 M in hexane, 3.46 mL, 8.66 mmol) was then added dropwise. Once the addition was completed, the reaction mixture was stirred for a further 30 minutes at -78 °C. The reaction was then warmed to room temperature and stirred for 30 minutes. The reaction mixture was cooled again to -78 °C and 4,7-di(thiophen-2-yl)benzo[c][1,2,5]thiadiazole (1.00 g, 3.33 mmol) in THF (15 mL) was added dropwise. The reaction was left to stir at 45 minutes for -78 °C. Trimethyltin chloride (1.66 g, 8.32 mmol) in THF (15 mL) was added dropwise. The reaction mixture was gradually warmed to room temperature and left to stir overnight. Brine (25 mL) was added to quench the reaction mixture. The crude material was extracted with DCM (3 x 25 mL), washed with brine (3 x 50 mL), dried ($MgSO_4$), filtered and the solvent removed *in vacuo*. The crude material was recrystallised from ethanol to yield pure 4,7-bis(5-(trimethylstannyl)thiophen-2-yl)benzo[c][1,2,5]thiadiazole as red needles (1.46 g, 2.33 mmol, 70 %).[11] M.p. = 158 – 160 °C. ^{1}H NMR (400 MHz, $CDCl_3$): δ (ppm) 8.2 (d, J = 3.5 Hz, 2H), 7.90

(s, 2H), 7.32 (d, J = 3.5 Hz, 2H), 0.46 (s, 18H). ^{13}C NMR (400 MHz, $CDCl_3$): δ (ppm) 152. 7, 145. 1, 140. 2, 136. 2, 128. 4, 128. 2, 125. 8, -6. 3. GC-MS: mass calcd. for $C_{20}H_{24}N_2S_3Sn_2$, 625.914; found, 625.9**.** Elem. Anal. Calcd. for $C_{20}H_{24}N_2S_3$: C 38.37; H 3. 86; N 4.47; S 15.37. Found: C 38.35; H 3.78; N 4.34; S 15.08.

3-Ethyl-4-methyl-2-aminothiophene-3,4-dicarboxylate (9)

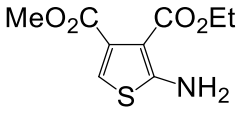

In an inert nitrogen atmosphere, ethyl cyanoacetate (8.5 g, 75.14 mmol), methyl 2-oxopropanoate (8.5 g, 83.2 mmol) and sulfur (2.81 g, 87.8 mmol) were dissolved in DMF (75 ml). A solution of triethylamine (57 mL) in DMF (40 mL) was added dropwise at room temperature. After complete addition, the temperature was raised to 50 °C and the reaction left to stir overnight. The mixture was cooled to room temperature and the reaction was quenched with water. The reaction mixture was left for 48 hours, after which time, long white needles were formed. The needles were filtered off and washed with ice-cold water to give the title product (9.98 g, 43.57 mmol, 58 %).[12] M.p. = 109 – 111 °C. ^{1}H NMR (400 MHz, $CDCl_3$) δ (ppm): 6.63 (s, 1H), 6.01 (s, 2H), 4.28 (q, *J* = 14.28 and 7.04 Hz, 2H), 3.86 (s, 3H), 1.33 (t, *J* = 7.1 Hz, 3H). ^{13}C NMR (400 MHz, $CDCl_3$) δ (ppm): 165.58, 164.59, 162.82, 132.44, 111.35, 104.92, 60.22, 52.22, 14.23. EI-MS (*m/z*): $[M]^+$ calculated for $C_9H_{11}NO_4S$ 229.0; Found 230.0. Elem. Anal. Calculated for $C_9H_{11}NO_4S$: C, 47.15; H, 4.84; N, 6.11; S, 13.99. Found: C, 46.49; H, 4.56; N, 5.91; S, 15.56.

Thiophene-3,4-dicarboxylic acid (10)

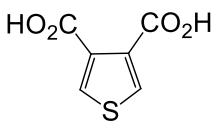

3-Ethyl-4-methyl-2-aminothiophene-3,4-dicarboxylate (**9**) (3.00 g, 12.4 mmol) was dissolved in anhydrous THF (270 mL). Under an inert atmosphere, this solution was added dropwise to a two-neck round bottom flask containing a boiling solution of *t*-butyl nitrite (1.7 mL, 1.47 g, 14.3 mmol) in anhydrous THF (360 mL). The mixture was maintained under reflux for 3 hours. Upon completion, the solvent was removed *in vacuo* and the crude product was purified by silica gel column chromatography using petroleum ether : ethylacetate (7:3) as the eluent. The solvent was removed *in vacuo*. To this material was added a dilute solution of NaOH (90 mL, 10 % w/w aq. sol). The mixture was stirred at 90 °C and left overnight. Upon completion, the solution was acidified to pH 1 with HCl and extracted with diethyl ether (3 x 300 mL). The organic layers were combined, dried with $MgSO_4$, filtered and the solvent removed *in vacuo* to yield the title compound as a white solid (0.62 g, 3.6 mmol, 29 %).[13]

M.p. = 226 – 228 °C. ^{1}H NMR (400 MHz, Acetone-d_6) δ (ppm): 8.58 (s, 2H). ^{13}C NMR (400 MHz, acetone-d_6) δ (ppm): 164. 3, 138. 8, 131. 6. EI-MS (*m/z*): $[M]^+$ calculated for $C_6H_4O_4S$ 171.98; Found 172.0. Elem. Anal. Calculated for $C_6H_4O_4S$: C, 41.86; H, 2.34; S, 18.63. Found: C, 44.64; H, 3.19; S, 16.04.

Thieno[3,4-c]furan-1,3-dione (11)

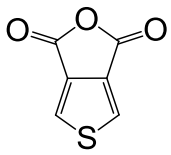

Thiophene-3,4-dicarboxylic acid (**10**) (3.00 g, 17.44 mmol) was dissolved in acetic anhydride (25 mL) and stirred at 110 °C for 2 h. The reaction mixture was cooled to room temperature resulting in the formation of brown, prism shaped crystals. The crystals were filtered off and then washed with ice-cold hexane to yield the title product as brown crystals (2.5 g, 16.23 mmol, 93 %).[14] M.p. = 155 – 157 °C. ^{1}H NMR (400 MHz, acetone-d_6) δ (ppm): 8.20 (s, 2H). ^{13}C NMR (400 MHz, acetone-d_6) δ (ppm): 157. 7, 136. 0, 131. 3. EI-MS (*m/z*): $[M]^+$ calculated for $C_6H_2O_3S$ 154.0; Found 154.0. Elem. Anal. Calculated for $C_6H_2O_3S$: C, 46.75; H, 1.31; S, 20.80. Found: C, 46.37; H, 1.75; S, 19.32.

5-Octyl-4H-thieno[3,4-c]pyrrole-4,6(5H)-dione (M6)

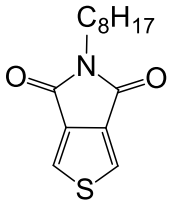

Under the protection of an argon atmosphere, thieno[3,4-c]furan-1,3-dione (**11**) (1.00 g, 3.21 mmol) was placed in a two neck round bottom flask and dissolved in anhydrous THF (5mL). *n*-Octylamine (0.47 g, 0.6 ml, 3.63 mmol) was then added dropwise to the mixture. Upon completion, the temperature was raised to 50 °C and left to stir for 3 hours. Upon completion, thionyl chloride (4.1 g, 2.5 ml, 34 mmol) was added dropwise and the reaction was left stirring at 50 °C overnight. The reaction mixture was precipitated in a H_2O : CH_3OH (75 mL : 37.5 mL) mixture. The precipitate was filtered off and purified by silica gel column chromatography using $CHCl_3$ as the eluent. The solvent was removed *in vacuo* to produce the final monomer as white powder (1.06 g, 2.50 mmol, 78 %).[15] M.p. = 121 – 123 °C. ^{1}H NMR (400 MHz, $CDCl_3$) δ (ppm): 7.82 (s, 2H), 3.62 (t, *J* = 7.48 Hz, 2H), 1.70-1.61 (m, 2H), 1.37–1.22 (br, 10H), 0.88 (t, *J* = 6.88 Hz, 3H). ^{13}C NMR (400 MHz, $CDCl_3$) δ (ppm): 162. 7, 136. 7, 125. 5, 38. 5, 31. 8, 29. 7, 29. 2, 28. 5, 26. 9, 22. 7, 14. 1. EI-MS (*m/z*): $[M]^+$ calculated for $C_{14}H_{19}NO_2S$ 265.11; Found 265.1. Elem. Anal. Calculated for $C_{14}H_{19}NO_2S$: C, 63.36; H, 7.22; N, 5.28; S, 12.08. Found: C, 63.40; H, 7.33; N, 4.85; S, 11.15.

5-(4-Hexylphenyl)-4H-thieno[3,4-c]pyrrole-4,6(5H)-dione (M7)

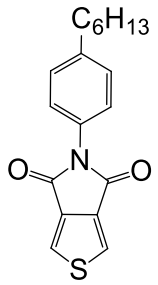

The title product was synthesised as described previously in the preparation of **M6**, using a mixture of thieno[3,4-c]furan-1,3-dione (**11**) (0.5 g, 3.24 mmol), 4-hexylaniline (0.66 g, 0.72 ml, 3.73 mmol) and thionyl chloride (4.1 g, 2.5 ml, 34 mmol) in anhydrous THF (5 mL). The desired product was obtained as a white powder (0.80 g, 2.55 mmol, 79 %).[15] M.p. = 158 – 160 °C. ^{1}H NMR (400 MHz, $CDCl_3$) δ (ppm): 7.97 (s, 2H), 7.31 (q, *J* = 13.47 and 8.06 Hz, 4H), 2.66 (t, *J* = 7.74 Hz, 2H), 1.70-1.61 (br, 4H), 1.43–1.30 (br, 4H), 0.91 (t, *J* = 6.88 Hz, 3H). ^{13}C NMR (400 MHz, $CDCl_3$) δ (ppm): 161. 7, 143. 4, 136. 3, 129. 4, 129. 1, 126. 5, 35. 7, 31. 7, 31. 3, 29. 1, 22. 6, 14. 3. EI-MS (*m/z*): $[M]^+$ calculated for $C_{18}H_{19}NO_2S$ 313.11; Found 313.1. Elem. Anal. Calculated for $C_{18}H_{19}NO_2S$: C, 68.98; H, 6.11; N, 4.47; S, 10.23. Found: C, 68.84; H, 6.09; N, 4.38 S, 10.00.

1,2-Bis(octyloxy)benzene (14)

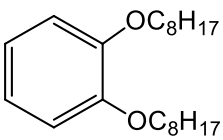

Under an inert nitrogen atmosphere catechol (20 g, 181.8 mmol) was dissolved in dry DMF (100 mL). 1-bromooctane (80.5 g, 72 mL, 0.4168 mol) and K_2CO_3 (76 g, 0.55 mol) were then added to the reaction vessel. The reaction was stirred for 40 hours at 100 °C. Upon completion, the mixture was left to cool down to room temperature. Water (100 mL) was added and the material was extracted with DCM (3 x 100 mL). The combined organic phases were dried over $MgSO_4$, filtered and the solvent was removed *in vacuo*. The crude product was recrystallized with ethanol to produce 1,2-bis(octyloxy)benzene as white needle like crystals (52.9 g, 0.16 mol, 88 %).[6] M.p. = 24 – 26 °C. ^{1}H NMR (400 MHz, $CDCl_3$) δ (ppm): 6.92 (s, 4H); 4.02 (t, 4H, *J* = 6.6 Hz); 1.90 – 1.80 (m, 4H); 1.51 – 1.41 (m, 4H), 1.41 – 1.26 (m, 16H), 0.91 (t, 6H, *J* = 6.65 Hz). ^{13}C NMR (400 MHz, $CDCl_3$) δ (ppm): 149. 2, 121. 0, 114. 1, 69. 3, 31. 8, 29. 4, 29. 4, 29. 3, 26. 1, 22. 7, 14. 1. EI-MS (*m/z*): $[M]^+$ calculated for $C_{22}H_{38}O_2$ 334.54, found 334.30. Elem. Anal. Calculated for $C_{22}H_{38}O_2$: C, 78.99; H, 11.45. Found: C, 78.84; H, 11.28.

1,2-Dinitro-4,5-bis(octyloxy)benzene (15)

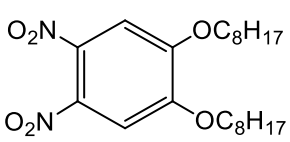

To a two neck round-bottom flask 1,2-bis(octyloxy)benzene (**14**) (20.00 g, 60.06 mmol) was introduced into a two-neck round bottom flask and dissolved in DCM (280 mL) and acetic acid (280 mL). The solution was cooled down to 0 °C and nitric acid (40 mL, 65 %) was added dropwise. Upon complete addition,

the mixture was warmed to room temperature and stirred for one hour. The reaction was again cooled down to 0 °C and nitric acid (100 mL, 100 %) was added dropwise. Upon complete addition, the reaction was warmed to room temperature and stirred for 40 hours. Upon completion, the solution was poured into ice-water and the organic layer separated. The material was extracted with DCM (3 x 100 mL). The organic phases were combined and washed with H_2O (3 x 100 mL), saturated aqueous of $NaHCO_3$ (3 x 100 mL) and brine (3 x 100 mL). The solution was dried over $MgSO_4$, filtered and the solvent was removed *in vacuo*. The crude product was recrystallized from ethanol to produce 1,2-dinitro-4,5-bis(octyloxy)benzene as a yellow solid (23.5 g, 0.055 mol, 92 %).[6] M.p. = 87 - 89 °C. ^{1}H NMR (400 MHz, $CDCl_3$) δ (ppm): 7.31 (s, 2H), 4.12 (t, 4H, *J* = 6.45 Hz), 1.94 – 1.81 (m, 4H), 1.51 – 1.41 (m, 4H), 1.41 – 1.26 (m, 16H), 0.91 (t, 6H, *J* = 6.7 Hz). ^{13}C NMR (400 MHz, $CDCl_3$) δ (ppm): 151. 8, 136. 5, 107. 9, 70. 2, 31. 8, 29. 2, 28. 7, 25. 8, 22. 7, 14. 1. EI-MS (*m/z*): $[M]^+$ calculated for $C_{22}H_{36}N_2O_6$ 424.53. Found 424.30. Elem. Anal. calculated for $C_{22}H_{36}N_2O_6$: C, 62.24; H, 8.55; N, 6.60. Found: C, 62.48; H, 8.45; N, 6.58.

4,5-Bis(octyloxy)benzene-1,2-diaminium chloride (16)

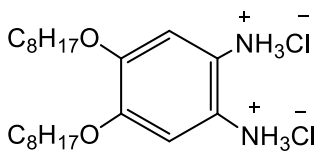

1,2-Dinitro-4,5-bis(octyloxy)benzene (**15**) (10.00 g, 23.55 mmol) and Sn(II)Cl_2 (42.4 g, 188.02 mmol) were dissolved in ethanol (250 mL) and HCl (100 mL, 35 %). The mixture was heated to 85 °C and left to stir overnight. After cooling to room temperature, the crude product was filtered and washed with H_2O (30 mL) and methanol (60 mL). The crude product was dried under a stream of nitrogen to produce the target product as an off-white solid (9.10 g, 0.020 mol, 88 %).[16] The instability of the product meant the product was used without any purification. ^{1}H NMR (400 MHz, DMSO-d_6) δ (ppm): 6.75 (s, 2H), 3.84 (t, 4H, *J* = 6.26 Hz), 1.71 – 1.62 (m, 4H), 1.51 – 1.41 (m, 4H), 1.41 – 1.26 (m, 16H), 0.86 (t, 6H, *J* = 6.83 Hz). ^{13}C NMR (400 MHz, DMSO-d_6) δ (ppm): 145. 1, 108. 00, 69. 1, 31. 2, 28. 6, 28. 7, 25. 5, 22. 1, 13. 9.

5,6-Bis(octyloxy)benzo[c][1,2,5]thiadiazole (17)

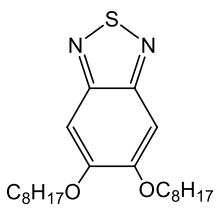

4,5-Bis(octyloxy)benzene-1,2-diaminium chloride(**16**) (9.00 g, 20.57 mmol) and triethylamine (6.30 mL, 46.10 mmol) were placed in a two-neck round bottom flask and dissolved in DCM (330 mL). Thionyl chloride (7 mL, 93.84 mmol) in DCM (25 mL) was added dropwise. The mixture was refluxed overnight. Upon completion, the reaction was poured into water (500 mL) and the crude material

was extracted with DCM (3 x 100 mL). The organic layers were combined, washed with water (3 x 100 mL), dried over $MgSO_4$ and filtered. The solvent was removed *in vacuo* and the crude product was recrystallized from ethanol to obtain the title product as an off-white solid (6.70 g, 0.02 mol, 83 %).[6] M.p. = 96 - 98 °C. ^{1}H NMR (400 MHz, $CDCl_3$) δ (ppm): 7.16 (s, 2H), 4.11 (t, 4H, *J* = 6.62 Hz), 2.2 – 1.83 (m, 4H), 1.6 – 1.5 (m, 4H), 1.47 – 1.25 (m, 16H), 0.91 (t, 6H, J = 6.73 Hz). ^{13}C NMR (400 MHz, $CDCl_3$) δ (ppm): 154. 1, 151. 4, 98. 4, 69. 1, 31. 8, 29. 3, 29. 3, 28. 7, 26. 0, 22. 7, 14. 1. EI-MS (*m/z*): $[M]^+$ calculated for $C_{22}H_{36}N_2O_2S$ 392.250. Found 392.32. Elem. Anal. Calculated for $C_{22}H_{36}N_2O_2S$: C, 67.30; H, 9.24; N, 7.14; S, 8.17 Found: C, 65.48; H, 8.45; N, 6.96; S, 7.90.

4,7-Dibromo-5,6-bis(octyloxy)benzo[c][1,2,5]thiadiazole (18)

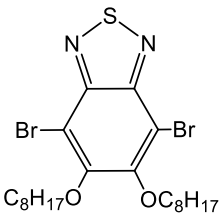

5,6-Bis(octyloxy)benzo[c][1,2,5]thiadiazole(**17**) (3.00 g, 7.64 mmol) was dissolved in a mixture of acetic acid (66 mL) and DCM (150 mL). Bromine (4 mL, 77.86 mmol) was then added dropwise. The mixture was left to stir in the dark for 48 hours at room temperature. Upon completion, the reaction mixture was poured into water (500 mL) and extracted with DCM (5 x 50 mL). The organic layer was washed with H_2O (3 x 80 mL), saturated $NaHCO_3$ (3 x 80 mL) and 1M $Na_2S_2O_3$ (3 x 80 mL). The solvent was removed *in vacuo* and the crude product was recrystallized from ethanol twice to produce 4,7-dibromo-5,6-bis(octyloxy)benzo[c][1,2,5]thiadiazole as a white fluffy solid (3.40 g, 6.18 mmol, 81 %).[6] M.p. = 44 - 46 °C. ^{1}H NMR (400 MHz, $CDCl_3$) δ (ppm): 4.18 (t, 4H, *J* = 6.51 Hz), 1.95 – 1.85 (m, 4H), 1.63 – 1.50 (m, 4H), 1.45 – 1.25 (m, 16H), 0.91 (t, 6H, *J* = 6.07 Hz). ^{13}C NMR (400 MHz, $CDCl_3$) δ (ppm): 154. 5, 150. 4, 106. 3, 75. 2, 31. 8, 30. 3, 29. 4, 29. 3, 26. 00, 22. 7, 14. 1. EI-MS (*m/z*): $[M]^+$ calculated for $C_{22}H_{34}Br_2N_2O_2S$ 550.069. Found 550.1. Elem. Anal. Calculated for $C_{22}H_{34}Br_2N_2O_2S$: C, 48.01; H, 6.23; N, 5.09; Br, 29.04; S, 5.83 Found: C, 47.63; H, 6.23; N, 4.96; Br, 28.86; S, 5.71.

5,6-Bis(octyloxy)-4,7-di(thiophen-2-yl)benzo[c][1,2,5]thiadiazole (19)

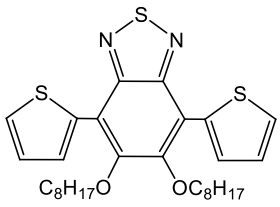

4,7-Dibromo-5,6-bis(octyloxy)benzo[c][1,2,5]thiadiazole (**18**) (3.00 g, 5.45 mmol), tri-*o*-tolylphosphine (531 mg, 1.74 mmol) and Pd_2dba_3 (200 mg, 0.22 mmol) were placed in a one neck round bottom flask, degassed and placed under an argon atmosphere. Anhydrous toluene (160 mL) was added to the mixture followed by 2-tributylstannylthiophene (5.20 mL, 13.93 mmol). The reaction

mixture was maintained under reflux for 16 hours under the protection of argon. Upon completion, the solvent was removed *in vacuo* and the crude product was purified by silica gel column chromatography using a gradient eluent (petroleum:$CHCl_3$). The title product was obtained as an orange oil (2.80 g, 5.03 mmol, 93 %).[6] M.p. = 74 - 76 °C.^{1}H NMR (400 MHz, $CDCl_3$) δ (ppm): 8.50 (dd, 2H, *J* = 3.81 and 1.12 Hz), 7.53 (dd, 2H, *J* = 5.17 and 1.10 Hz), 7.26 (dd, 2H, *J* = 5.16 and 3.80 Hz), 4.13 (t, 4H, *J* = 7.17 Hz), 2.00 – 1.9 (m, 4H), 1.51 – 1.41 (m, 4H), 1.41 – 1.26 (m, 16H), 0.92 (t, 6H, *J* = 6.87 Hz). ^{13}C NMR (400 MHz, $CDCl_3$) δ (ppm): 152. 0, 151. 0, 134. 1, 130. 6, 127. 3, 126. 8, 117. 6, 74. 8, 31. 8, 30. 4, 29. 5, 29. 3, 26. 0, 22. 7, 14. 1. EI-MS (*m/z*): $[M]^+$ calculated for $C_{30}H_{40}N_2O_2S_3$ 556.225, found 556.0. Elem. Anal. Calculated for $C_{30}H_{40}N_2O_2S_3$: C, 64.71; H, 7.24; N, 5.03; S, 17.27 Found: C, 62.40; H, 7.10; N, 4.90; S, 16.50.

4,7-Bis(5-bromothiophen-2-yl)-5,6-bis(octyloxy)benzo[c][1,2,5] thiadiazole (20)

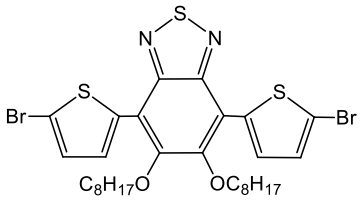

5,6-Bis(octyloxy)-4,7-di(thiophen-2-yl)benzo[c][1,2,5]thiadiazole (**19**) (1.50 g, 2.70 mmol) was dissolved in glacial acetic acid (50 mL) and $CHCl_3$ (50 mL). NBS (1.00 g, 5.65 mmol was added to the reaction mixture. The reaction was lift to stir for 20 hours at room temperature in the dark. Upon completion, the solvent was removed and the crude product was purified using silica gel column chromatography using a gradient eluent (petroleum:$CHCl_3$) to produce the title product as an orange solid (1.62 g, 2.27 mmol, 84 %).[6] M.p. = 75 - 76 °C. ^{1}H NMR (400 MHz, $CDCl_3$) δ (ppm): 8.39 (d, 2H, *J* = 4.15 Hz), 7.20 (d, 2H, *J* = 4.17 Hz), 4.14 (t, 4H, *J* = 7.08 Hz), 2.02 – 1.9 (m, 4H), 1.53 – 1.43 (m, 4H), 1.43 – 1.27 (m, 16H), 0.92 (t, 6H, *J* = 6.72 Hz). ^{13}C NMR (400 MHz, $CDCl_3$) δ (ppm): 151. 5, 150. 4, 135. 7, 131. 0, 129. 7, 117. 0, 115. 5, 74. 8, 31. 9, 30. 3, 29. 5, 29. 3, 26. 0, 22. 7, 14. 1. EI-MS (*m/z*): $[M]^+$ calculated for $C_{30}H_{38}Br_2N_2O_2S_3$ 714.04. Found 714.0. Elem. Anal. Calculated for $C_{30}H_{38}Br_2N_2O_2S_3$: C, 50.42; H, 5.36; N, 3.92; Br, 22.36; S, 13.46 Found: C, 50.37; H, 5.17; N, 3.87; Br, 22.43; S, 13.47.

5,6-Bis(octyloxy)-4,7-bis(5-(trimethylstannyl)thiophen-2yl) benzo[c][1,2,5]thiadiazole (M8)

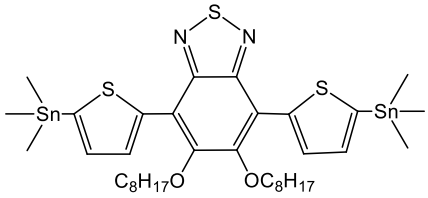

Under an inert atmosphere, 4,7-bis(5-bromothiophen-2-yl)-5,6-bis(octyloxy)benzo[c][1,2,5] thiadiazole (**20**) (0.25 g, 0.35 mmol) was dissolved in anhydrous THF (20 mL). The solution was cooled to -78 °C and *n*-BuLi (2.5 M in hexanes, 0.44 mL, 1.1 mmol) was added dropwise. The reaction was stirred for 3 hours at -78 °C. Trimethyltin

chloride (0.22 g, 1.1 mmol) in anhydrous THF (3 mL) was then added dropwise. The reaction mixture was allowed to warm to room temperature and left stirring overnight. The solution was poured onto brine and extracted with diethyl ether (5 x 70 mL). The organic layers were combined, washed with H_2O (4 x 100 mL), dried over $MgSO_4$ and filtered. The solvent was removed *in vacuo* to afford the monomer as a green oil (0.28 g, 0.31 mmol, 91 %). ^{1}H NMR (400 MHz, $CDCl_3$) δ (ppm): 8.53 (d, 2H, J = 3.53 Hz), 7.34 (d, 2H, *J* = 3.49 Hz), 4.13 (t, 4H, *J* = 6.96 Hz), 1.98 – 1.89 (m, 4H), 1.52 – 1.42 (m, 4H), 1.40 – 1.26 (m, 16H), 0.91 (t, 6H, *J* = 6.90 Hz). ^{13}C NMR (400 MHz, $CDCl_3$) δ (ppm): 152. 0, 151. 0, 134. 8, 131. 3, 127. 2, 126. 7, 117. 6, 74. 3, 31. 9, 30. 4, 29. 6, 29. 3, 26. 1, 22. 7, 14. 1, -8. 1. EI-MS (*m/z*): $[M]^+$ calculated for $C_{36}H_{56}N_2O_2S_3Sn$, 882.15. Found, 882.1. Elem. Anal. Calculated for $C_{36}H_{56}N_2O_2S_3Sn$: C, 49.00; H, 6.40; N, 3.17; S, 10.90 Found: C, 51.58; H, 6.62; N, 3.02; S, 10.47.

4,7-Di([2,2'-bithiophen]-5-yl)-5,6-bis(octyloxy)benzo[c][1,2,5] thiadiazole (21)

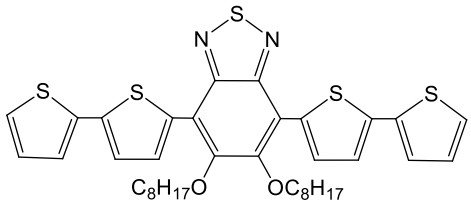

4,7-Dibromo-5,6-bis(octyloxy)benzo[c][1,2,5]thiadiazole (**18**) (1.41 g, 2.56 mmol), tri-o-tolylphosphine (25.50 mg, 83.70 μmol) and $Pd(OAc)_2$ (9.40 mg, 42.50 μmol) were placed in a one neck round bottom flask, degassed and placed under an argon atmosphere. Anhydrous toluene (25 mL) was added to the reaction followed by [2,2]bithiophenyl-5-yl-trimethyl-stannane (1**2**) (2.20 g, 6.70 mmol). The reaction mixture was refluxed for 24 hours. Upon completion, the crude product was purified using silica gel column chromatography using a gradient eluent (petroleum:$CHCl_3$) to give the title product as a red solid (1.03 g, 1.43 mmol, 56 %).[8] M.p. = 87 - 89 °C. ^{1}H NMR (400 MHz, $CDCl_3$) δ (ppm): 8.52 (d, 2H, *J* = 4.05 Hz), 7.32 (d, 2H, *J* = 1.17 Hz), 7.31 (d, 2H, *J* = 1.11 Hz), 7.29 (d, 2H, *J* = 1.08 Hz), 7.09 (dd, 2H, *J* = 5.12 and 3.64 Hz), 4.19 (t, 4H, *J* = 7.15 Hz), 2.05-1.95 (m, 4H), 1.56–1.26 (br, 20H), 0.90 (t, 6H, *J* = 6.54 Hz). ^{13}C NMR (400 MHz, $CDCl_3$) δ (ppm): 151. 6, 150. 8, 138. 9, 137. 6, 133. 2, 131. 2, 128. 0, 124. 7, 123. 8, 123. 6, 117. 3, 31. 9, 30.5, 29. 6, 29. 4, 26. 1, 22. 7, 14. 1. Elem. Anal. Calculated for $C_{38}H_{44}N_2O_2S_5$: C, 63.29; H, 6.15; N, 3.88. S, 22.23. Found: C, 63.11; H, 6.09; N, 3.78; S, 22.15.

4,7-Bis(5'-bromo-[2,2'-bithiophen]-5-yl)-5,6-bis(octyloxy)benzo[c] [1,2,5]thiadiazole (22)

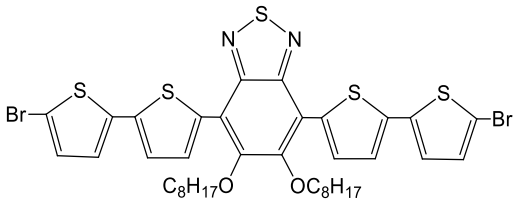

4,7-Di([2,2'-bithiophen]-5-yl)-5,6-bis(octyloxy) benzo [c][1,2,5]thiadiazole (**21**) (1.00 g, 1.38 mmol) and NBS (0.48 g, 2.70 mmol) were placed in a one neck round bottom flask and dissolved in dry chlorobenzene (25 mL). The reaction mixture was left to stir for 3 hours at 50 °C in the dark. Upon completion, the temperature was raised to 100 °C and the reaction stirred for a further 15 minutes. The solvent was removed *in vacuo* and the crude product was purified using silica gel column chromatography using petroleum ether:$CHCl_3$ (4:1) as the solvent system to give the title product as a red solid (0.84 g, 0.95 mmol, 70 %).[8] M.p. = 92 - 93 °C. ^{1}H NMR (400 MHz, $CDCl_3$) δ (ppm): 8.51 (d, 2H, *J* = 4.02 Hz), 7.25 (d, 2H, *J* = 4.02 Hz), 7.04 (q, 4H), 4.18 (t, 4H, *J* = 7.09 Hz), 2.04-1.94 (m, 4H), 1.56–1.26 (br, 20H), 0.91 (t, 6H, *J* = 6.54 Hz). ^{13}C NMR (400 MHz, $CDCl_3$) δ (ppm): 151. 7, 150. 7, 139. 1, 137. 8, 133. 6, 131. 7, 130. 8, 123. 8, 117. 2, 111. 3, 74. 6, 31. 9, 31. 9, 30. 5, 29. 6, 29. 4, 26. 1, 22. 4, 14. 2. EI-MS (*m/z*): $[M]^+$ calculated for $C_{38}H_{42}Br_2N_2O_2S_5$: 878.02. Found, 878.14. Elem. Anal. Calculated for $C_{38}H_{42}Br_2N_2O_2S_5$: C, 51.93; H, 4.82; Br, 18.18; N, 3.19; S, 18.24 Found: C, 52.06; H, 4.90; Br, 18.26; N, 3.08; S, 17.99.

5,6-Bis(octyloxy)-4,7-bis(5'-(trimethylstannyl)-[2,2'-bithiophen]-5-yl)benzo[c][1,2,5]thiadi azole (M9)

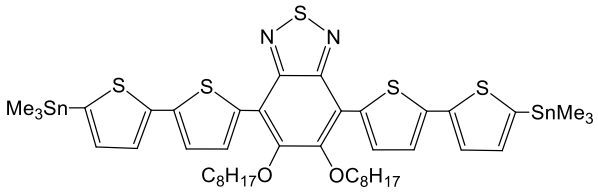

Under an inert atmosphere, 4,7-bis(5'-bromo-[2,2'-bithiophen]-5-yl)-5,6-bis(octyloxy)benzo [c][1,2,5]thiadiazole (**22**) (0.20 g, 0.23 mmol) was dissolved in dry THF (20 mL). The solution was cooled to -78 °C and *n*-BuLi (2.5 M in hexane, 0.29 mL, 0.72 mmol) was added dropwise. The mixture was stirred for 3 hours at -78 °C. Trimethyltin chloride (0.14 g, 0.71 mmol) in THF (3 mL) was then added dropwise. Upon complete addition, the reaction mixture was gradually warmed to room temperature and stirred overnight. The solution was poured into brine and extracted with diethyl ether (5 x 50 mL). The organic layers were combined, washed with H_2O (3 x 100 mL), dried over $MgSO_4$ and filtered. The solvent was removed *in vacuo* to produce the final monomer as a red oil (0.23 g, 0.22 mmol, 97 %). ^{1}H NMR (400 MHz, $CDCl_3$) δ (ppm): 8.52 (d, 2H, *J* = 3.93 Hz), 7.42 (d, 2H, *J* = 3.18 Hz), 7.31 (d, 2H, *J* = 3.80 Hz), 7.16 (d, 2H, *J* = 3.15 Hz), 4.18 (t, 4H, *J* = 6.91 Hz), 2.06-1.95 (m, 4H), 1.57–1.21 (br, 20H), 0.90 (t, 6H, *J* = 6.54 Hz), 0.43

(s, 18H). ^{13}C NMR (400 MHz, $CDCl_3$) δ (ppm): 151. 6, 150. 8, 139. 0, 137. 9, 133. 0, 131. 7, 128. 0, 123. 8, 117. 2, 111. 3, 74. 6, 31. 8, 31. 9, 30. 5, 29. 6, 29. 4, 26. 1, 22. 4, 14. 1. EI-MS (*m/z*): $[M]^+$ calculated for $C_{44}H_{60}N_2O_2S_5Sn_2$: 1046.70; found 1045.9**.** Elem. Anal. Calculated for $C_{44}H_{60}N_2O_2S_5Sn_2$: C, 50.49; H, 5.78; N, 2.68; S, 15.32. Found: C, 52.90; H, 6.12; N, 2.56; S, 14.20.

6.5. Preparation of polymers

Poly(4,5,9,10-tetrakis((2-hexyldecyl)oxy)-pyrene-2,7-diyl-alt-(4,7-dithiophen-2-yl)- 2',1',3'-benzothiadiazole-5,5-diyl] (PP_{HD}-DTBT)

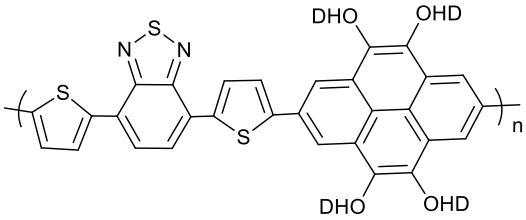

A mixture of 2,7-dibromo-4,5,9,10-tetrakis((2-hexyldecyl)oxy)pyrene (**M1**) (160 mg, 0.12 mmol), 4,7-bis(5-(trimethylstanyl)thiophene-2-yl)benzo[c][1, 2,5]thiadiazole (**M3**) (75 mg, 0.12 mmol), $Pd(OAc)_2$ (2.00 mg, 8.9 μmol) and tri(*o*-tolyl)phosphine (5.38 mg, 17.7 μmol) were placed in a one neck round bottom flask and placed under an inert argon atmosphere. Anhydrous toluene (10 mL) was added, the system was degassed and placed under an inert argon atmosphere. The reaction was heated to 100 °C and left to stir for 48 hours. Upon completion, the reaction was allowed to cool to room temperature. 2-(Tributylstannyl)thiophene (11.7 μL, 0.037 mmol) was added, the system was degassed and the solution maintained under reflux for 1 hour. Upon completion, the reaction was cooled to room temperature and 2-bromothiophene (45.1 mg, 0.28 mmol) was added. The reaction vessel was degassed again and the solution heated to 100 °C and maintained under reflux for a further hour. Upon completion, the reaction was cooled to room temperature. Chloroform (250 mL) was then added to the reaction mixture followed by addition of an ammonium hydroxide solution (28% in H_2O, 40 mL) and the mixture was stirred at 60 °C for 3 hour. The mixture was cooled and the organic phase was separated and washed with water (5 x 100 mL). The organic phase was collected, concentrated to 40 mL *in vacuo* and precipitated in methanol (300 mL). The solids were filtered through a membrane and subjected to Soxhlet extraction in turn with methanol, acetone, hexane and toluene. The toluene fraction was concentrated *in vacuo* and precipitated in methanol. The precipitate was stirred overnight. The pure polymer was filtered through a membrane filter and collected as a dark purple solid (65 mg, 37 %). GPC toluene fraction: M_n = 20,500 Da; M_w = 30,200 Da; Đ = 1.47. ^{1}H NMR (500 MHz, $C_2D_2Cl_4$, 100 °C) δ (ppm): 8.83 (s,

4H), 8.35 (br.d, 2H), 8.00 (br.s, 2H), 7.80 (br.d, 2H), 4.30 (br.d, 8H), 2.20-2.00 (m, 4H), 1.90-1.75 (m, 4H), 1.75-1.20 (m, 90H), 0.90 (br.t, 24H). Elem. Anal. Calcd. for $C_{94}H_{142}N_2O_4S_3$: C 77.20, H 9.90, N 1.90, S 6.58. Found: C 75.49, H 9.24, N 1.98, S 8.12.

Poly(4,5,9,10-tetrakis((2-hexyldecyl)oxy)pyrene-2,7-diyl-alt-(5,6-difluoro-4,7-di(thiophen-2-yl)-2',1',3'-benzothiadiazole-5,5-diyl] (PP_{HD}-DTffBT)

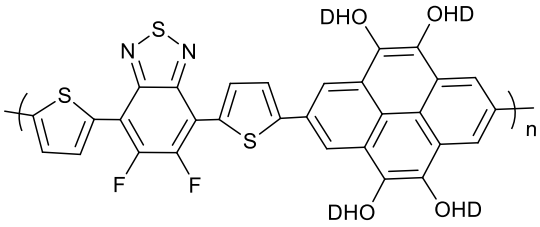

The title product was synthesised as described previously in the preparation of **PP_{HD}-DTBT**, using a mixture of **M1** (160 mg, 0.12 mmol), 5,6-difluoro-4,7-bis(5-(trimethylstannyl)thiophen-2-yl)benzo[c][1,2,5]thiadiazole (80 mg, 0.12 mmol), $Pd(OAc)_2$ (2.00 mg, 8.9 μmol) and tri(*o*-tolyl)phosphine (5.38 mg, 17.7 μmol) in toluene (10 mL). The product was obtained as a dark purple solid (115 mg, 64 %). GPC toluene fraction: M_n = 20,700 Da; M_w = 40,400 Da; Đ = 1.95. ^{1}H NMR (500 MHz, $C_2D_2Cl_4$, 100 °C) δ (ppm): 8.86 (br.s, 4H), 8.50 (br.d, 2H), 7.83 (br.d, 2H), 4.30 (br.d, 8H), 2.20-2.00 (m, 4H), 1.90-1.75 (m, 4H), 1.75-1.20 (m, 90H), 0.90 (br.t, 24H). Elem. Anal. Calcd. for $C_{94}H_{142}F_2N_2O_4S_3$: C 75.35, H 9.55, N 1.87, S 6.41. Found C 72.13, H 8.90, N 2.38, S 8.02.

Poly(4,5,9,10-tetrakis((2-ethylhexyl)oxy)pyrene-2,7-diyl-alt-(4,7-dithiophen-2-yl)-2',1',3'-benzothiadiazole-5,5-diyl] (PP_{EH}-DTBT)

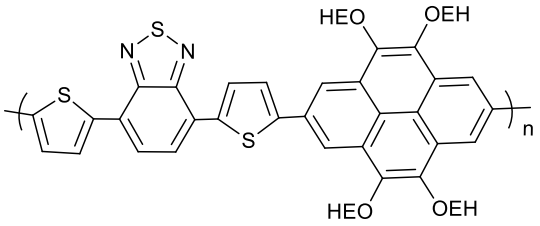

The title product was synthesised as described previously in the preparation of **PP_{HD}-DTBT**, using a mixture of **M2** (120 mg, 0.13 mmol), **M3** (86 mg, 0.13 mmol), $Pd(OAc)_2$ (2.20 mg, 8.9 μmol) and tri(*o*-tolyl)phosphine (6.00 mg, 20.00 μmol) in toluene (8 mL). The product was obtained as a dark purple solid (38 mg, 35 %). GPC chloroform fraction: M_n = 12,800 Da; M_w = 20,000 Da; Đ = 1.56. ^{1}H NMR (500 MHz, $C_2D_2Cl_4$, 100 °C) δ (ppm): 8.80 (br.s, 4H), 8.27 (br.d, 2H), 8.00 (br.s, 2H), 7.73 (br.d, 2H), 4.3 (br.d, 8H), 2.05 (m, 4H), 1.94-1.27 (m, 32H), 1.14 (br.t, 12H), 0.98 (t, 12H). Elem. Anal. Calcd. for $C_{62}H_{78}N_2O_4S_3$: C 73.62, H 7.77, N 2.77, S 9.51. Found C 77.48, H 10.52, N 1.49, S 5.24.

Poly-4,5,9,10-tetrakis((2-ethylhexyl)oxy)pyrene-2,7-diyl-alt-(5,6-difluoro-4,7-di(thiophen-2-yl)-2',1',3'-benzothiadiazole-5,5-diyl] (PP_{EH}-DTffBT)

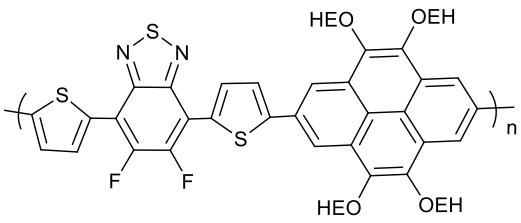

PP_{EH}-DTffBT was synthesised as outlined previously in the preparation of **PP_{HD}-DTBT**, using a mixture of **M2** (105 mg, 0.12 mmol), 5,6-difluoro-4,7-bis(5-(trimethylstannyl)thiophen-2-yl)benzo[c][1,2,5]thiadiazole (80 mg, 0.12 mmol), $Pd(OAc)_2$ (2.00 mg, 8.9 μmol) and tri(*o*-tolyl)phosphine (5.38 mg, 17.7 μmol) in toluene (10 mL). The product was obtained as a dark purple solid (30 mg, 24 %). GPC chloroform fraction: M_n = 5,300 Da; M_w = 6,300 Da; Đ = 1.18. ^{1}H NMR (500 MHz, $C_2D_2Cl_4$, 100 °C) δ (ppm): 8.85 (br.s, 4H), 8.50 (br.d, 2H), 7.82 (br.d, 2H), 4.3 (br.d, 8H), 2.05 (m, 4H), 1.94-1.27 (m, 32H), 1.14 (br.t, 12H), 0.98 (t, 12H). Elem. Anal. Calcd. For $C_{62}H_{76}F_2N_2O_4S_3$: C 71.09, H 7.31, N 2.67, S 9.18. Found C 62.00, H 6.40, N 2.60, S 9.00.

Poly((2,2'-(4,5,9,10-tetrakis((2-ethylhexyl)oxy)pyrene-2,7-diyl)dithiophene)-alt-(5-octyl-thieno[3,4,c]pyrrole-4,6-dione)) (PP_{EH}DT-TPD_O)

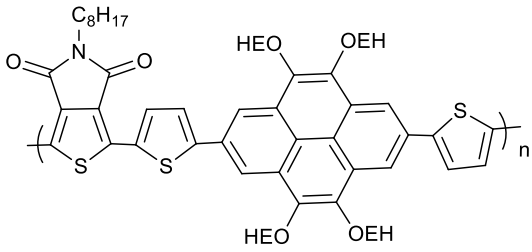

A mixture of 5,5'-(4,5,9,10-tetrakis((2-ethylhexyl)oxy)pyrene-2,7-diyl)bis(2-bromothiophene) (**M4**) (170 mg, 0.16 mmol), 5-octyl-4H-thieno[3,4-c]pyrrole-4,6(5H)-dione (**M6)** (43.48 mg, 0.164 mmol), $PdCl_2(MeCN)_2$ (1.3 mg, 5.00 μmol), $P(C_6H_4$-o-$OMe)_3$ (1.8 mg, 5.00 μmol), Cs_2CO_3 (160 mg, 0.5 mmol) and pivalic acid (PivOH) (16.7 mg, 0.16 mmol) were put in a Schlenk tube and placed under an inert argon atmosphere. Anhydrous THF (1 mL) was added to the mixture. The reaction mixture was stirred at room temperature for 30 minutes and then at 100 °C for 48 hours. The solution was cooled down to room temperature and washed with water (3 x 150 mL). The organic phases were combined, concentrated *in vacuo* and precipitated in methanol. The resulting solid was collected via filtration and subject to Soxhlet extraction with methanol, acetone, hexane, toluene and chloroform. The chloroform fraction was concentrated *in vacuo* and precipitated into methanol. The solid was filtered by a membrane filter and the polymer was obtained as a dark red solid (44 mg, 0.038 mmol, 24 %). GPC chloroform fraction: M_n = 19,700 Da; M_w = 38,400 Da; Đ = 1.95. ^{1}H NMR (500 MHz, $C_2D_2Cl_4$, 100 °C) δ (ppm): 8.75 (s, 4H), 8.60 (d, 2H), 8.30 (d, 2H), 4.3 (d, 8H), 3.80 (t, 2H), 2.10-1.20 (br, 48H), 1.20-

0.85 (br, 27H). Elem. Anal. Calculated for $C_{70}H_{93}NO_6S_5$: C, 73.71; H, 8.22; N, 1.23; S, 8.43; Found: C, 73.32; H, 8.56; N, 1.00; S, 7.37.

Synthesis of Poly((2,2'-(4,5,9,10-tetrakis((2-ethylhexyl)oxy)pyrene-2,7-diyl)dithiophene)-alt-(5-(4-hexylphenyl)-thieno[3,4-c]pyrrole-4,6-dione)) ($PP_{EH}DT$-TPD_{HP})

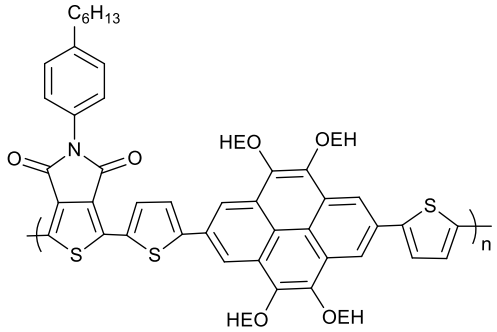

$PP_{EH}DT$-TPD_{HP} was synthesised according to the polymerisation method outlined for **$PP_{EH}DT$-TPD_O**, using a mixture of **M4** (140 mg, 0.135 mmol), **M7** (42.30 mg, 0.135 mmol), $PdCl_2(MeCN)_2$ (1.3 mg, 5.00 µmol), $P(C_6H_4$-o-$OMe)_3$ (1.8 mg, 5.00 µmol), Cs_2CO_3 (160 mg, 0.5 mmol) and PivOH (16.7 mg, 0.16 mmol) in THF (1.2 ml). The product was obtained as a dark red solid (28 mg, 0.023 mmol, 18 %). GPC toluene fraction: M_n = 5,700; M_w = 8700; Đ = 1.53. ^{1}H NMR (500 MHz, $C_2D_2Cl_4$, 100 °C) δ (ppm): 8.80-8.65 (br, 4H), 8.60 (d, 2H), 8.30 (d, 2H), 7.45-7.30 (q, 4H), 4.30 (d, 8H), 2.66 (t, 2H), 2.10-1.93 (br, 4H), 1.90-1.20 (br, 40H), 1.20-0.85 (br, 27H). Elem. Anal. Calculated for $C_{74}H_{93}NO_6S_5$: C, 74.77; H, 7.89; N, 1.18; S, 8.09. Found: C, 75.08; H, 11.00; N, 0.80; S, 6.90.

Poly((5,5''-(4,5,9,10-tetrakis((2-ethylhexyl)oxy)pyrene-2,7-diyl)di-2,2'-bithiophene)-alt-(5-octyl-thieno[3,4,c]pyrrole-4,6-dione)) ($PP_{EH}DT2$-TPD_O)

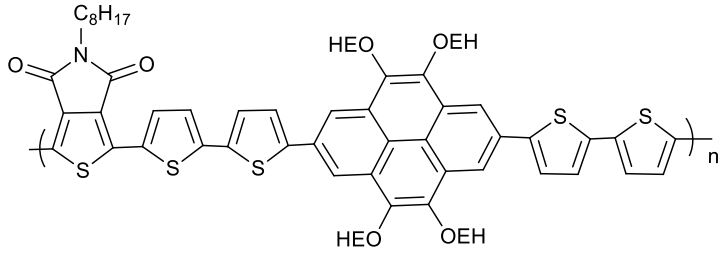

$PP_{EH}DT2$-TPD_O was synthesised according to the polymerisation method outlined for **$PP_{EH}DT$-TPD_O**, using a mixture of **M5** (140 mg, 0.116 mmol), **M6** (30.92 mg, 0.116 mmol), $PdCl_2(MeCN)_2$ (1.3 mg, 5.00 µmol), $P(C_6H_4$-o-$OMe)_3$ (1.8 mg, 5.00 µmol), Cs_2CO_3 (160 mg, 0.5 mmol) and PivOH (16.7 mg, 0.16 mmol) in THF (1.2 ml). The polymer was obtained as a dark red solid (42 mg, 0.032 mmol, 24 %). GPC chloroform fraction: M_n = 9,100, M_w = 12,700, Đ = 1.40. ^{1}H NMR (500 MHz, $C_2D_2Cl_4$, 100 °C) δ (ppm): 8.70-8.55(br, 4H), 7.46 (d, 2H), 7.35 (dd, 2H), 7.20 (dd, 4H), 4.3 (d, 8H), 3.70 (t, 2H), 2.20-0.70 (br, 75H). Elem. Anal. Calculated for $C_{78}H_{97}NO_6S_5$: C, 71.79; H, 7.49; N, 1.07; S, 12.29. Found: C, 67.00; H, 7.00; N, 1.00; S, 11.10.

Poly{(5,5''-(4,5,9,10-tetrakis((2-ethylhexyl)oxy)pyrene-2,7-diyl)di-2,2'-bithiophene)-alt-(5-(4-hexylphenyl)-thieno[3,4-c]pyrrole-4,6-dione)) ($PP_{EH}DT2\text{-}TPD_{HP}$)

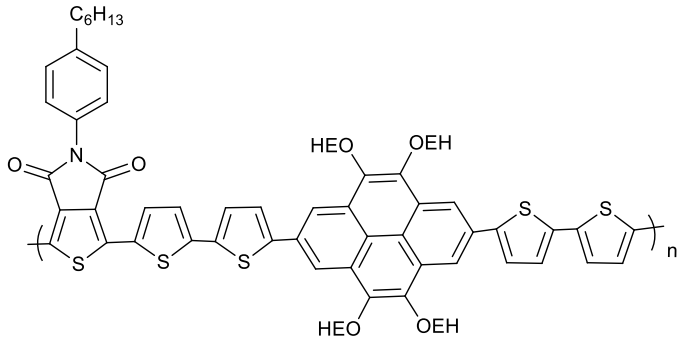

$PP_{EH}DT2\text{-}TPD_{HP}$ was synthesised according to the polymerisation method outlined for **$PP_{EH}DT\text{-}TPD_{O}$**, using a mixture of **M5** (110 mg, 0.091 mmol), **M7** (28.70 mg, 0.091 mmol), $PdCl_2(MeCN)_2$ (1.3 mg, 5.00 µmol), $P(C_6H_4\text{-}o\text{-}OMe)_3$ (1.8 mg, 5.00 µmol), Cs_2CO_3 (160 mg, 0.5 mmol) and PivOH (16.7 mg, 0.16 mmol) in THF (1.2 ml). The polymer was obtained as a black solid (55 mg, 0.040 mmol, 44 %). GPC chloroform fraction: M_n = 5,500, M_w = 9,200, Đ = 1.66. ^{1}H NMR (500 MHz, $C_2D_2Cl_4$, 100 °C) δ (ppm): 8.80-8.65 (br, 4H), 8.60 (d, 2H), 8.30 (d, 2H), 7.45-7.30 (q, 4H), 4.30 (d, 8H), 2.66 (t, 2H), 2.10-1.93 (br, 4H), 1.90-1.20 (br, 44H), 1.20-0.85 (br, 27H). Elem. Anal. Calculated for $C_{82}H_{97}NO_6S_5$: C, 72.79; H, 7.23; N, 1.04; S, 11.85. Found: C, 69.00; H, 6.81; N, 0.90; S, 10.42.

Poly [4,5,9,10-tetrakis((2-ethylhexyl)oxy)pyrene-alt-5,6-bis(octyloxy)-4,7-di(thiophene-2yl) benzo[c][1,2,5]thiadiazole (PP_{EH}-DTBT-8)

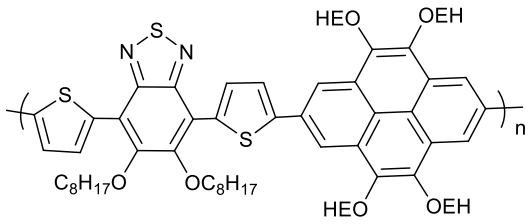

PP_{EH}-DTBT-8 was synthesised as described previously in the preparation of **PP_{HD}-DTBT**, using a mixture of **M2** (0.140 g, 0.160 mmol), **M8** (0.141 g, 0.160 mmol), $Pd(OAc)_2$ (2.00 mg, 11 µmol) and tri(*o*-toly)phosphine (7.00 mg, 23 µmol) in toluene (5 mL). The product was obtained as a dark red solid (50 mg, 0.04 mmol, 25 %). GPC hexane fraction: M_n = 4,700 Da; M_w = 7,000 Da; Đ = 1.49. ^{1}H NMR (500 MHz, $C_2D_2Cl_4$, 100 °C) δ (ppm): 8.85 (br.s, 4H), 8.63 (br.d, 2H), 7.83 (br.d, 2H), 4.40-4.14 (m, 12H), 2.13-1.95 (m, 8H), 1.95-1.20 (m, 52H), 1.13 (br.t, 12H), 0.95 (br.t, 12H), 0.80 (br.t, 6H). Elem. Anal. Calculated for $C_{78}H_{110}N_2O_6S_3$: C, 73.89; H, 8.74; N, 2.21; S, 7.59. Found: C, 72.73; H, 8.53; N, 2.22; S, 7.33.

Poly[4,5,9,10-tetrakis((2-ethylhexyl)oxy)pyren-alt-4,7-di([2,2'-bithiophen]-5-yl)-5,6-bis (octyloxy)benzo[c][1,2,5]thiadiazole (PP_{EH}-DT2BT-8)

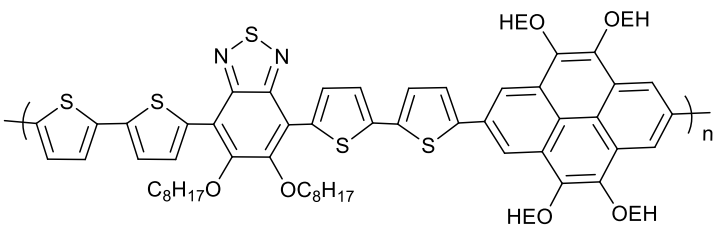

PP_{EH}-DT2BT-8 was synthesised according to the polymerisation method outlined for **PP_{EH}-DTBT-8**, using a mixture of **M2** (0.117 g, 0.134 mmol), **M9** (0.140 g, 0.134 mmol), $Pd(OAc)_2$ (2.00 mg, 11 μmol) and tri(*o*-toly)phosphine (7.00 mg, 23 μmol) in toluene (5 mL). However, the main fraction of the polymer was extracted with toluene. The polymer was obtained as a dark purple solid (0.130 mg, 0.09 mmol, 68 %). GPC toluene fraction: M_n = 11,200 Da; M_w = 20,900 Da; Đ = 1.87. ^{1}H NMR (500 MHz, $C_2D_2Cl_4$, 100 °C) δ (ppm): 8.70 (br.s, 4H), 8.50 (br.d, 2H), 7.56 (br.d, 2H), 7.40 (br.d, 4H), 4.33-4.10 (m, 12H), 2.10-1.90 (m, 8H), 1.95-1.20 (m, 52H), 1.10 (br.t, 12H), 0.97 (br.t, 12H), 0.87 (br.t, 6H). Elem. Anal. Calculated for $C_{86}H_{114}N_2O_6S_5$: C, 72.12; H, 8.02; N, 1.96; S 11.19. Found: C, 70.51; H, 7.70; N, 2.01; S, 10.88.

6.6. References

1 V. V Filichev, I. V Astakhova, A. D. Malakhov, V. A. Korshun and E. B. Pedersen, *Chem. Eur. J.*, 2008, **14**, 9968–9980.

2 J. Hu, D. Zhang and F. W. Harris, *J. Org. Chem.*, 2005, **70**, 707–708.

3 J. A. Letizia, S. Cronin, R. P. Ortiz, A. Facchetti, M. A. Ratner and T. J. Marks, *Chem. - A Eur. J.*, 2010, **16**, 1911–1928.

4 S. Kawano, M. Baumgarten, D. Chercka, V. Enkelmann and K. Mu, *Chem. Commun.*, 2013, **49**, 5058–5060.

5 N. Wang, X. Bao, Y. Yan, D. Ouyang, M. Sun, V. A. L. Roy, C. S. Lee and R. Yang, *J. Polym. Sci. Part A Polym. Chem.*, 2014, **52**, 3198–3204.

6 M. H. Petersen, S. A. Gevorgyan, F. C. Krebs and R. A. J. Janssen, *Chem. Mater.*, 2009, **21**, 4669–4675.

7 S. Ellinger, A. Kreyes, U. Ziener, C. Hoffmann-Richter, K. Landfester and M. Möller, *Eur. J. Org. Chem.*, 2007, 5686–5702.

8 H. Yi, S. Al-Faifi, A. Iraqi, D. C. Watters, J. Kingsley and D. G. Lidzey, *J. Mater. Chem.*, 2011, **21**, 13649.

9 G. A. Wiley, R. L. Hershkowitz, B. M. Rein and B. C. Chung, *J. Am. Chem. Soc.*, 1964, **86**, 964-965.

10 K. Parab, K. Venkatasubbaiah and F. Jäkle, *J. Am. Chem. Soc.*, 2006, **128**, 12879-12885.

11 B. Fu, J. Baltazar, Z. Hu, A.-T. Chien, S. Kumar, C. L. Henderson, D. M. Collard and E. Reichmanis, *Chem. Mater.*, 2012, **24**, 4123–4133.

12 P. Berrouard, E. Gagnon, C. Tessier, M. Leclerc and V. La, *Org. Lett.*, 2011, **13**, 38-41.

13 P. Berrouard, S. Dufresne, A. Pron, J. Veilleux and M. Leclerc, *J. Org. Chem.*, 2012, **77**, 8167–8173.

14 E. Zhu, B. Ni, B. Zhao, J. Hai, L. Bian, H. Wu and W. Tang, *Macromol. Chem. Phys.*, 2014,

215, 227-234.

15 J. Warnan, A. El Labban, C. Cabanetos, E. T. Hoke and P. Kumar, *Chem. Mat.*, 2014, **26**, 2299-2306.

16 P. Ding, B. Liu, B. Peng, Y. Zou, Y. He and K. Zhou, *Macromol. Chem. Phys.*, 2010, **211**, 2555-2561.

17 M. Wakioka, N. Ichihara, Y. Kitano and F. Ozawa, *Macromolecules*, 2014, **47**, 626-631.

Chapter VII:

Supplementary Information

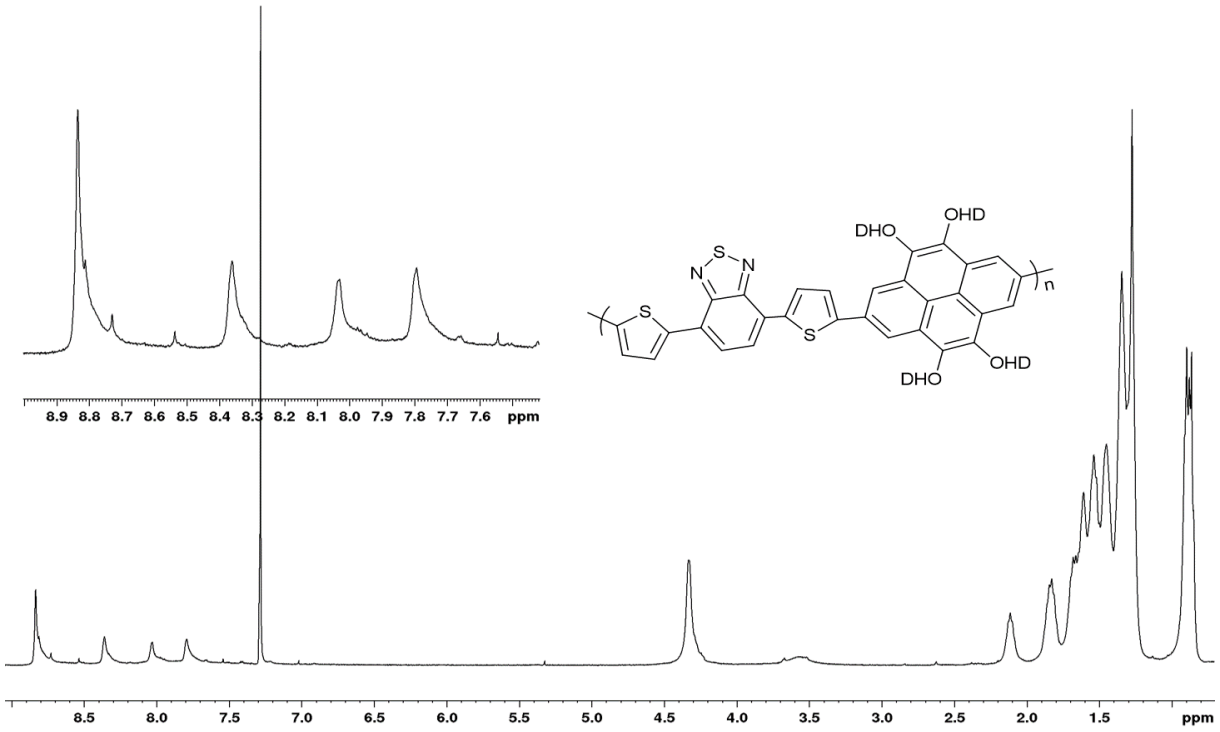

Figure 1. ^{1}H NMR spectrum of **PP_{HD}-DTBT** in $CDCl_3$.

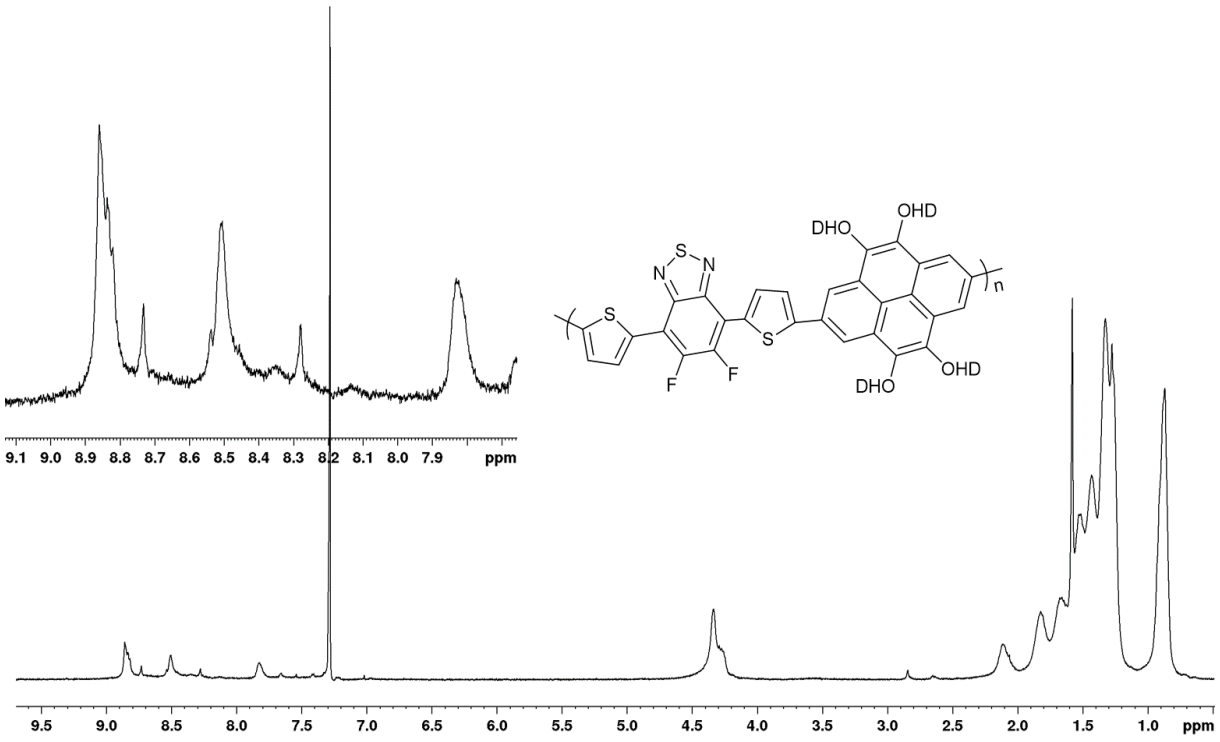

Figure 2. ^{1}H NMR spectrum of **PP_{HD}-DTffBT** in $CDCl_3$.

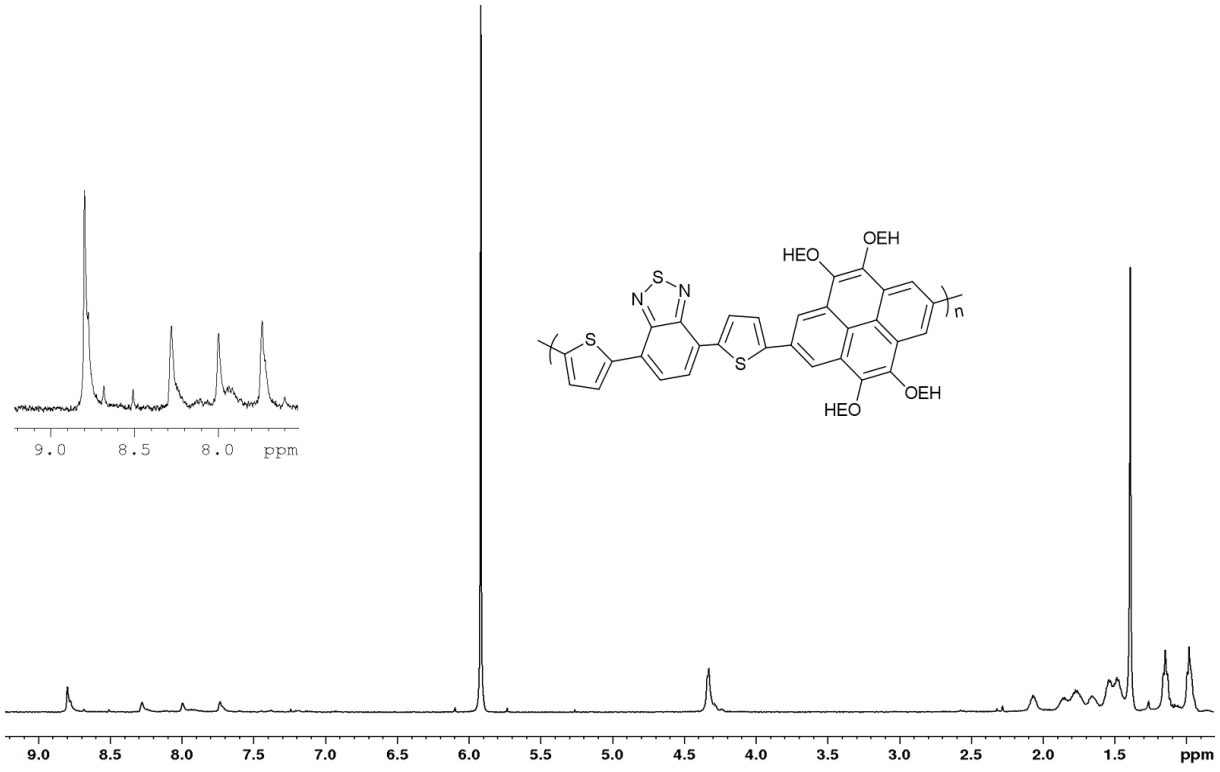

Figure 3. ^{1}H NMR spectrum of **PP_{EH}-DTBT** at 100 ºC in $C_2D_2Cl_4$.

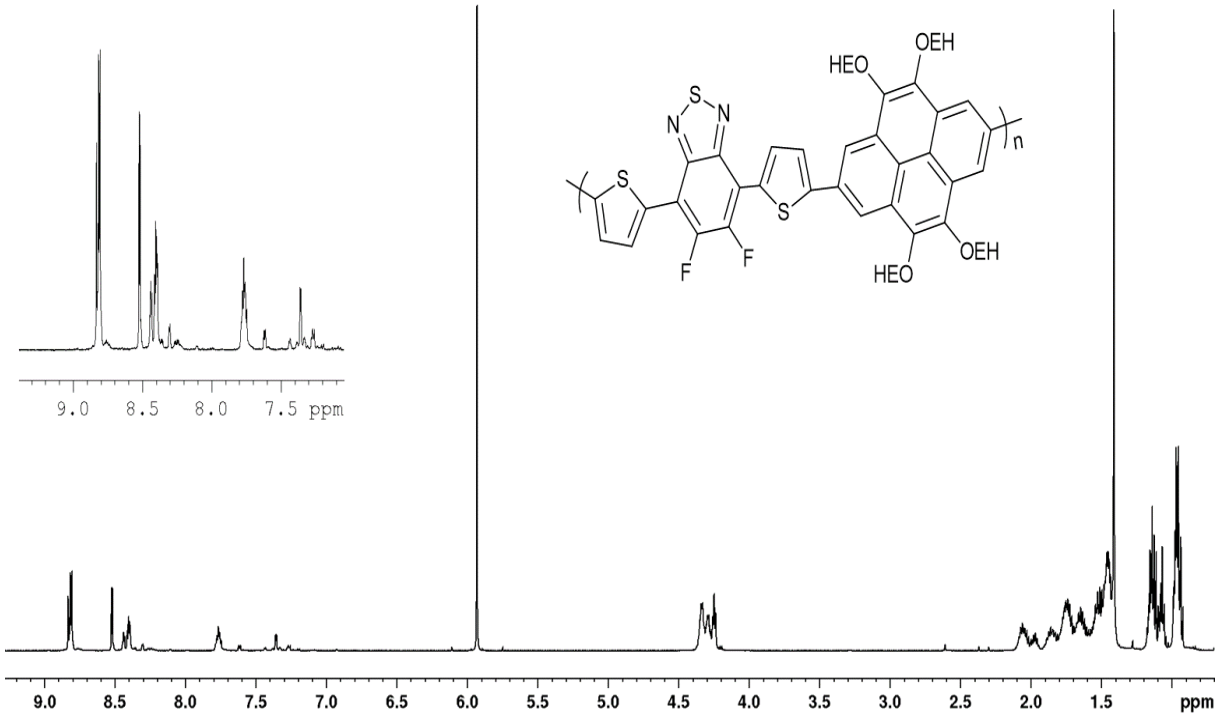

Figure 4. ^{1}H NMR spectrum of **PP_{EH}-DTffBT** at 100 ºC in $C_2D_2Cl_4$.

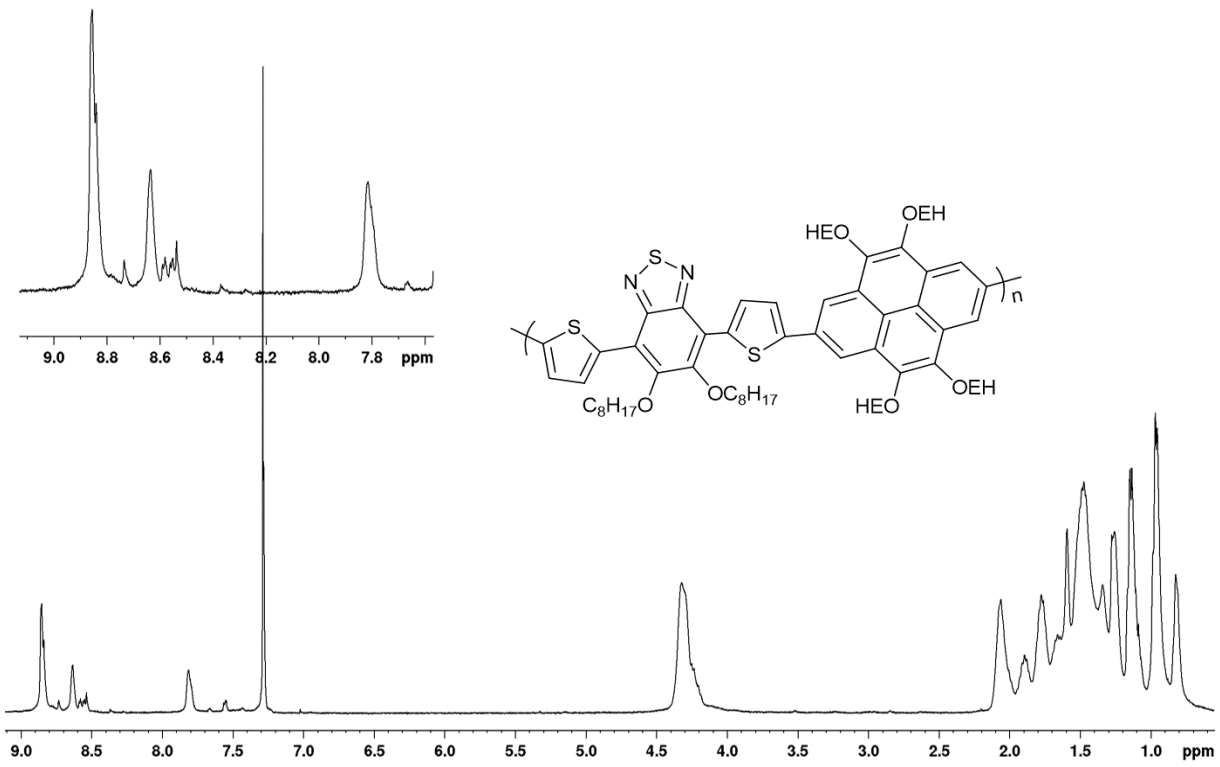

Figure 5. ^{1}H NMR spectrum of **PP$_{EH}$-DTBT-8** in $CDCl_3$.

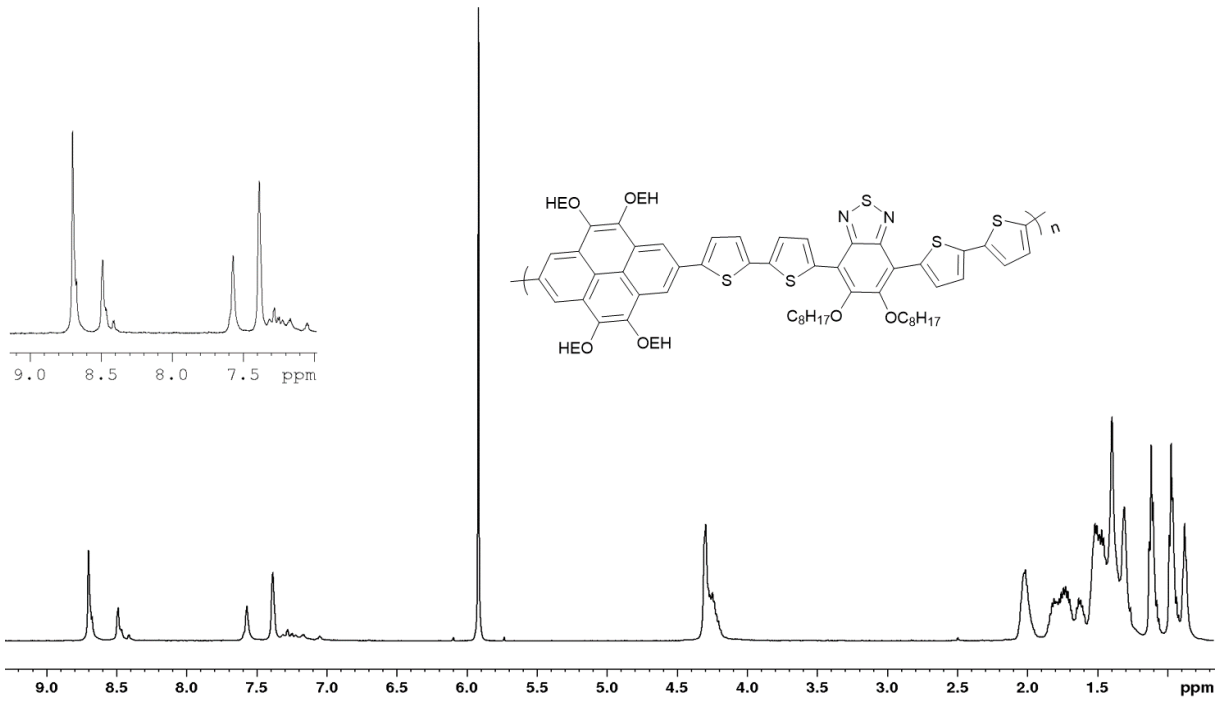

Figure 6. ^{1}H NMR spectrum of **PP$_{EH}$-DT2BT-8** at 100 ^{o}C in $C_2D_2Cl_4$.

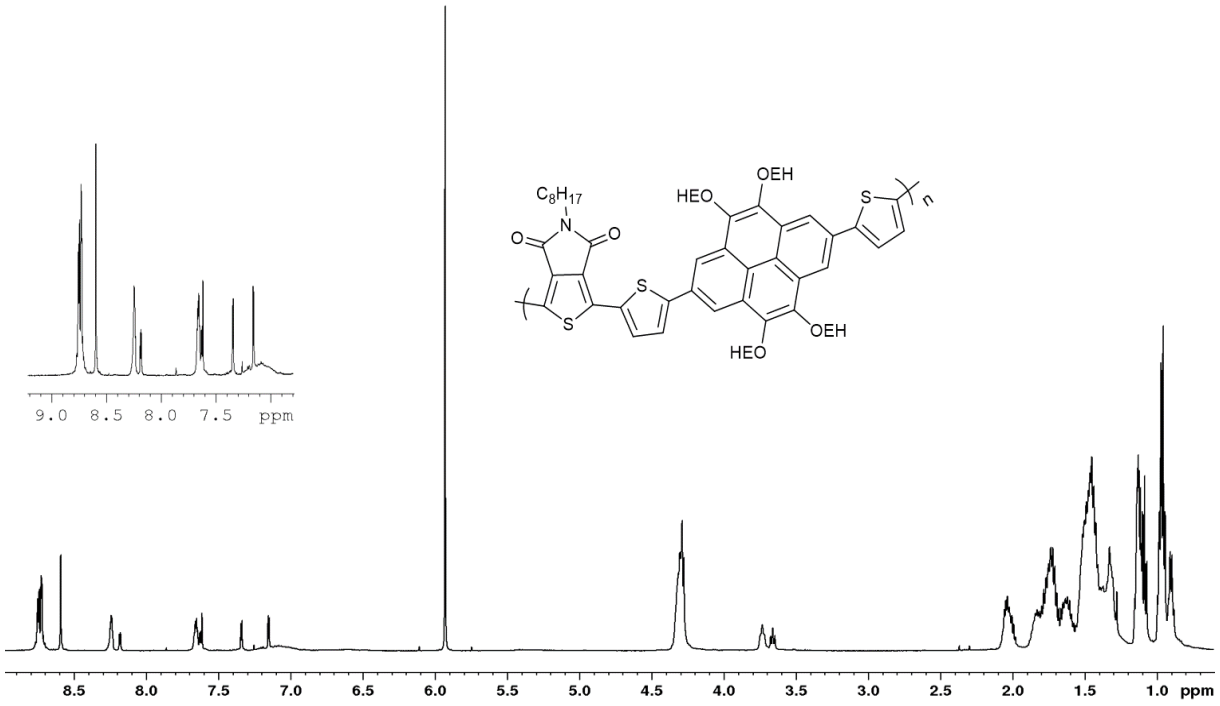

Figure 7. ^{1}H NMR spectrum of **$PP_{EH}DT$-TPD_O** at 100 ^{o}C in $C_2D_2Cl_4$.

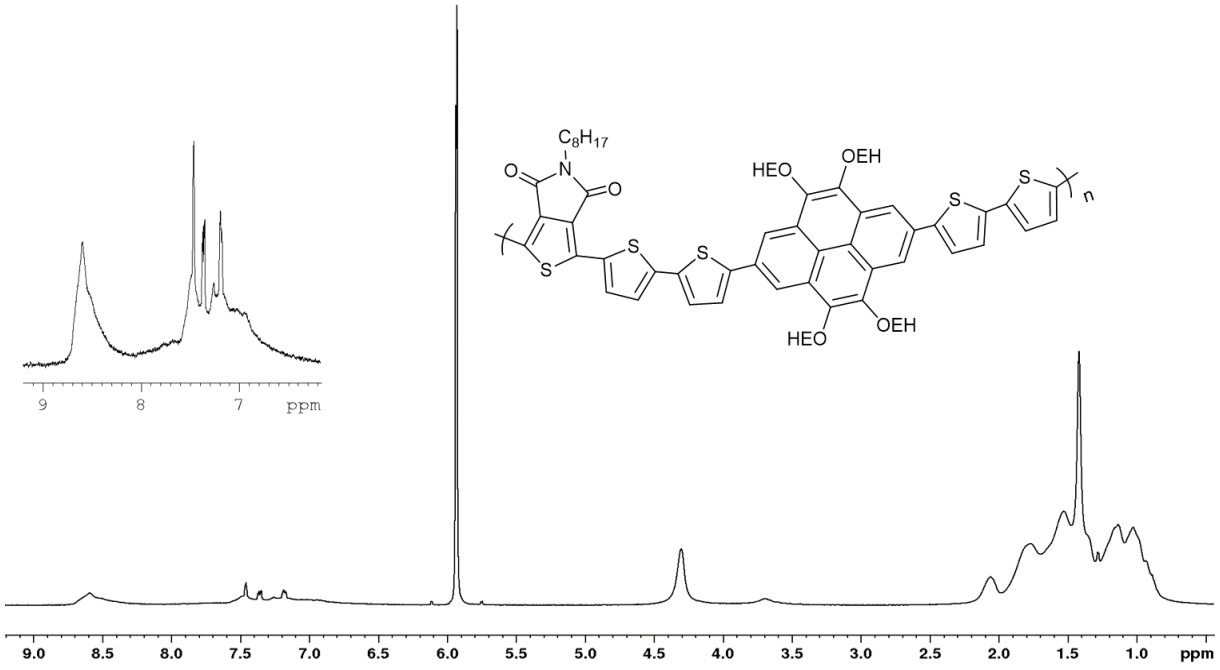

Figure 8. ^{1}H NMR spectrum of **$PP_{EH}DT2$-TPD_O** at 100 ^{o}C in $C_2D_2Cl_4$.

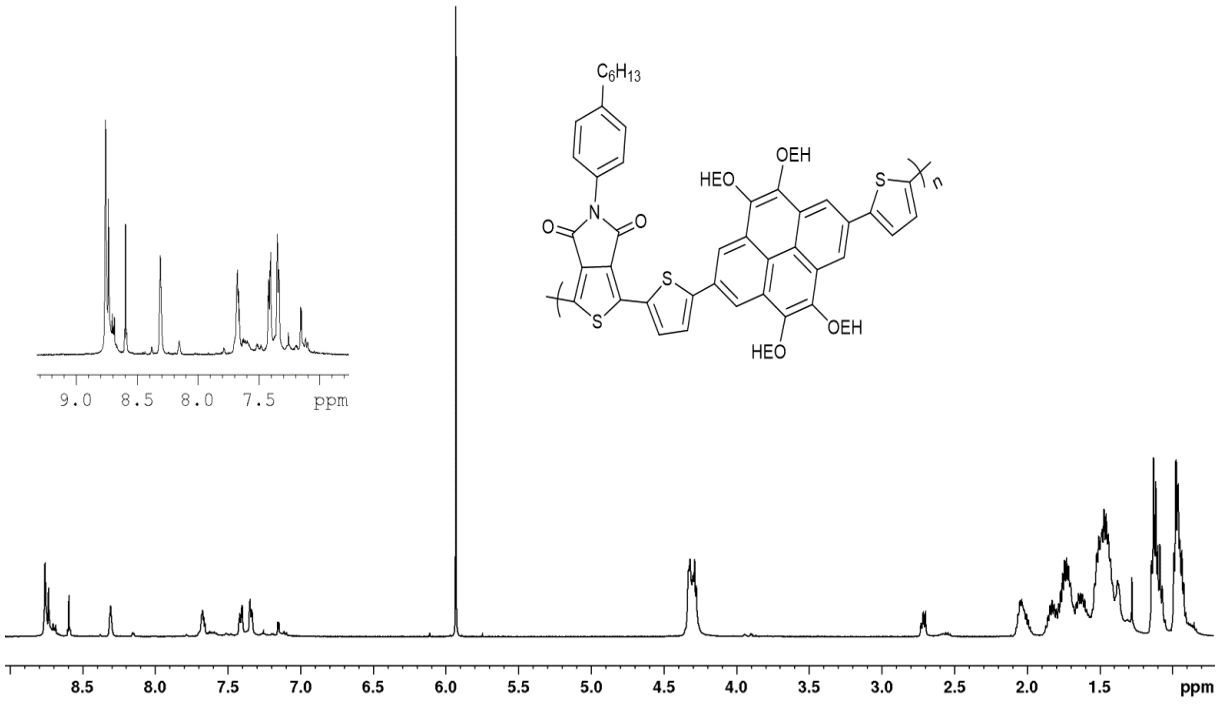

Figure 9. ^{1}H NMR spectrum of **$PP_{EH}DT$-TPD_{HP}** at 100 ^{o}C in $C_2D_2Cl_4$.

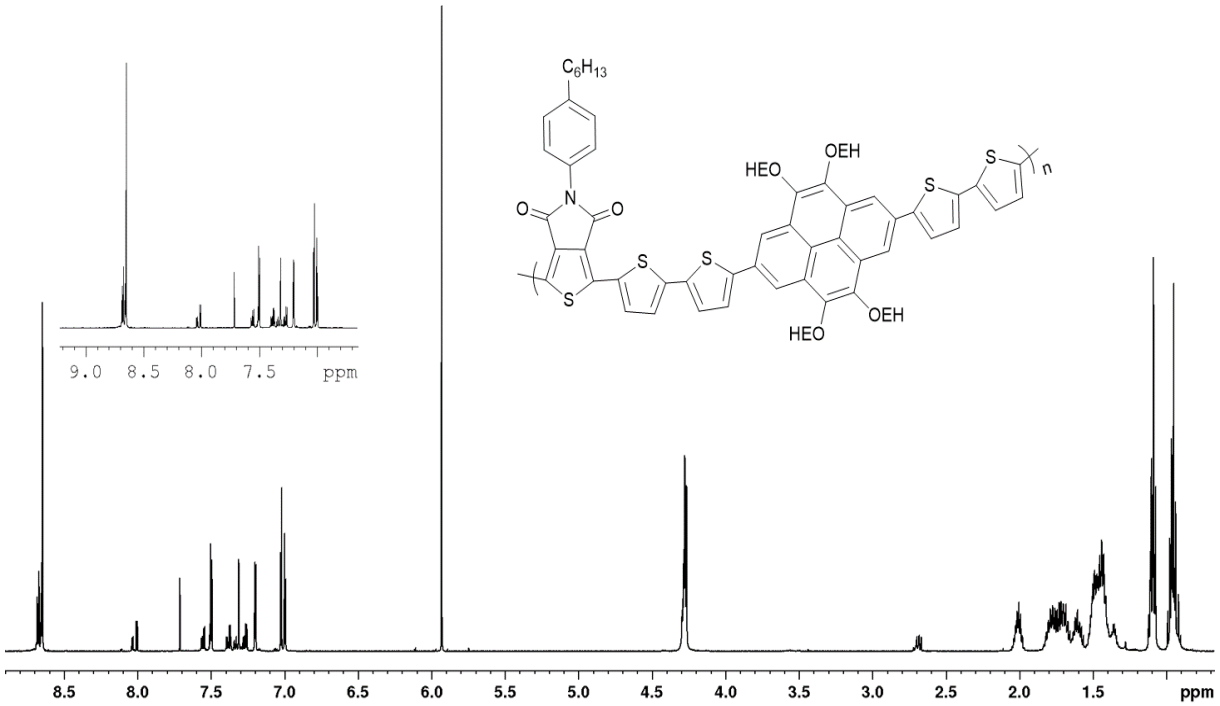

Figure 10. ^{1}H NMR spectrum of **$PP_{EH}DT2$-TPD_{HP}** at 100 ^{o}C in $C_2D_2Cl_4$.